AD-A075 379 MASSACHUSETTS INST OF TECH CAMBRIDGE ACOUSTICS AND V--ETC F/G 20/4
WALL PRESSURE FLUCTUATIONS DURING TRANSITION ON A FLAT PLATE.(U)
APR 79 C J GEDNEY N00014-77-C-0084
UNCLASSIFIED A/V-84618-1 NL

1 OF 2
AD A075379

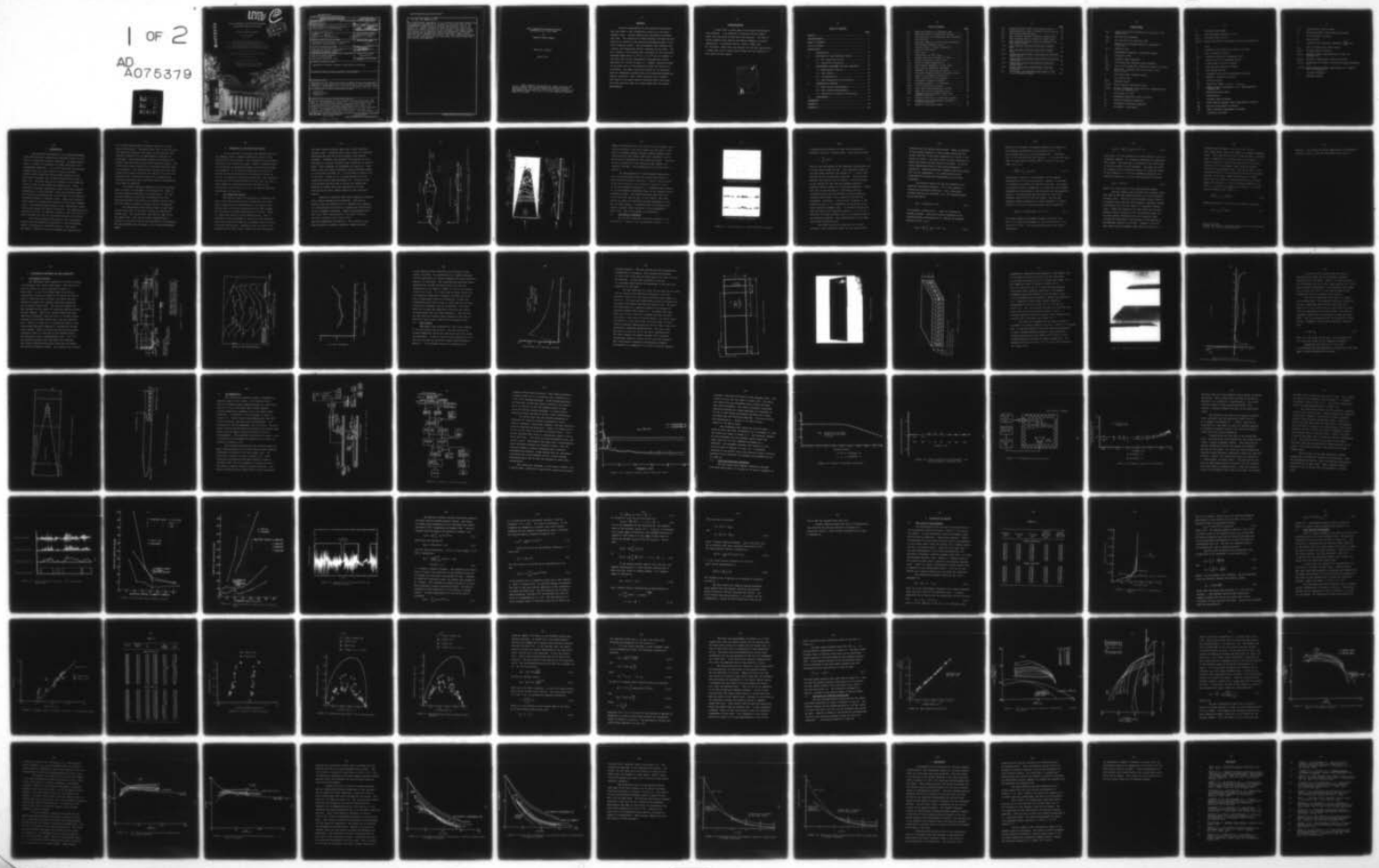

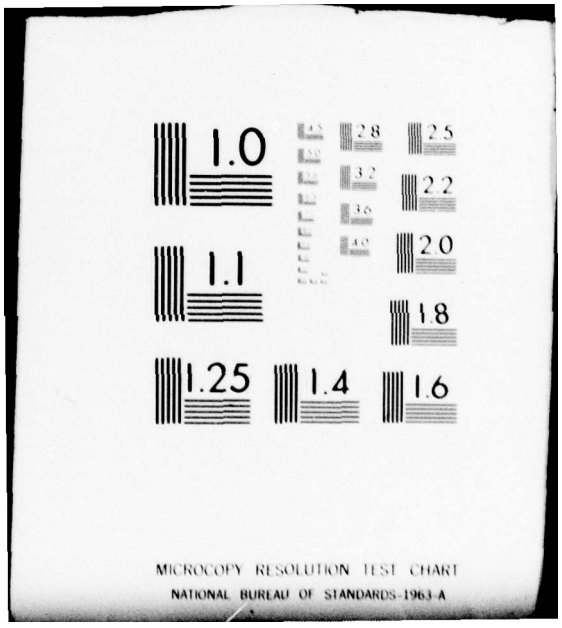
1.0
1.1
1.25
1.4
1.6
1.8
2.0
2.2
2.5
2.8
3.2
3.6
4.0
MICROCOPY RESOLUTION TEST CHART
NATIONAL BUREAU OF STANDARDS-1963-A

LEVEL II

AD A075379

WALL PRESSURE FLUCTUATIONS DURING TRANSITION ON A FLAT PLATE

by

CHARLES JOSEPH GEDNEY

Report No. 84618-1
April 1979

This research was carried out under the
Naval Sea Systems Command General Hydromechanics
Research Program administered by the
David W. Taylor Naval Ship Research and Development Center
under Office of Naval Research Contract N00014-77-C-0084

Approved for public release; distribution unlimited

Acoustics and Vibration Laboratory

Massachusetts Institute of Technology
Cambridge, Massachusetts 02139

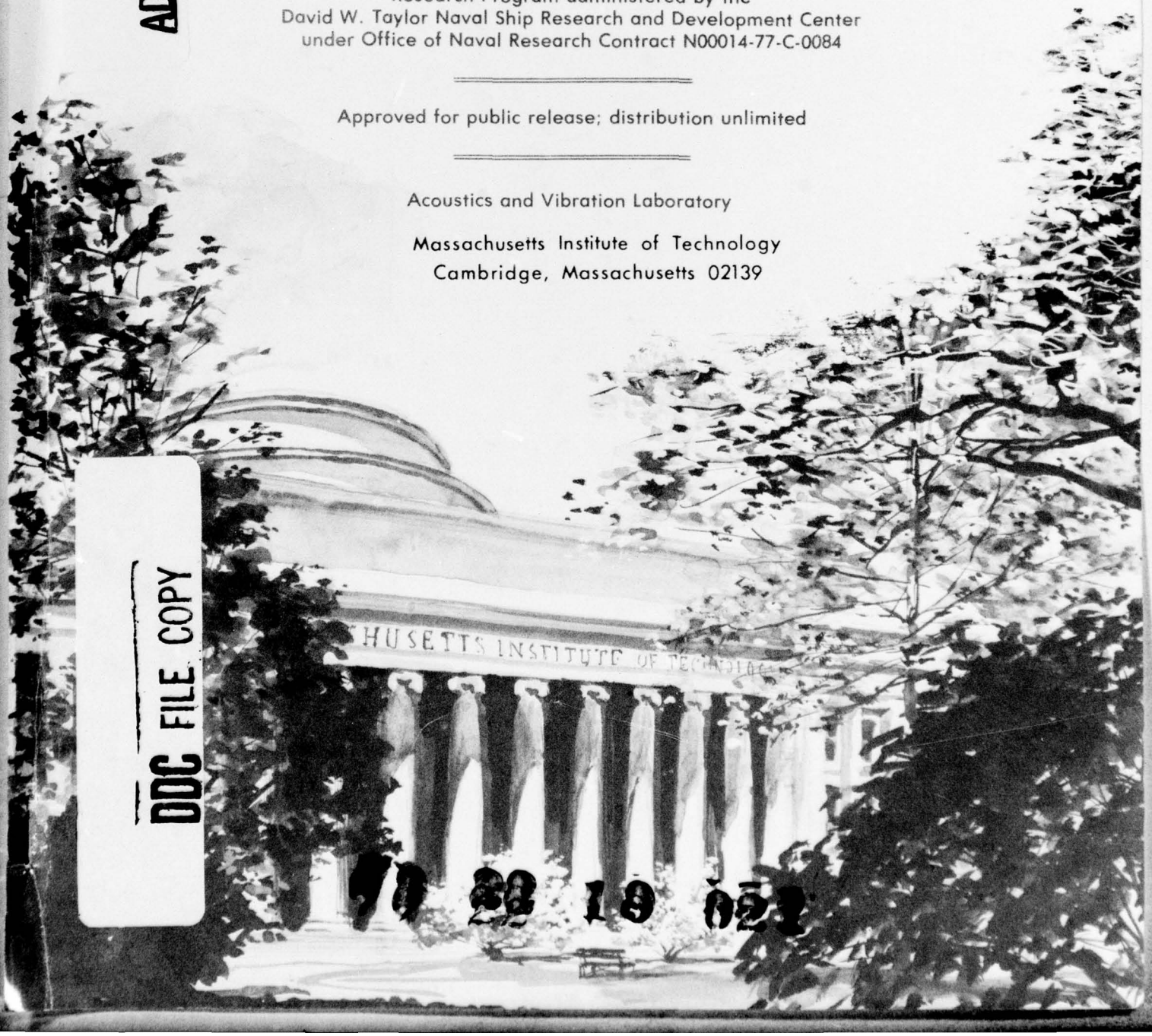

DDC
OCT 22 1979
E

DDC FILE COPY

79 10 19 021

UNCLASSIFIED

SECURITY CLASSIFICATION OF THIS PAGE (When Data Entered)

REPORT DOCUMENTATION PAGE

READ INSTRUCTIONS BEFORE COMPLETING FORM

1. REPORT NUMBER: A/V-84618-1	2. GOVT ACCESSION NO.
3. RECIPIENT'S CATALOG NUMBER	
4. TITLE (and Subtitle): Wall Pressure Fluctuations During Transition on a Flat Plate	5. TYPE OF REPORT & PERIOD COVERED: Final / October 1976 thru April 1979
	6. PERFORMING ORG. REPORT NUMBER
7. AUTHOR(s): Charles Joseph Gedney	8. CONTRACT OR GRANT NUMBER(s): N00014-77-C-0084
9. PERFORMING ORGANIZATION NAME AND ADDRESS: Massachusetts Institute of Technology, Cambridge, Massachusetts 02139	10. PROGRAM ELEMENT, PROJECT, TASK AREA & WORK UNIT NUMBERS: 12 114
11. CONTROLLING OFFICE NAME AND ADDRESS: David W. Taylor Naval Ship Research and Development Center, Code 1505, Bethesda, Maryland 20084	12. REPORT DATE: 11 April 1979
	13. NUMBER OF PAGES
14. MONITORING AGENCY NAME & ADDRESS (if different from Controlling Office): Office of Naval Research, 800 N. Quincy Street, Arlington, Virginia 22217	15. SECURITY CLASS. (of this report): Unclassified
	15a. DECLASSIFICATION/DOWNGRADING SCHEDULE

16. DISTRIBUTION STATEMENT (of this Report)

Approved for public release; distribution unlimited.

17. DISTRIBUTION STATEMENT (of the abstract entered in Block 20, if different from Report)

18. SUPPLEMENTARY NOTES

Sponsored by the Naval Sea Systems Command General Hydromechanics Research Program administered by the David W. Taylor Naval Ship Research & Development Ctr., Code 1505, Bethesda, Maryland 20084

19. KEY WORDS (Continue on reverse side if necessary and identify by block number)

flow noise
boundary layers
transition

20. ABSTRACT (Continue on reverse side if necessary and identify by block number)

Detailed measurements of wall pressure fluctuations have been made in the intermittent region of a flat plate boundary layer. Digital sampling and processing techniques were used. The properties of these pressure fluctuations were found to be similar to the previous measurements made in the fully turbulent region. The measurements were repeated with a single two dimensional surface roughness on the plate. The only changes in

over

DD FORM 1 JAN 73 1473 EDITION OF 1 NOV 65 IS OBSOLETE S/N 0102-014-6601

UNCLASSIFIED

SECURITY CLASSIFICATION OF THIS PAGE (When Data Entered)

405 028

JCD

2.0 to 1.2 million per foot

the results were a decrease in the transition Reynolds number from 2×10^6 to 1.2×10^6 and an increase in the decay rate of the longitudinal cross-spectral density magnitude by a factor of about 1.5. Emmons' analytical model of the burst rate in the transition region was found to be inaccurate. His model treats the sources of the turbulent spots as independent random events with prescribed probability density functions. Both a delta function and a constant were used as the source density functions and in each case the burst rate was about two times higher than the present measurements.

WALL PRESSURE FLUCTUATIONS DURING TRANSITION ON A FLAT PLATE

by

CHARLES JOSEPH GEDNEY

Report No. 84618-1

April 1979

This research was carried out under the Naval Sea Systems Command General Hydromechanics Research Program administered by the David W. Taylor Naval Ship Research and Development Center under Office of Naval Research Contract N00014-77-C-0084.

ABSTRACT

Detailed measurements of wall pressure fluctuations have been made in the intermittent region of a flat plate boundary layer. Digital sampling and processing techniques were used. The properties of these pressure fluctuations were found to be similar to the previous measurements made in the fully turbulent region. The measurements were repeated with a single two dimensional surface roughness on the plate. The only changes in the results were a decrease in the transition Reynolds number from 2×10^6 to 1.2×10^6 and an increase in the decay rate of the longitudinal cross-spectral density magnitude by a factor of about 1.5. Emmons' analytical model of the burst rate in the transition region was found to be inaccurate. His model treats the sources of the turbulent spots as independent random events with prescribed probability density functions. Both a delta function and a constant were used as the source density functions and in each case the burst rate was about two times higher than the present measurements.

ACKNOWLEDGMENTS

I would like to thank some of the people who helped in this research. I am indebted to Professor Patrick Leehey, whose time and patience made this work possible. The help of fellow students Paul Shapiro and Charles Thompson is greatly appreciated. Discussions with Dr. Fred C. DeMetz and Dr. William K. Blake were very helpful and are also appreciated. I would also like to thank Cheryl Gibson for her diligence in the typing of this report.

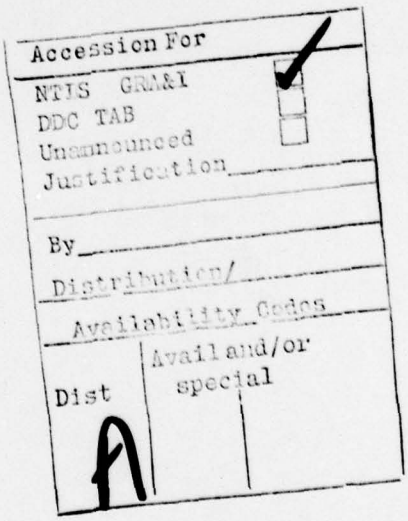

TABLE OF CONTENTS

		Page
ABSTRACT		2
ACKNOWLEDGMENTS		3
TABLE OF CONTENTS		4
LIST OF FIGURES		5
NOMENCLATURE		7
1.	INTRODUCTION	10
2.	PROPERTIES OF THE TRANSITION REGION	12
	2.1 The Transition Process	12
	2.2 Statistical Properties	16
3.	EXPERIMENTAL EQUIPMENT AND DATA PROCESSING	24
	3.1 Experimental Facility	24
	3.2 Test Fixture	28
	3.3 Instrumentation	40
	3.4 Data Acquisition and Processing	45
4.	DISCUSSION OF RESULTS	61
	4.1 Mean Velocity Measurements	61
	4.2 Mean Pressure Measurements	65
	4.3 Statistics of Pressure Fluctuations	74
5.	CONCLUSIONS	89
REFERENCES		92
APPENDIX A		95
APPENDIX B		106

LIST OF FIGURES

		Page
2.1	Shape and Growth of a Turbulent Spot	14
2.2	Idealized Sketch of Transition Process	15
2.3	Time Histories of Intermittent Wall Pressures .	17
3.1	Test Facility	25
3.2	Frequency Spectra of Free Stream Turbulence ...	26
3.3	Free Stream Turbulence Level	27
3.4	Acoustic Noise in Tunnel Blockhouse	29
3.5	Layout of Test Plate	31
3.6	Test Plate	32
3.7	Construction of Test Plate	33
3.8	Leading and Trailing Edges of Plate	35
3.9	Pressure Gradient on Test Plate.....	36
3.10	Extent of Edge Contamination	38
3.11	Step Surface Roughness in Test Plate	39
3.12	Mean Velocity Measuring Equipment	41
3.13	Schematic of Electronic Circuitry	42
3.14	Turbulent Pressure Spectra and Noise Floors ...	44
3.15	Results of Equipment Calibration	46
3.16	Phase Calibration of Microphones	47
3.17	Microphone Calibration Setup	48
3.18	Frequency Response of Microphones	49
3.19	Signal Conditioning Process	52
3.20	Burst Rate Versus Smoothing Interval	53
3.21	Burst Rate Versus Triggering Level	54
3.22	Computer Plot of Pressure Signal and Indicator Function	55
4.1	Velocity Profiles in Intermittent Region	63
4.2	Boundary Layer Displacement Thickness in Intermittent Region	66
4.3	Extent of Transition Region	68

		Page
4.4	Normalized Burst Rates (Line Source Density) ...	69
4.5	Normalized Burst Rates (Constant Source Density).	70
4.6	Mean Square Pressure Ratio	75
4.7	Wall Pressure Spectral Densities (Smooth Wall) .	76
4.8	Wall Pressure Spectral Densities (Rough Wall) ...	77
4.9	Wall Pressure Spectral Densities Scaled by the Wall Shear Stress	79
4.10	Wall Pressure Convection Velocities (Smooth Wall)	81
4.11	Wall Pressure Convection Velocities (Rough Wall)	82
4.12	Normalized Longitudinal Cross-Spectral Densities (Smooth Wall)	84
4.13	Normalized Longitudinal Cross-Spectral Densities (Rough Wall)	85
4.14	Normalized Lateral Cross-Spectral Densities (Smooth Wall)	87
4.15	Normalized Lateral Cross-Spectral Densites (Rough Wall)	88
B.1	Retrograde and Truncated Cones Shown in the x,y,t Coordinate System	107

NOMENCLATURE

C_{fL}	local skin friction coefficient ($\tau_w/1/2\rho U_\infty^2$) for laminar flow
C_{fm}	skin friction measured
C_{fT}	skin friction for turbulent flow
d	diameter of microphone pinhole or distance of $(x-x_o)$ tanα
E[ ]	expected value
f	experimental frequency (cycles per second)
f_j	frequency of FFT
f_B	turbulent burst frequency
f_B^*	non-dimensional turbulent burst frequency
g(P)	source rate probability function at point P on plate
H(x)	Heaviside function, H=0 if x<0, H=1 if x>0, H=1/2 if x=0
k	two dimensional roughness height
n	line source rate
p(t)	pressure signal
P(f,T)	finite Fourier transform of p(t)
$\tilde{P}_j, \tilde{Q}_j$	Fourier transforms of p(t) and q(t) approximated by an FFT (at frequency f_j)
q	total head, 1/2 ρU_∞^2
$\bar{r}$	microphone separation vector distance
r_L	lateral microphone separation
r_S	streamwise microphone separation
R	retrograde cone region

R'	truncated cone region
Re_x	Reynolds number based on x, Ux/ν
$R_p(\tau)$	autocorrelation of p(t)
$R_p(\bar{r},\tau)$	cross-correlation of pressures at points separated by $\bar{r}$
t	time
Δt	turbulent burst duration at point P on plate
$\bar{u}$	mean streamwise velocity
$\bar{U}_c(\omega)$	convection velocity of pressure field
U_g	growth velocity of turbulent bursts
U_ℓ	leading edge velocity of bursts
U_t	trailing edge velocity of bursts
U_∞	free stream velocity
x,y	streamwise and vertical coordinates on plate
$\bar{x}$	reduced x coordinate, $(x-x_t)/\Delta X_T$
x_t	transition point
ΔX_T	transition length, $x\|_{\gamma=0.99} - x\|_{\gamma=0.01}$
$\tilde{z}_j$	complex Fourier transform of z(t), approximated by a complex FFT
α	burst spread half angle
γ	intermittency
δ	boundary layer thickness
δ_L^*	local laminar boundary layer displacement thickness
δ_m^*	Measured displacement thickness
δ_T^*	local turbulent displacement thickness
η	integration variable

$\theta(\omega)$	cross-spectral density phase
θ_m	measured boundary layer momentum thickness
ν	fluid kinematic viscosity
ρ	fluid density
σ^*	turbulent spot convection parameter, $\frac{U_\infty U_g}{U_\ell U_t} \tan\alpha$
τ_{wT}	local turbulent wall shear stress
$\Phi_p(\omega)$	pressure spectral density
$\tilde{\Phi}_p(f_j)$	spectral density approximated by an FFT (at frequency f_j)
$\bar{\Phi}_p(f_j)$	average of approximate spectral densities
$\phi_p(\bar{r},\omega)$	cross-spectral density of pressure signals separated by $\bar{r}$
$\tilde{\phi}_p(\bar{r},f_j)$	cross-spectral density approximated by a complex FFT (at frequency f_j)
ω	circular frequency
$< >$	temporal average

1. INTRODUCTION

Wall pressure fluctuations in the turbulent boundary layer have long been recognized as important sources of vibration of marine and aircraft structures. In marine applications, the effect of turbulence on sonar structures is of considerable importance. It is well known that the turbulent boundary layer is a major source of sonar self-noise. Boundary layer flows have received much attention in the past and an excellent list of publications may be found in White [1]. Two works that are of interest in this study are those by Blake [2] and DeMetz and Casarella [3]. Blake presented a thorough experimental study of the wall pressure fluctuations in fully turbulent, flat plate boundary layers. The statistics he measured are of great value in the design of structures exposed to turbulent flows. DeMetz and Casarella investigated the intermittent portion of a flat plate boundary layer. They presented many details of the intermittent region but did not measure any spatial statistics. The properties of the intermittent region are important because it may cover most of a small structure and cause an appreciable amount of excitation.

This report presents the results of an experimental study of the wall pressure fluctuations in the intermittent region of transition to turbulent flow on a flat plate. The study is similar to the one of DeMetz and Casarella [3]

but includes measurements of spatial statistics (cross-spectral densities). Experiments were done in the low noise, low turbulence acoustic wind tunnel in the Acoustics and Vibration Laboratory at the Massachusetts Institute of Technology. Two phase-matched condenser microphones with pinhole caps were used to obtain wall pressure signals. The statistics of these signals were calculated digitally using a minicomputer. The intermittency, average burst rate and average burst period along with the auto and cross-spectral densities were calculated for many test configurations. Convection velocities were calculated from the longitudinal cross-spectral densities.

The results obtained compare well with the measurements of Blake [2] and DeMetz and Casarella [3]. Most of the data showed no dependence on intermittency. The auto-spectral densities varied with intermittency but this variation was most likely due to an improper scaling along with the effect of spatial averaging over the microphone.

The measurements were repeated with a single downstream facing step in the plate located just behind the leading edge. The results were very much the same as for the smooth case. The only noticeable changes were an increase in the decay rate of the longitudinal cross-spectral density magnitude and a decrease in the transition Reynolds number.

2. PROPERTIES OF THE TRANSITION REGION

In the flow past a structure, the laminar portion of the boundary layer is usually considered passive in the excitation of the structure. This includes the non-turbulent portions of the transition region. However, turbulent spots can contribute an appreciable amount of excitation and must be considered. It is therefore important to be able to predict the start and extent of the transition region as well as its important statistical properties. The transition process has received much attention in the past, but only a small number of investigations have been done on the statistics of the intermittent region. The present work was concentrated in this area.

2.1 THE TRANSITION PROCESS

The natural process of transition to turbulent flow over a flat plate begins with the instability of certain small, random velocity fluctuations in the laminar flow. Fluctuations with certain characteristics become unstable and are known as Tollmien-Schlichting (T-S) waves. These T-S waves soon develop a three dimensionality. This is followed by vortex breakdown at regions of high localized shear and finally the formation of turbulent spots at areas of intense fluctuations. Turbulent spots (or bursts) are characterized by their highly random velocity fluctuations

and small scales of motion, much like a fully turbulent boundary layer. Turbulent spots grow as they are convected downstream and soon the entire boundary layer becomes turbulent. Schubauer and Klebanoff [4] measured the size and shape of a typical turbulent spot created by an electric spark. Their findings are reproduced in Figure 2.1. This figure shows the normal "arrowhead" shaped planform growing at a half-angle of about 11^{o}. It also shows a profile view of the spot. Figure 2.2 is an idealized sketch of the transition process taken from White [1]. Transition has received much attention and is fairly well understood. Hundreds of studies have been published on the many interesting and often complex aspects of the transition process.

Emmons [9] suggested that burst formation be modeled with a source probability distribution. This method requires that the probability of a turbulent spot forming at a certain location be given by a probability distribution in the streamwise coordinate. Dhawan and Narasimha [11] have since shown experimentally, that burst formation can best be modeled with a Dirac delta function probability distribution. The location of the delta function is usually called the transition point.

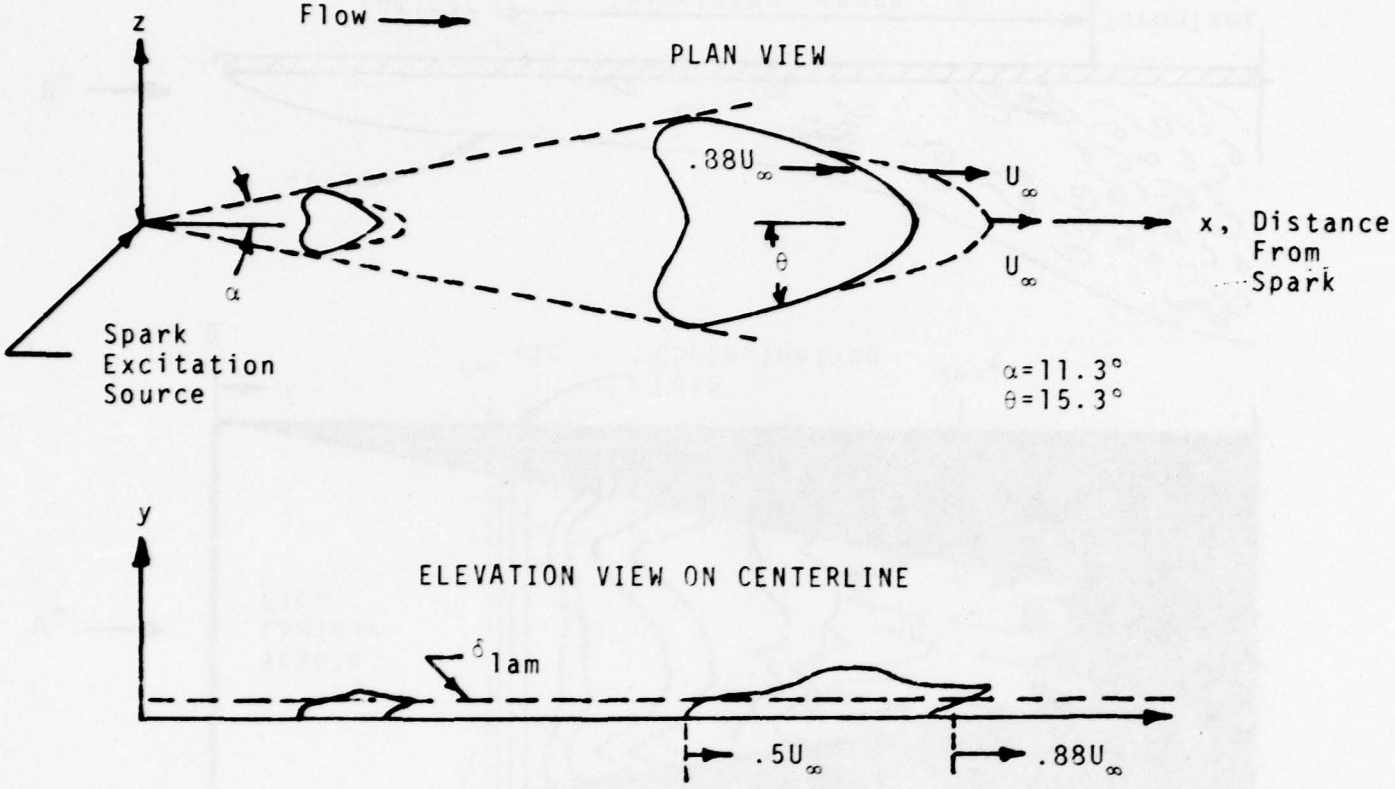

FIGURE 2.1 Shape and Growth of a Turbulent Spot. (Excited by an Electric Spark) From Schubauer and Klebanoff [4].

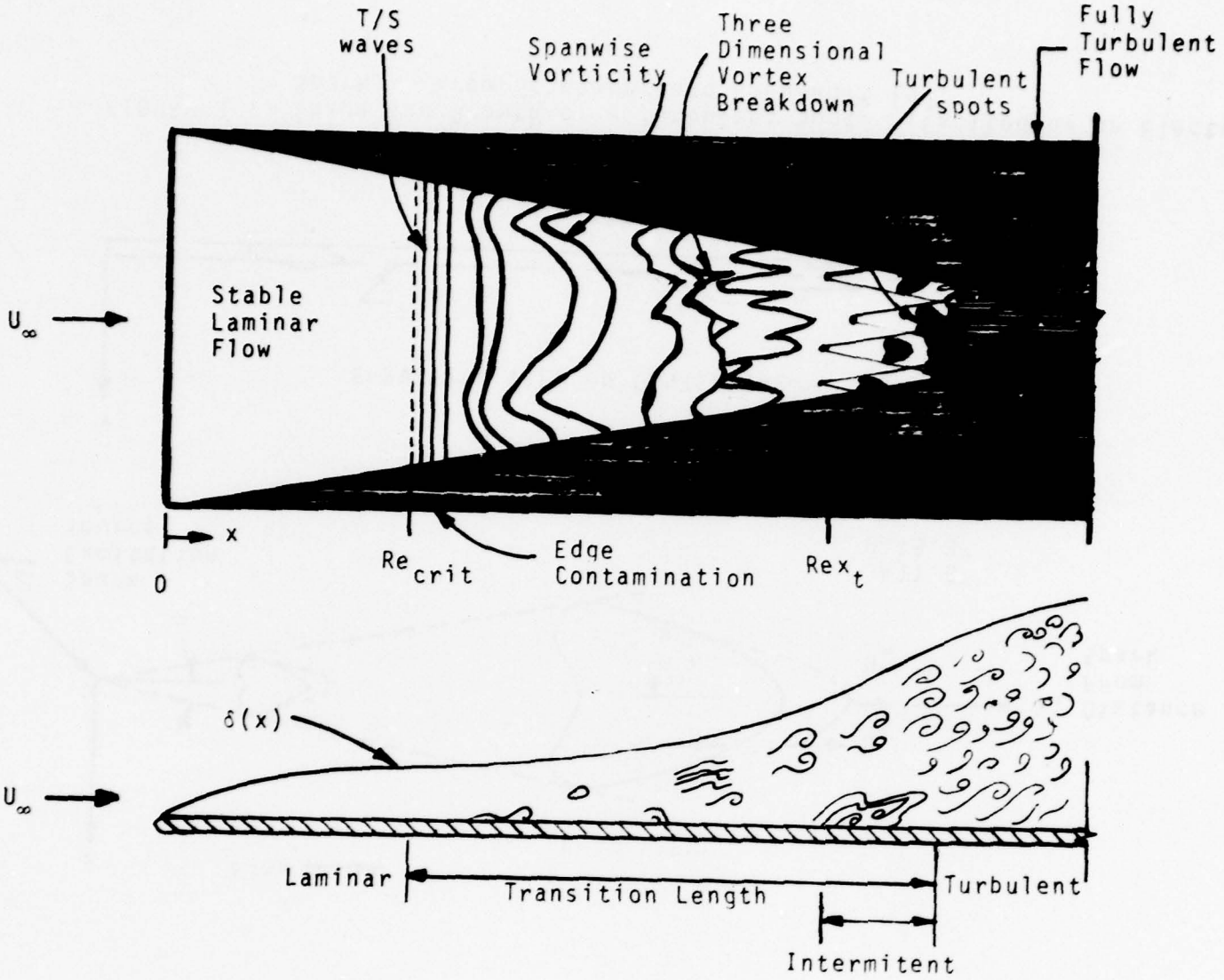

FIGURE 2.2 Idealized Sketch of Transition Process From White [1]

Dhawan and Narasimha have also shown that the boundary layer velocity profile in the burst region (as seen from a fixed point) fluctuates between a Blasius profile between bursts (originating at the leading edge) and a turbulent profile during bursts (beginning at the transition point). Therefore, the mean velocity is a time average of the laminar and turbulent portions. This observation will be used later in Chapter 4.

The characteristics of wall pressure fluctuations are of interest because they are the exciting forces in flow related structural vibrations. Typical time histories of the wall pressure in the transition region are shown in the oscillographs of Figure 2.3. A turbulent spot appears as a high frequency, disordered burst in the otherwise quiet, microphone signal. The downstream growth and convection of the spots can also be seen in this figure. The lower signal was taken at a position slightly downstream of that for the upper signal. A turbulent spot in the upper trace appears slightly larger and later in the corresponding lower trace due to the growth and convection.

2.2 STATISTICAL PROPERTIES

The one most important statistical property of the intermittent region is the intermittency factor, γ. It

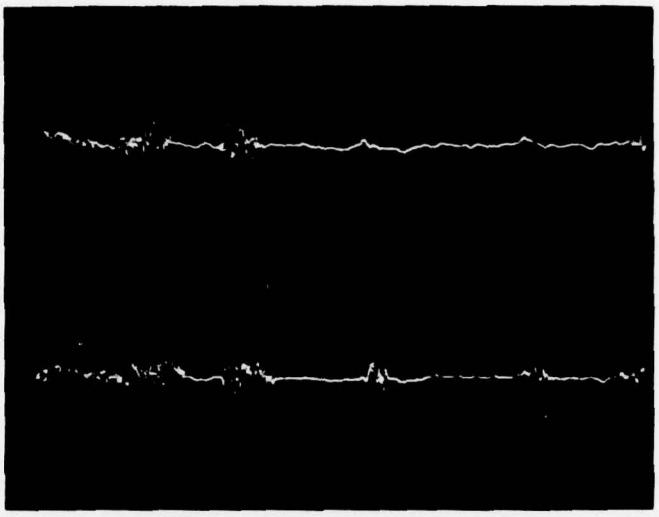

Streamwise Microphone Separation

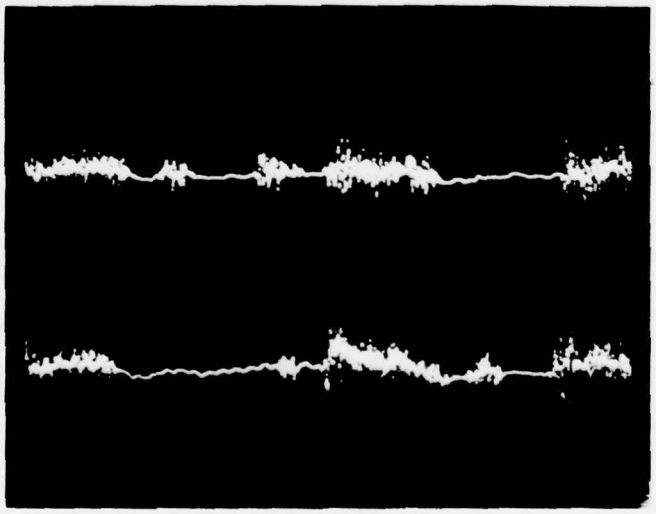

Lateral Microphone Separation

FIGURE 2.3 Time Histories of Intermittent Wall Pressure

is defined as the fraction of time the flow exhibits a turbulent nature at a certain point. This can be written:

$$\gamma = \sum_{i=1}^{N} t_i/T, \tag{2.1}$$

where t_i are the lengths of the turbulent time periods, and T is the total length of time. Since turbulent spots do not have square profiles (see Figure 2.2), γ varies with vertical as well as horizontal position. Since the wall pressure fluctuations are of interest, γ will be defined as the fraction of time the wall pressure exhibits a turbulent nature, unless it is specified otherwise. Notice that this is not the same as γ defined by velocity fluctuations near the wall because a certain amount of averaging takes place in the pressure field over the microphone. Obviously, γ varies from 0 (laminar) at the transition point to 1.0 (turbulent) at the start of the fully turbulent boundary layer. It should be pointed out that the ends of the transition region (γ = 0, 1.0) are difficult to locate accurately due to the random nature of the transition process. Fair approximations can be made using large averaging times.

Two other statistical properties of the wall pressure in the transition region are the average burst

frequency and the average burst period. These are defined as the average frequency at which bursts appear and the average duration of the bursts appearing at a point in the transition region. The usual units are burst frequency in bursts per second and burst period in seconds. It can be easily demonstrated that of these three statistical properties - intermittency, burst frequency and burst period only two are independent, (i.e. burst period can be calculated by dividing the intermittency by the burst frequency).

The spectral density of the wall pressure is an important statistical property. It is very useful in determining structural excitation. For a stationary, randomly varying wall pressure, $p(t)$, the autocorrelation may be defined by:

$$R_p(\tau) = E[p(t)p(t+\tau)], \tag{2.2}$$

(see Crandall and Mark [12]). Here E[ ] denotes an ensemble average. Taking the Fourier transform of the autocorrelation and dividing by 2π defines the spectral density of $p(t)$, $\Phi_p(\omega)$:

$$\Phi_p(\omega) = \frac{1}{2\pi} \int_{-\infty}^{\infty} R_p(\tau)\, e^{-i\omega\tau}\, d\tau. \tag{2.3}$$

Defined in this manner the spectral density is a measure of the frequency distribution of the energy in p(t). It can be shown that R_p is an even function of τ. Therefore $\Phi_p(\omega)$ is an even, positive real function. It can also be shown that the mean square pressure, $\overline{p^2(t)}$ is equal to the area under $\Phi_p(\omega)$, or:

$$\overline{p^2(t)} = \int_{-\infty}^{\infty} \Phi_p(\omega)\, d\omega. \qquad (2.4)$$

The spectral density is a good measure of the temporal characteristics of the wall pressure. However, it provides no information regarding the spatial variations. One method of obtaining spatial information is to make two wall pressure measurements simultaneously, and calculate the cross-spectral density. This method was used by Blake [2], Bull [13], Willmarth and Wooldridge [14] and others. For two wall pressure signals separated by a vector distance, $\bar{r}$, [$p(\bar{x},t)$ and $p(\bar{x} + \bar{r}, t)$] the cross-correlation may be defined by:

$$R_p(\bar{r},\tau) = E[p(\bar{x},t)p(\bar{x} + \bar{r}, t + \tau)]. \qquad (2.5)$$

E[ ] again denotes an ensemble average, and $p(\bar{x},t)$ and $p(\bar{x} + \bar{r}, t)$ must be stationary in time and spatially in the plane of the wall. The cross-spectral density may now be defined by:

$$\phi_p(\bar{r},\omega) = \frac{1}{2\pi}\int_{-\infty}^{\infty} R_p(\bar{r},\tau)e^{-i\omega\tau}\,d\tau. \qquad (2.6)$$

Since $R_p(\bar{r},\tau)$ is not necessarily an even function, $\phi(\bar{r},\omega)$ is in general complex. It is usually presented as a magnitude and a phase. The magnitude is a measure of the correlation of the two signals at each frequency. The phase can serve as a measure of the convection velocity of turbulent eddies. If the separation, $\bar{r}$ is in the streamwise direction, the convection velocity, $\bar{U}_c$ can be obtained from the relation:

$$\bar{U}_c(\omega) = \omega\bar{r}/\theta(\omega) \qquad (2.7)$$

where $\theta(\omega)$ is the phase of the cross-spectral density.

Previous studies have indicated that turbulent spots have many of the same characteristics as a fully turbulent boundary layer. Velocity or wall pressure signals taken in a turbulent spot show the high frequency, apparently random fluctuations that are also found in a turbulent boundary layer. DeMetz and Casarella [3] have shown that the wall pressure spectral density in the intermittent region has the same general characteristics as a turbulent layer, although the magnitude is less because of the presence of non-turbulent regions in the flow. Cantwell, et al [7] have shown that the boundary layer velocity profile in a

turbulent spot contains a law of the wall region and a wake region, just as is found in a turbulent boundary layer. These observations seem to indicate that a turbulent spot is essentially an isolated region of turbulence. It would be helpful if some of the statistics in the intermittent part of the boundary layer could be compared directly to the turbulent data. This may be done if the intermittent data is first corrected for the non-turbulent portions of the flow. DeMetz and Casarella [3] have shown that the following relationship holds for the mean square wall pressure in a fully turbulent boundary layer, $\overline{p^2(t)}|_{\gamma=1}$, and the mean square wall pressure in an intermittent boundary layer, $\overline{p^2(t)}|_{\gamma}$:*

$$\overline{p^2(t)}|_{\gamma=1} = \frac{1}{\gamma}\,\overline{p^2(t)}|_{\gamma}. \tag{2.8}$$

Combining equations (2.4) and (2.8) yields the relation:

$$\Phi_p(\omega)|_{\gamma=1} = \frac{1}{\gamma}\,\Phi_p(\omega)|_{\gamma}. \tag{2.9}$$

*Notice that $\overline{p^2(t)}|_{\gamma}$ is the mean square of the total pressure signal, not just the turbulent part.

Equation (2.9) allows the direct comparison of the turbulent statistic, $\Phi_p(\omega)|_{\gamma=1}$ and the intermittent one, $\Phi_p(\omega)|_{\gamma}$.

3. EXPERIMENTAL EQUIPMENT AND DATA PROCESSING

3.1 EXPERIMENTAL FACILITY

The experiments were conducted in the MIT low-noise, low-turbulence open circuit wind tunnel. This facility is shown in Figure 3.1 and is described in detail in Hanson [15]. It has a flow speed range of 20-50 m/s, controlled by varying the speed of a DC motor driving the blower. Since the work of Hanson, the tunnel has been modified to improve its inherent freestream turbulence and to further reduce noise. The settling chamber has been extended and the number of turbulence reducing screens has been doubled. Behind the screens holding the honey comb flow straighener, there are six 16 x 18 mesh screens, followed by two 48 mesh screens and a two foot settling zone. Figure 3.2 shows the 1/3 octave band levels of the free stream turbulence component u' obtained for various tunnel speeds. Figure 3.3 shows the resulting percentage turbulence level as a function of free stream velocity. The turbulence level is approximately 0.05%. Tani [16] and Spangler and Wells [17] have shown that reducing free stream turbulence below this level does not change the transition Reynolds number. The acoustic noise created

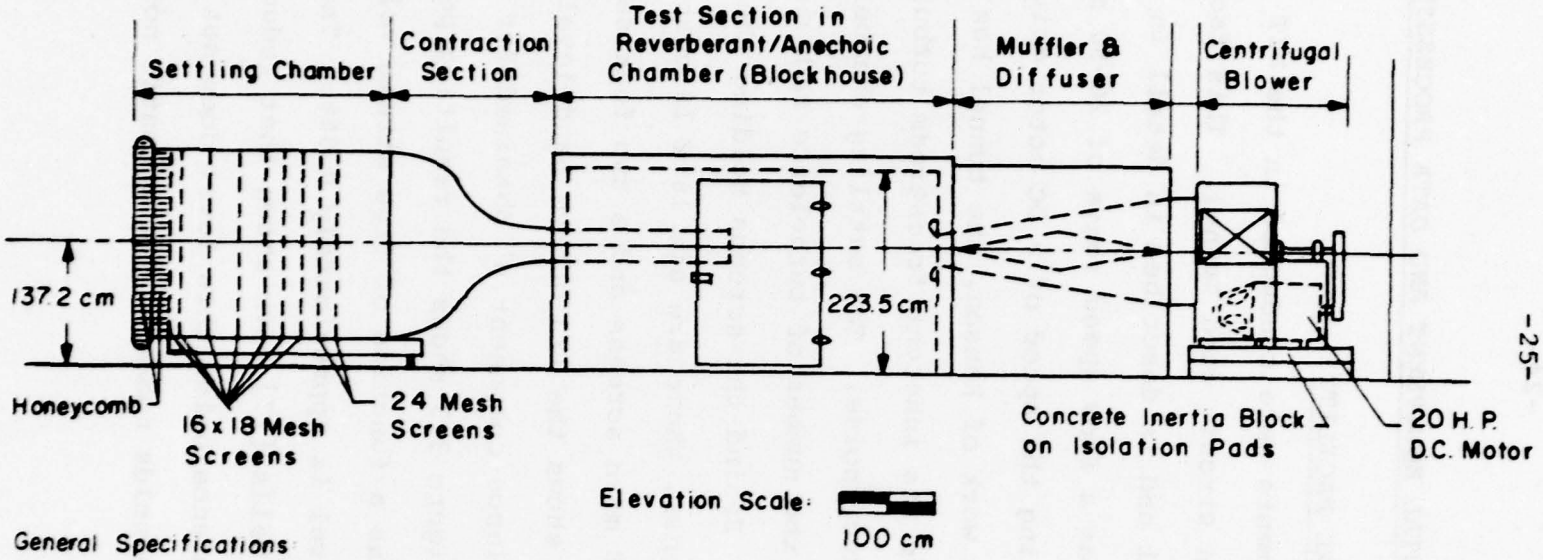

General Specifications:
Contraction Ratio: 20:1
Test Section: 38cm x 38cm, shown in open duct configuration

WIND TUNNEL FACILITY — ROOM 5-024
ACOUSTICS & VIBRATIONS LABORATORY
MASSACHUSETTS INSTITUTE OF TECHNOLOGY

FIGURE 3.1 Test Facility

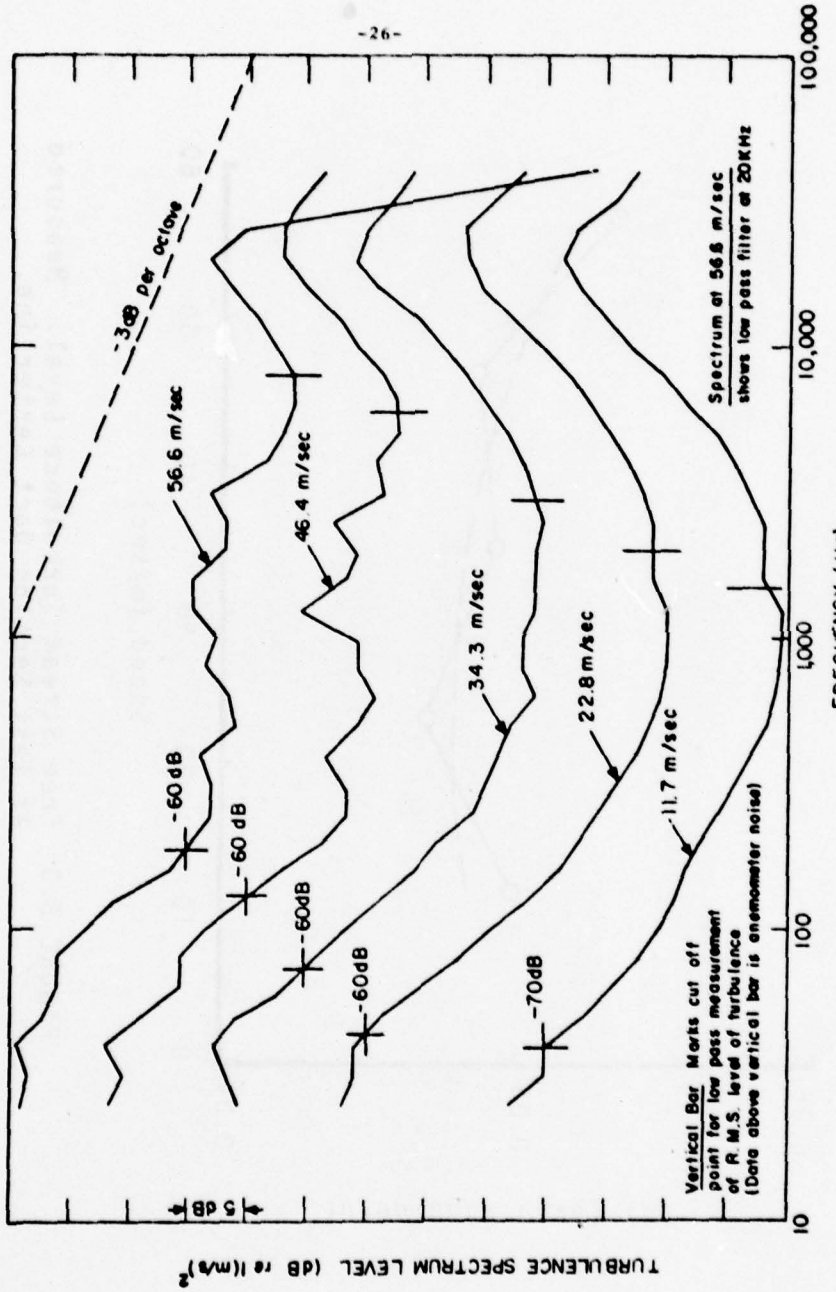

FIGURE 3.2 Frequency Spectra of Free Stream Turbulence. Measured at Test Section Duct Centerline in 1/3 Octave Bands.

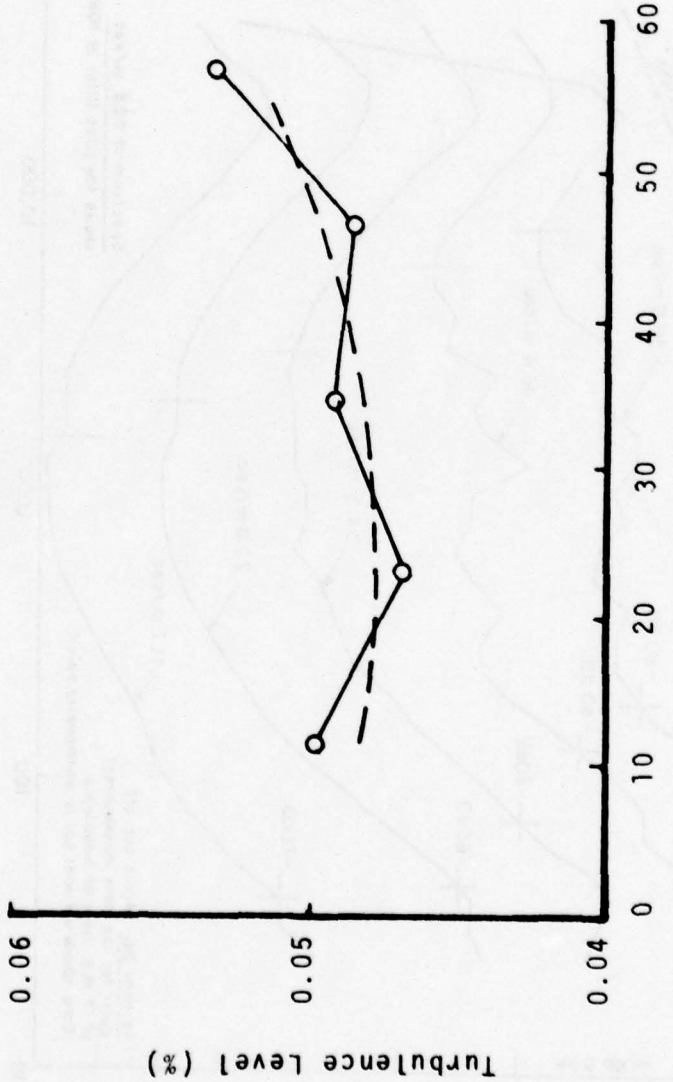

FIGURE 3.3 Free Stream Turbulence Level. Measured at Test Section Duct Centerline.

by the tunnel has been reduced by the isolation of the tunnel and blower, the installation of a muffler-diffuser and the application of vibration damping and sound absorptive material to the blower. The sound pressure spectrum levels measured just outside the mixing zone in an open jet configuration, are shown in Figure 3.4, for a free stream velocity of 50 m/s. It is felt that the noise levels are low enough, by comparison to Spangler and Wells, as to not have an appreciable effect on transition. An open jet configuration was used in order to allow some of the sound generated to propagate into the blockhouse. The blockhouse was airtight and completely lined with two inches of polyurethane foam for sound absorption. This facility has been used for boundary layer research in the past by Blake [2], Martin [18], Shapiro [19] and Moeller [20].

3.2 TEST FIXTURE

Experiments were performed on a flat plate mounted in the wind tunnel test section. The test section was located immediately behind the contraction and just inside the blockhouse. It was 15 inches (38 cm) square and 6 feet (183 cm) long and was lined with smooth sound absorptive material. It had movable walls for controlling the

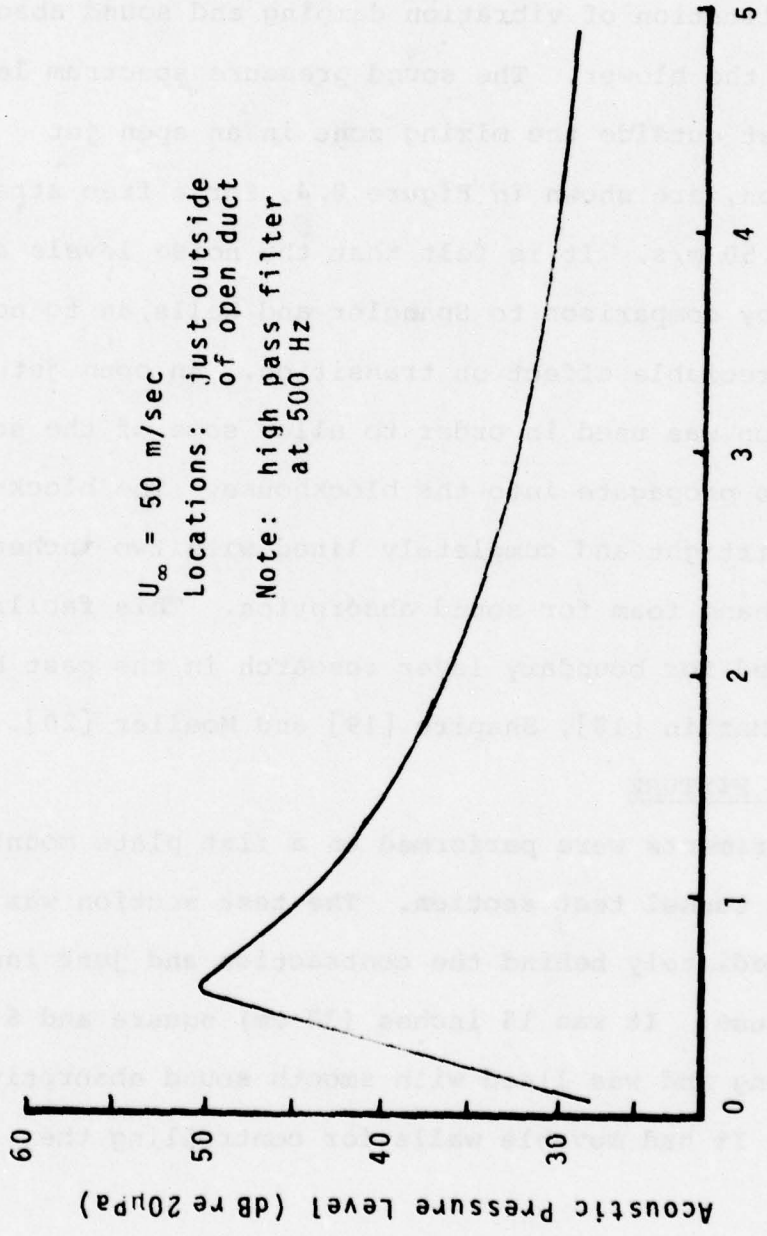

FIGURE 3.4 Acoustic Noise in Tunnel Blockhouse.

pressure gradient. The test section was also equipped with a mechanical x-y traverse. This traverse was accurate to 0.001 inch (0.025 mm) vertically and to 0.1 inch (0.25 cm) horizontally. It was used to position a hot wire or a pressure probe during the measurement of the mean flow properties on the plate.

The test plate was 15 inches (38 cm) wide and 48 inches (122 cm) long and was mounted horizontally in the test section 5 inches (12.7 cm) above the bottom (see Figures 3.5 and 3.6). The plate was located below center to minimize the secondary flow effects described by Shapiro [19]. The plate was constructed as a composite sandwich to increase the vibration damping (see Figure 3.7). The upper layer was made of 0.25 inch (0.635 cm) aluminum tool and jig plate to provide a flat, easy to polish, surface. The center layer was made of a 0.125 inch (0.317 cm) thick sheet of visco-elastic vibration-damping material (E-A-R C-1002, from E-A-R Corporation, Westwood, Massachusetts). The lower layer was made of 0.125 inch (0.317 cm) thick aluminum plate. The whole sandwich was bonded together with a two-part polyurethane adhesive, chosen for its high peel strength. This construction technique was developed by Shapiro, and resulted in a damping of 11 to 40% of critical damping

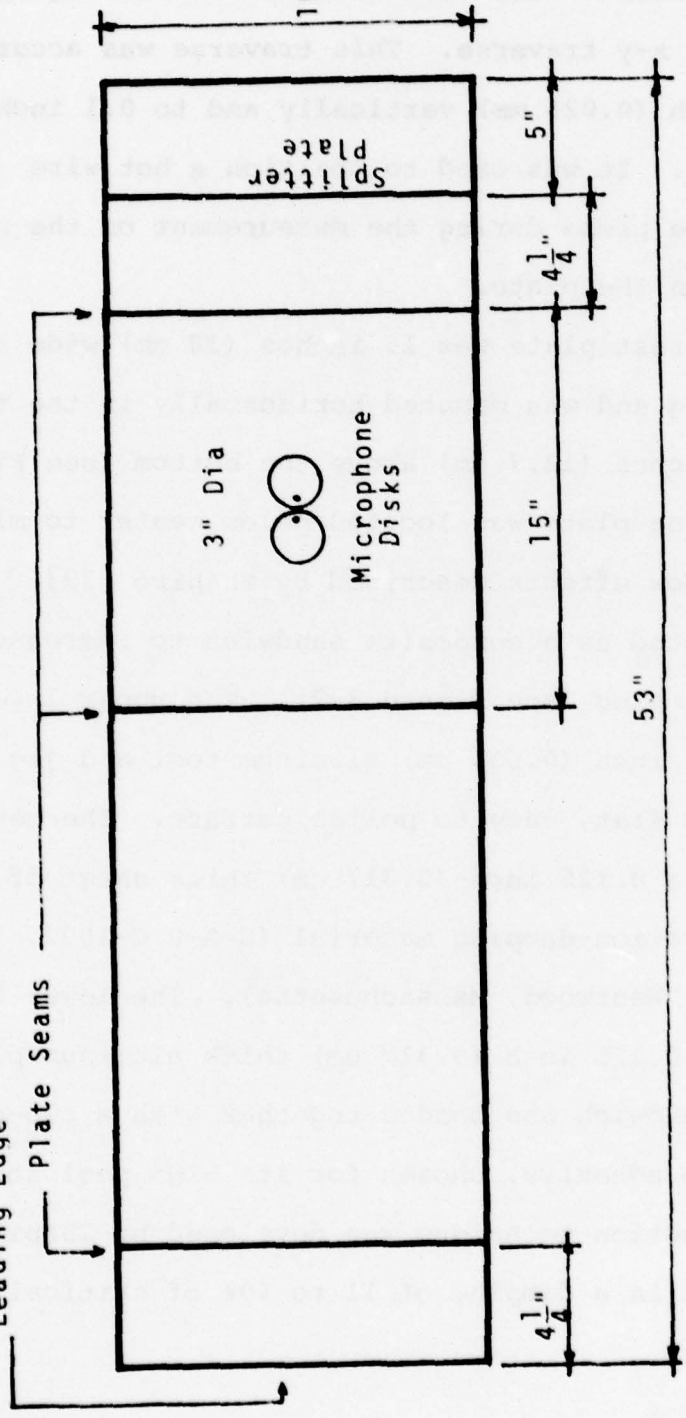

FIGURE 3.5 Layout of Test Plate

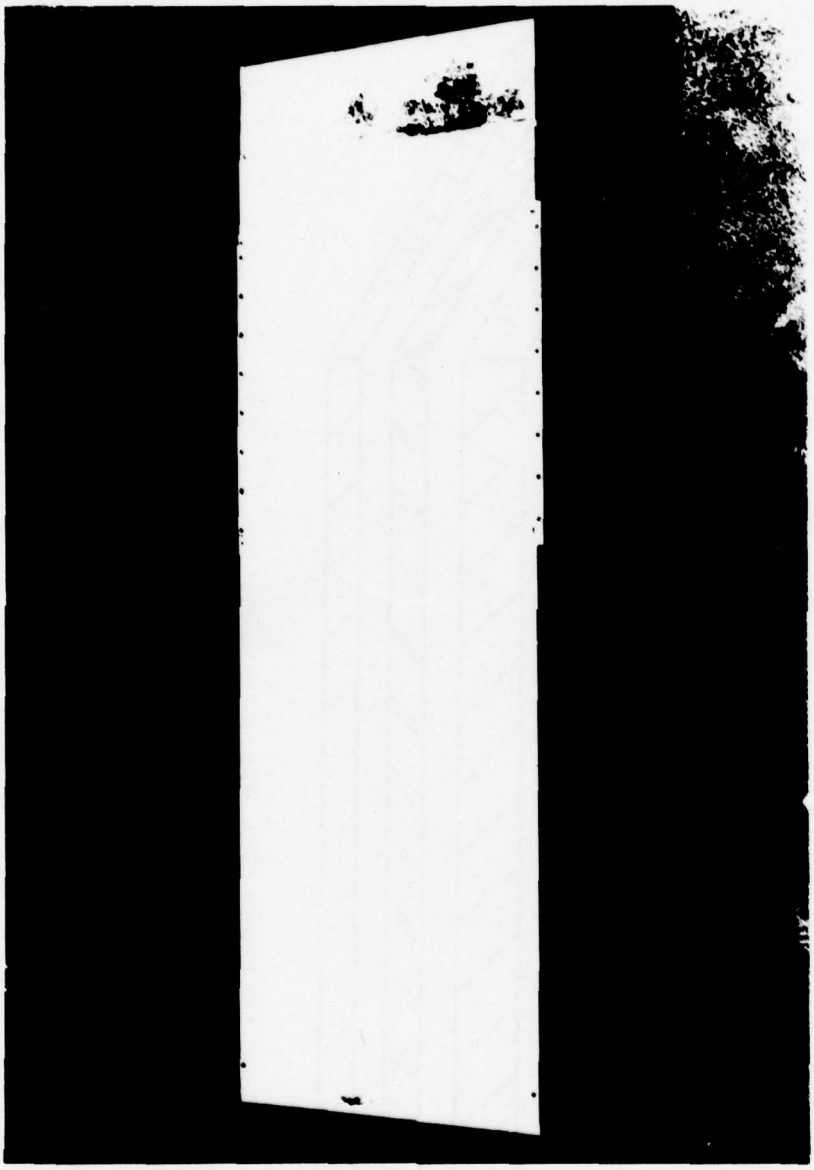

FIGURE 3.6 Test Plate

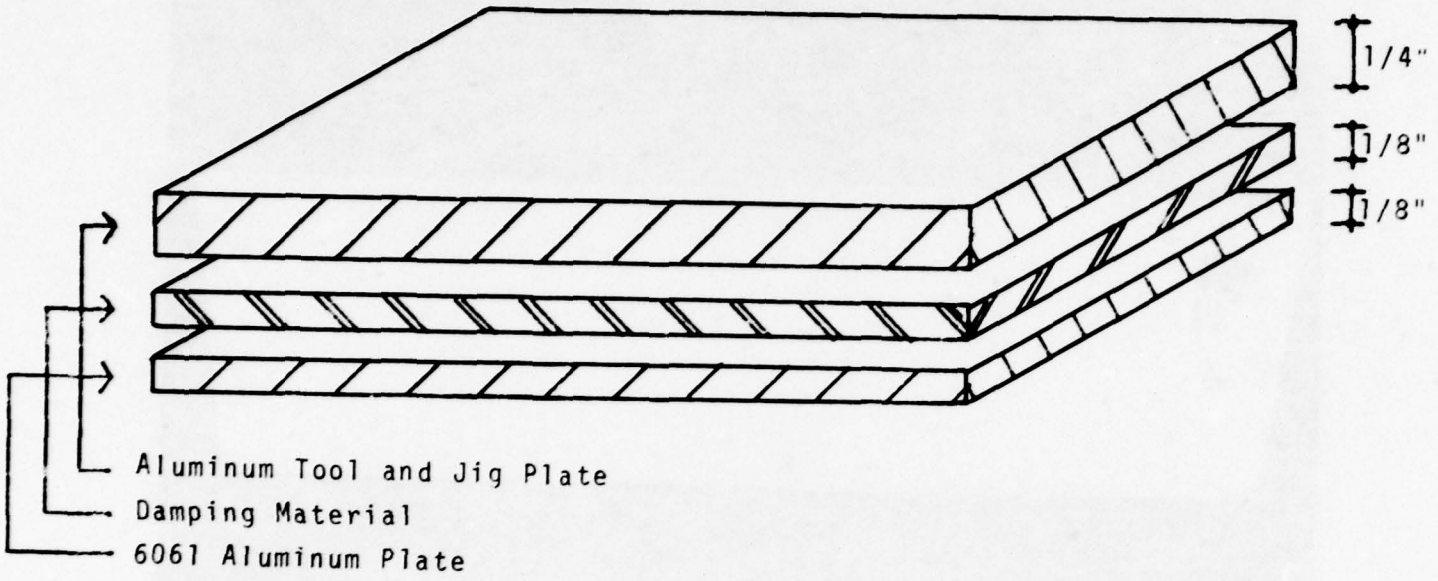

Figure 3.7 Construction of Test Plate

(depending on temperature and frequency). The leading edge of the plate was solid 0.50 inch (1.27 cm) thick tool and jig plate machined into a 6:1 ellipse (see Figure 3.8). This shape was chosen by Shapiro because of its practical shape and lack of a strong pressure gradient which could cause premature transition. The pressure transducers were flush mounted in two rotatable 3 inch (7.62 cm) diameter disks (similar to DeMetz and Casarella's [3]). Rotation of these disks allowed transducer separations of 0.275 to 5 inches (0.7 to 12.7 cm, see Figure 3.5). The trailing edge was made of a thin splitter plate, much like the one used by Shapiro, which extended rearward to prevent coherent vortex shedding from creating plate vibrations (see Figure 3.8).

The plate was assembled and the upper surface was polished to a surface roughness of about 5μ inches (0.127 microns) RMS. It was then mounted in the test section and adjusted to have a minimum pressure gradient. The variation in pressure obtained over the length of the plate at a free stream velocity of 35.8 m/s is shown in Figure 3.9. The maximum variation was about 1% of the total head (excluding the leading edge).

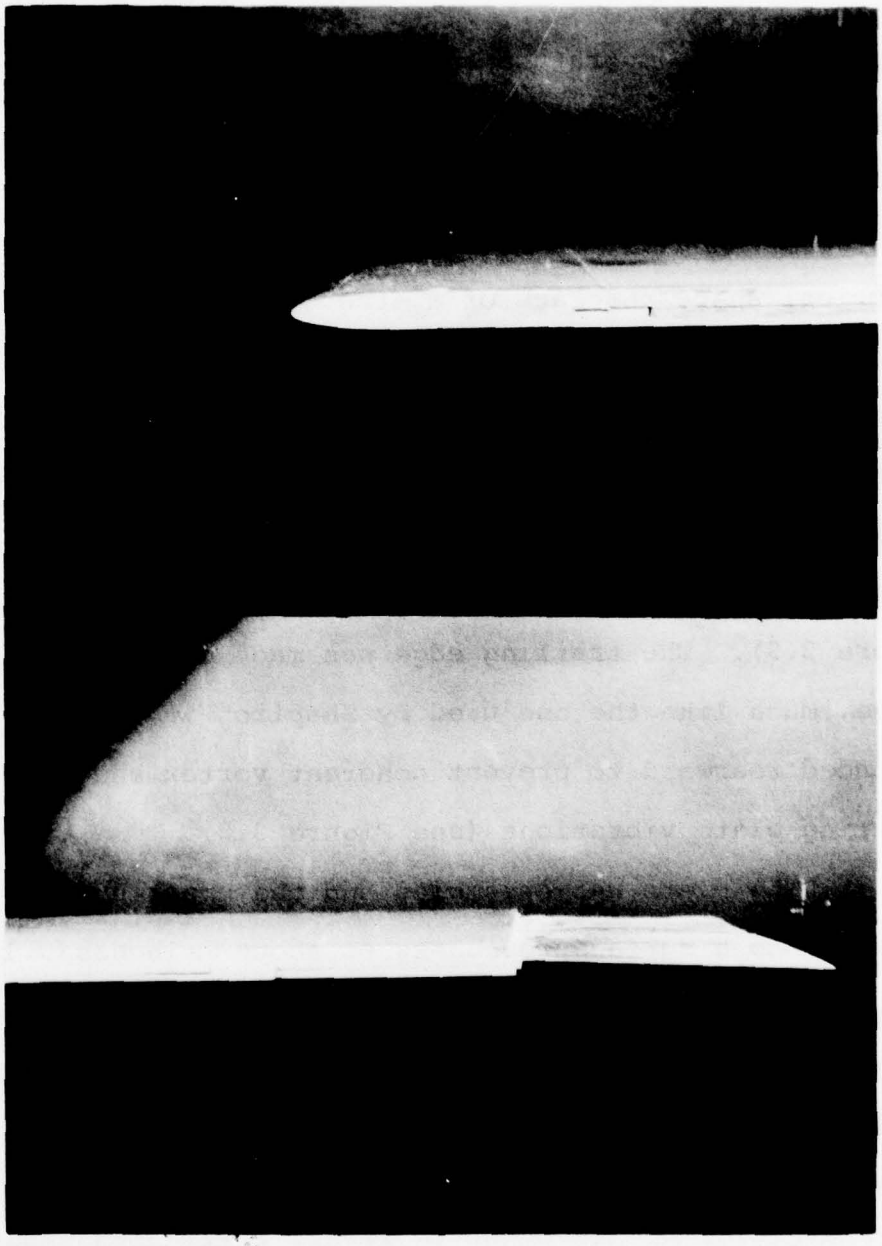

IGURE 3.8 Leading and Trailing Edges of Plate

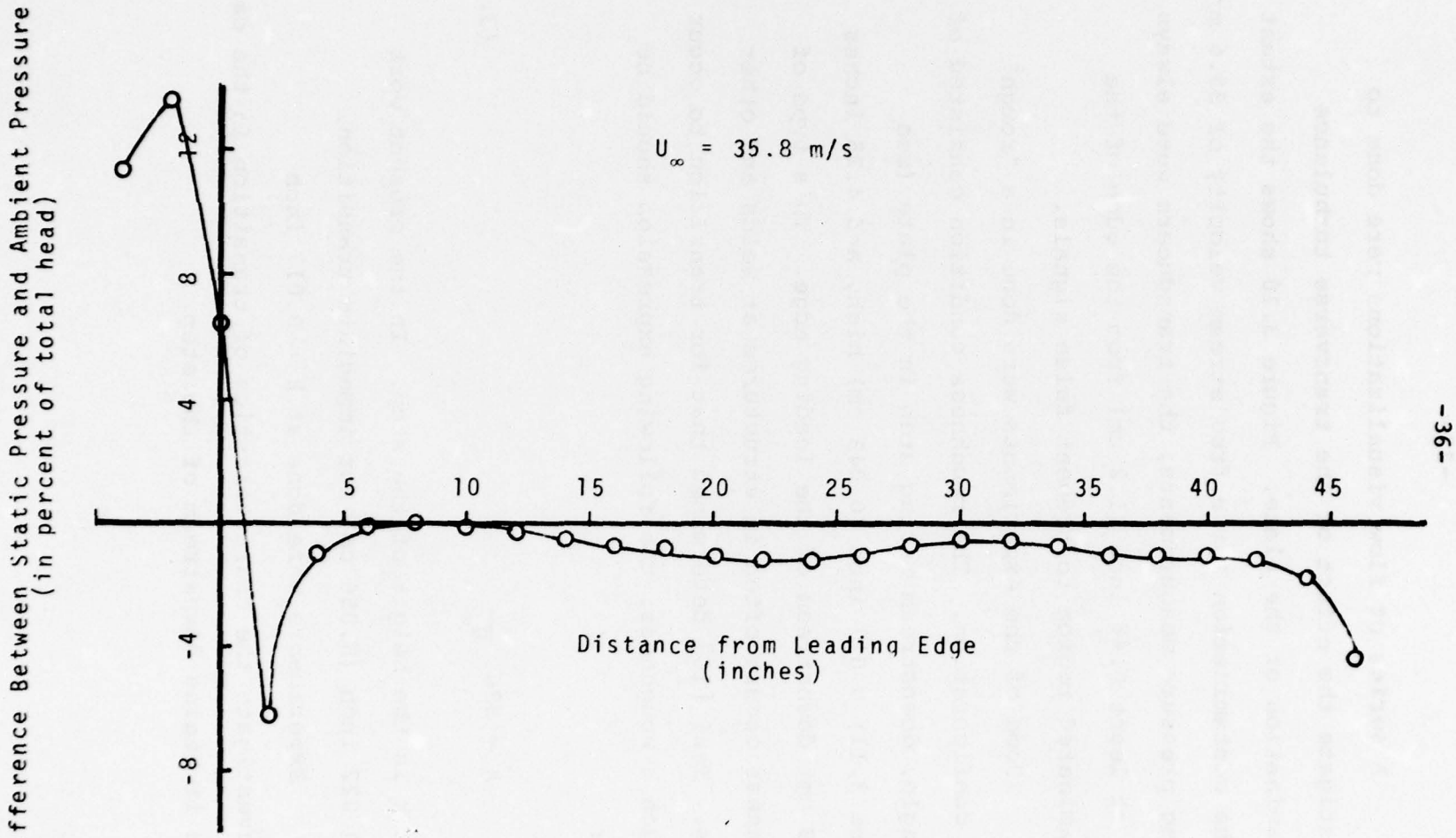

FIGURE 3.9 Pressure Gradient on Test Plate

A series of flow visualizations were done to investigate the effect of the transverse turbulence contamination of the plate. Figure 3.10 shows the extent of the contamination for a free stream velocity of 35.6 m/s. During pressure measurements, the transducers were always kept at least 0.48 inch (1.2 cm) from the edge of the contaminated region to prevent false signals.

Some of the experiments were done in a "rough" wall configuration. The roughness condition consisted of a single, downstream facing step in the plate (see Figure 3.11) 0.017 inch (0.043 cm) high, and 4.25 inches (10.8 cm) downstream of the leading edge. This type of roughness occurs often in structures at welds and other seams. Tani [16] determined that for transition to occur at such a roughness, the following expression should be true:

$$k \cong 826. \frac{\nu}{U_\infty} \qquad (3.1)$$

where k is the height of the step. In the present work $k \cong 0.022$ inch (0.056 cm) for immediate transition.

Experiments were done at k = 0.017 inch to investigate the characteristics of transition in the case where it begins downstream of the step.

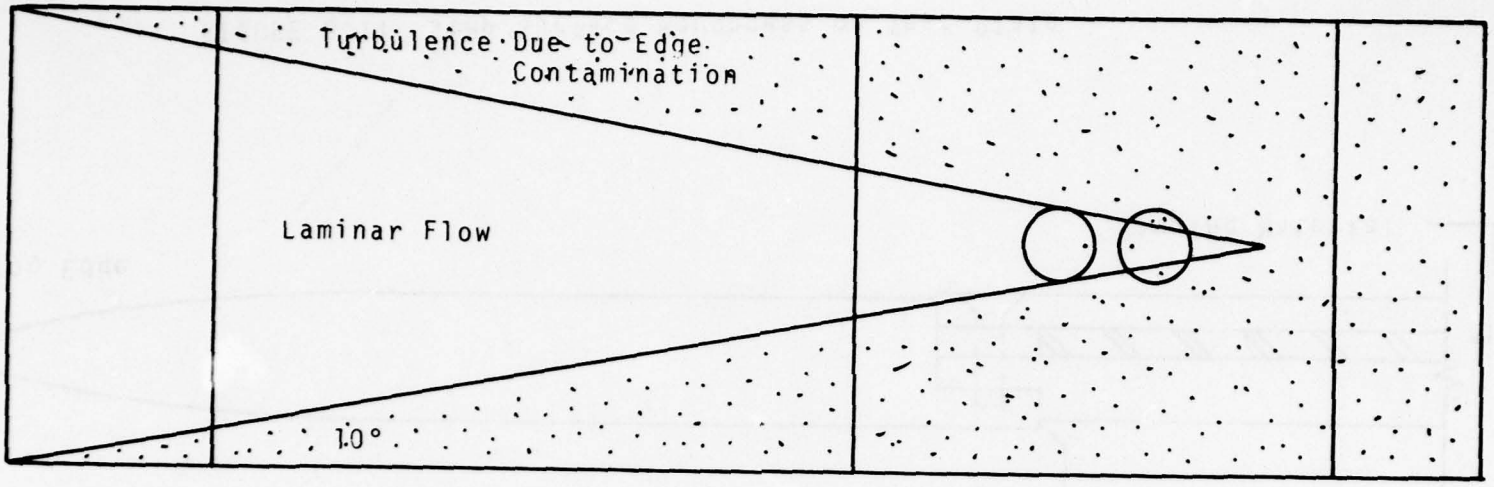

FIGURE 3.10 Extent of Edge Contamination

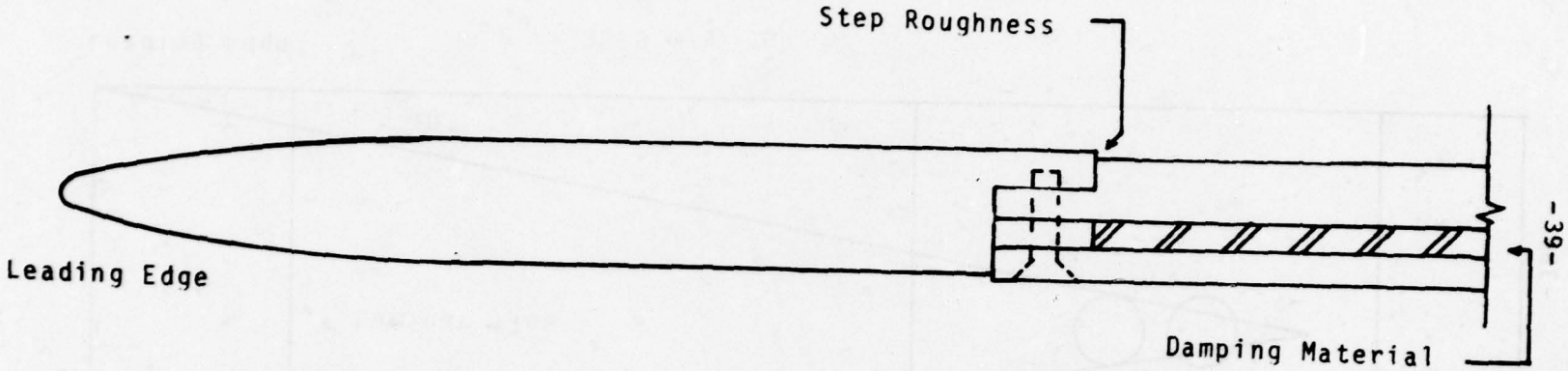

FIGURE 3.11 Step Surface Roughness on Test Plate

3.3 INSTRUMENTATION

The size of the transition region (including the starting point and the length) were measured using a hot wire anemometer probe (Thermo-Systems Inc. probe model 1261-T1,5) with a Disa model 55005 battery powered, constant temperature anemometer and a Disa model 555D15 linearizer. A schematic of this equipment is shown in Figure 3.12. Static pressure measurements were made with a static pressure tube and a Betz micromanometer. The resolution of this micromanometer was 0.1 mm H_2O. The free stream velocity was monitored by measuring the pressure drop across the wind tunnel contraction section with the micromanometer. This provided a resolution of about 0.1 m/s. A calibration was performed by Shapiro [19] to ensure an accuracy of about 0.1 m/s.

Wall pressure fluctuations were measured using two Bruel and Kjaer type 4138, 1/8 inch, phase matched condenser microphones fitted with 1/32 inch pinhole caps. The electronic circuitry is shown in Figure 3.13. Final statistical calculations were made digitally using an Interdata model M70 mini-computer in conjunction with a two channel eight-bit analog to digital converter. The digital calculations were made using the data acquisition

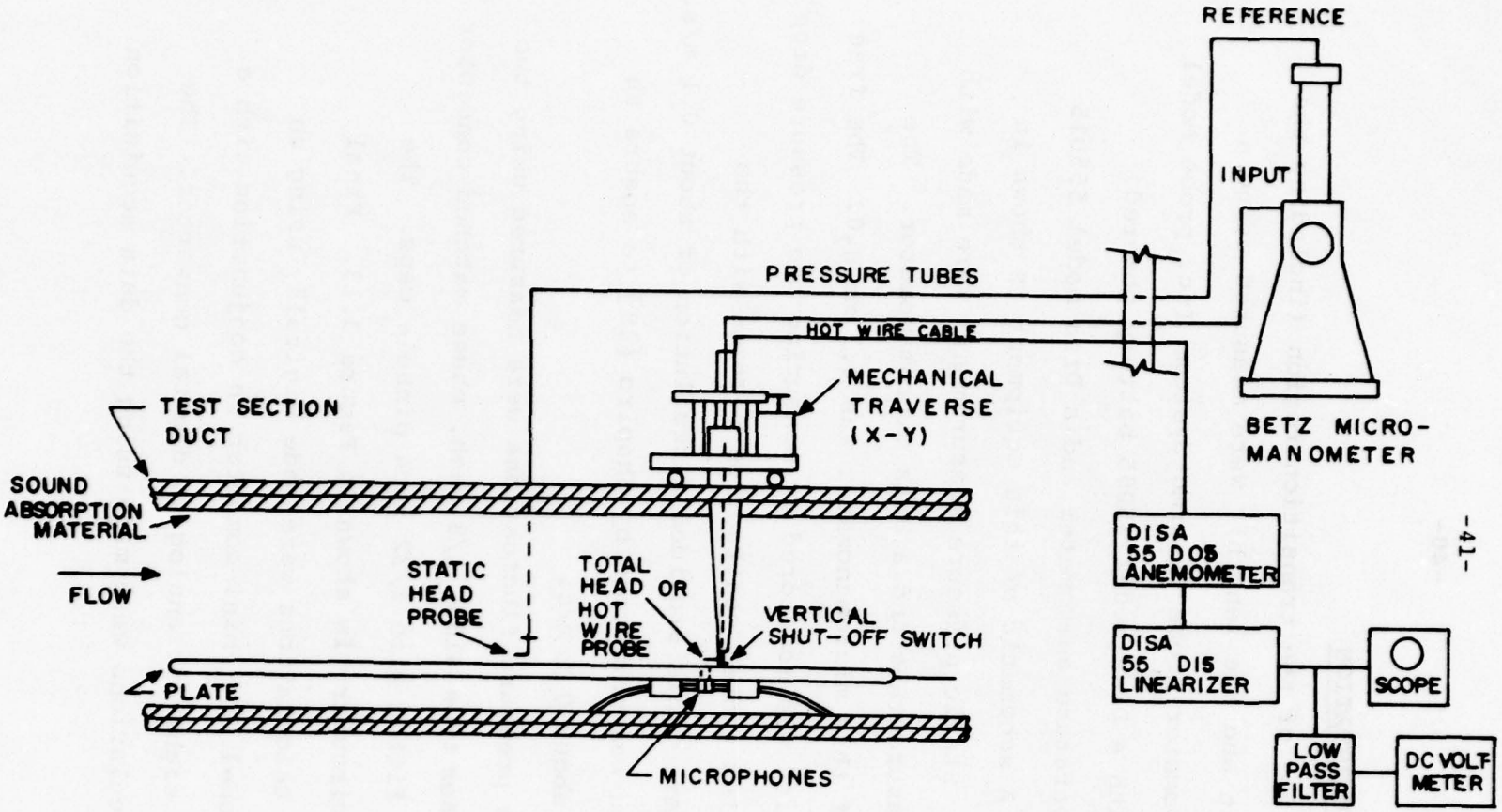

FIGURE 3.12 Mean Velocity Measuring Equipment

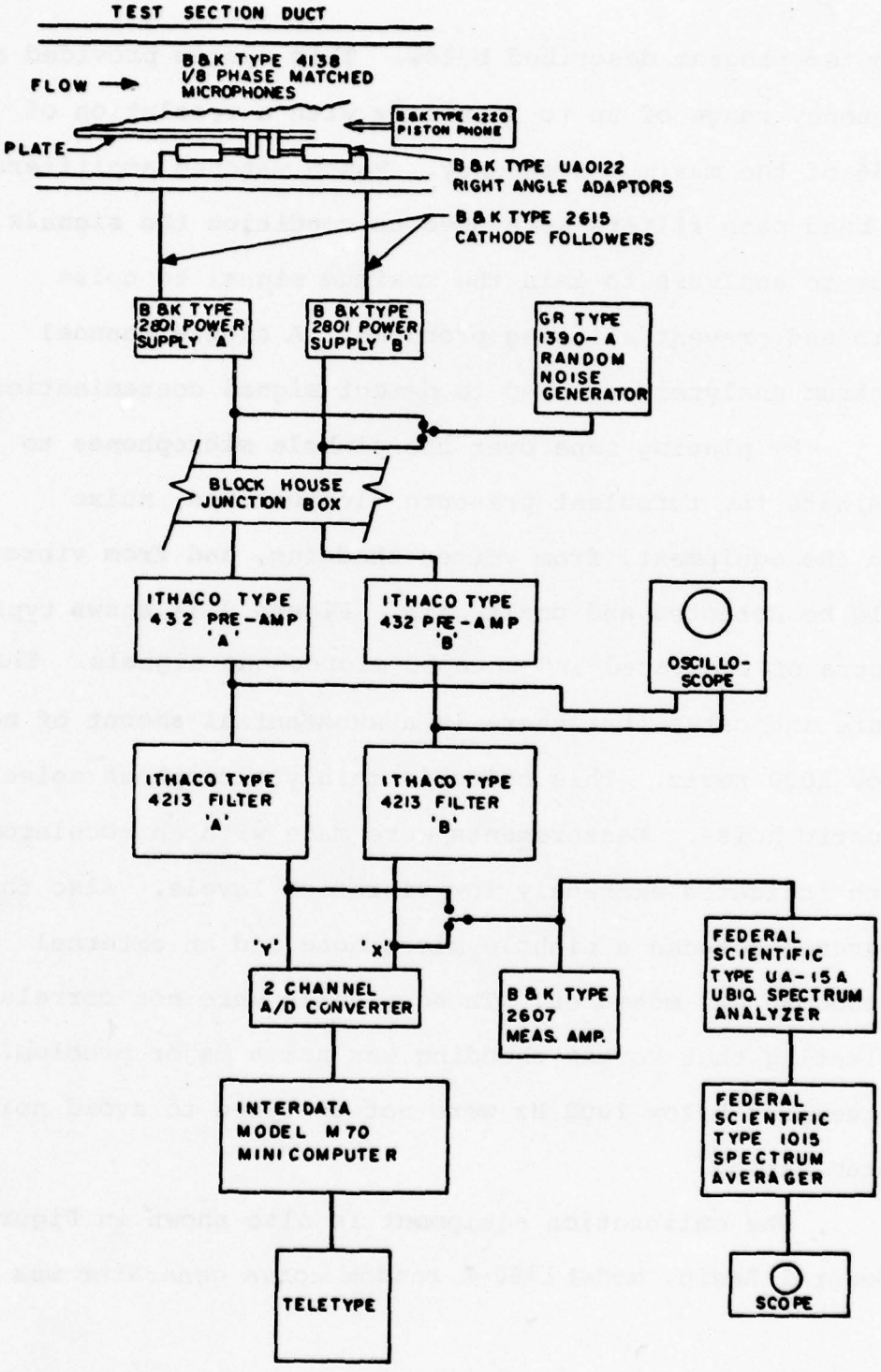

FIGURE 3.13 Schematic of Electronic Circuitry

computer program described below. This system provided a frequency range of up to 25,000 Hz with a resolution of 1/256 of the maximum frequency. Phase matched amplifiers and band pass filters were used to condition the signals prior to analysis to gain the maximum signal to noise ratio and prevent aliasing problems. A single channel spectrum analyzer was used to detect signal contamination.

By placing tape over the pinhole microphones to eliminate the turbulent pressure fluctuations, noise from the equipment, from vortex shedding, and from vibrations could be detected and dealt with. Figure 3.14 shows typical spectra of the taped and untaped microphone signals. This figure indicates that there is a substantial amount of noise below 1000 hertz. This noise is mainly microphone noise, and acoustic noise. Measurements were made with an accelerometer, which indicated extremely low vibration levels. Also the coherence between a pinhole microphone and an external microphone was measured. These signals were not correlated, indicating that vortex shedding was not a major problem. Frequencies below 1000 Hz were not analyzed to avoid noise contamination.

The calibration equipment is also shown in Figure 3.13. A General Radio, model 1390-A random noise generator was used to

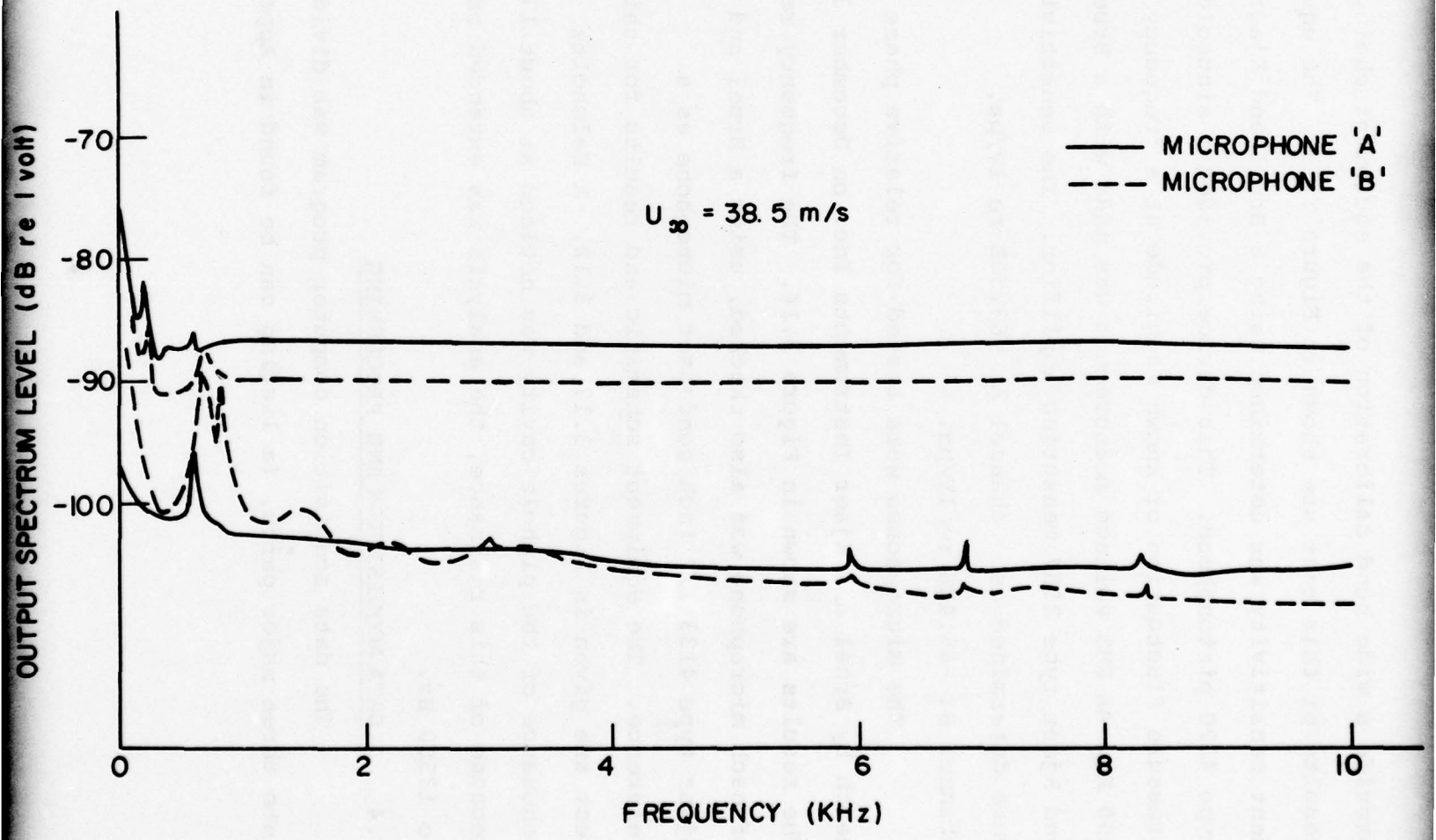

FIGURE 3.14 Turbulent Pressure Spectra and Noise Floors

provide a wide band calibration of the equipment chain. The results of this test are shown in Figure 3.15. The equipment sensitivity was determined using a Bruel and Kjaer type 4220 pistonphone. This device provided a sinusoidal pressure fluctuation of known magnitude at a frequency of 250 Hz. An RMS voltage measurement was made with a Bruel and Kjaer type 2607 measuring amplifier. The sensitivities were determined as channel A: -63.5dB re 1V/pa, channel B: -65.4dB re 1V/pa.

The microphones were tested for relative phase match by Bruel and Kjaer Instruments Inc. on December 30, 1974. The results are shown in Figure 3.16. The frequency response of each microphone was also checked, using a Bruel and Kjaer type 4133 1/2 inch condenser microphone as a reference. The equipment schematic and results for this test are given in Figures 3.17 and 3.18. A Helmholtz resonance of the pinhole cavity was noticed at about 17,000 Hz. Because of this resonance, the analysis was extended only up to 13500 Hz.

3.4 DATA ACQUISITION AND PROCESSING

The data acquisition computer program was divided into three major parts, (a listing can be found in Appendix A).

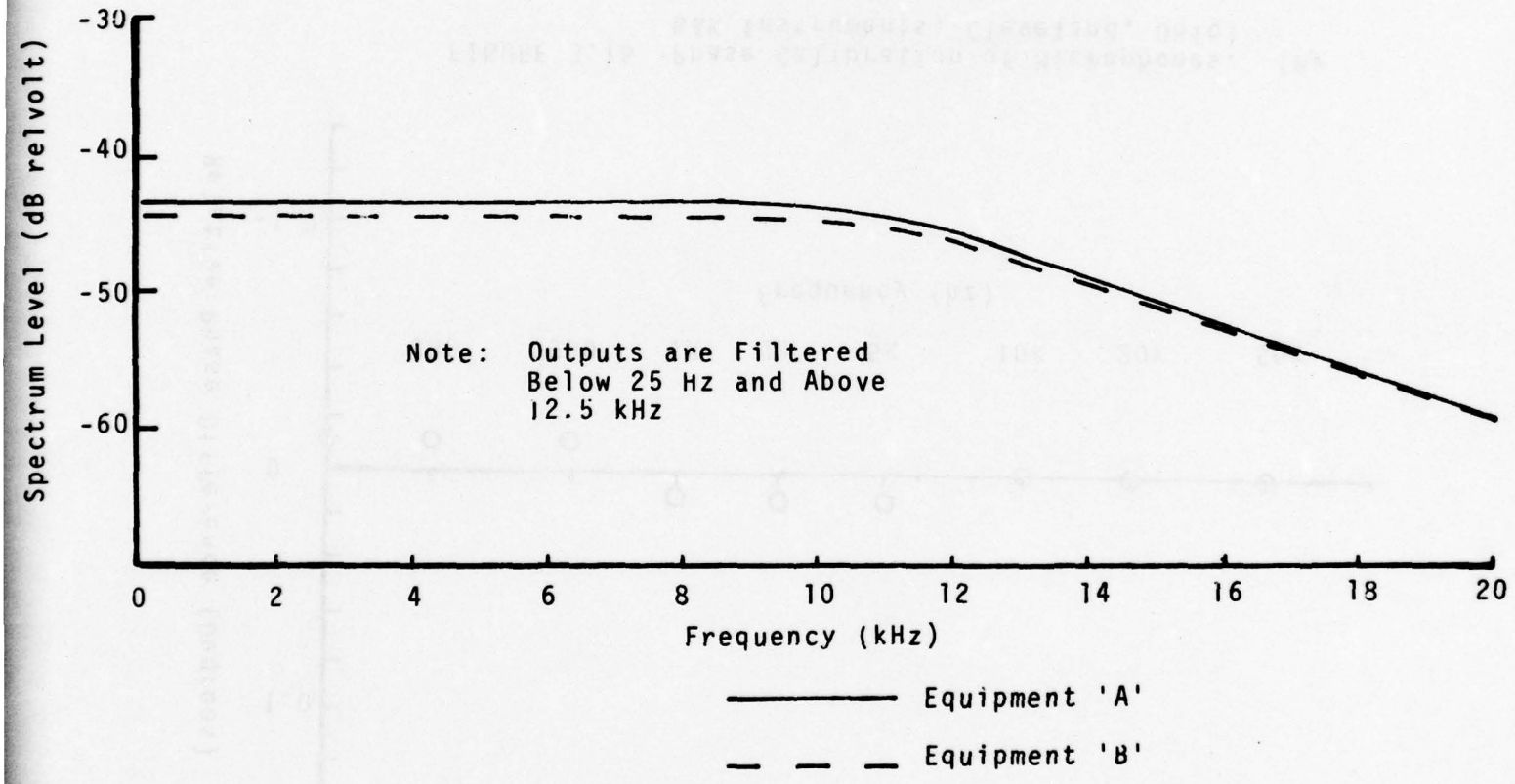

FIGURE 3.15 Results of Equipment Calibration

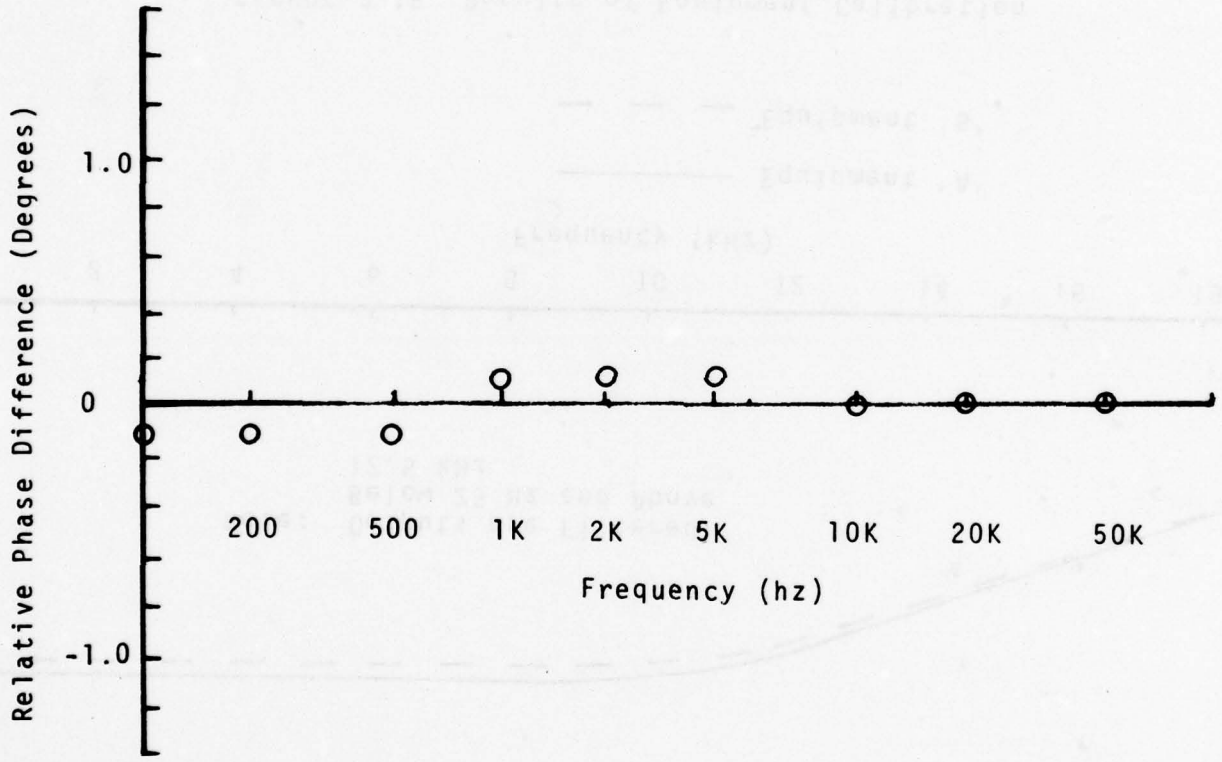

FIGURE 3.16 Phase Calibration of Microphones. (By B&K Instruments, Cleveland, Ohio)

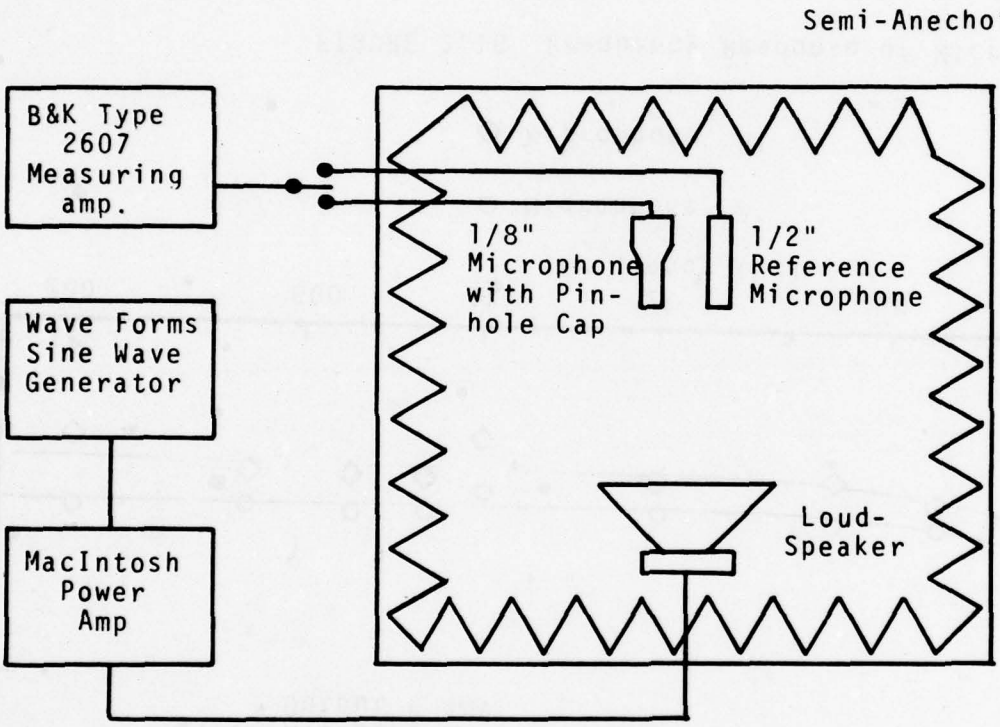

FIGURE 3.17 Microphone Calibration Set-up

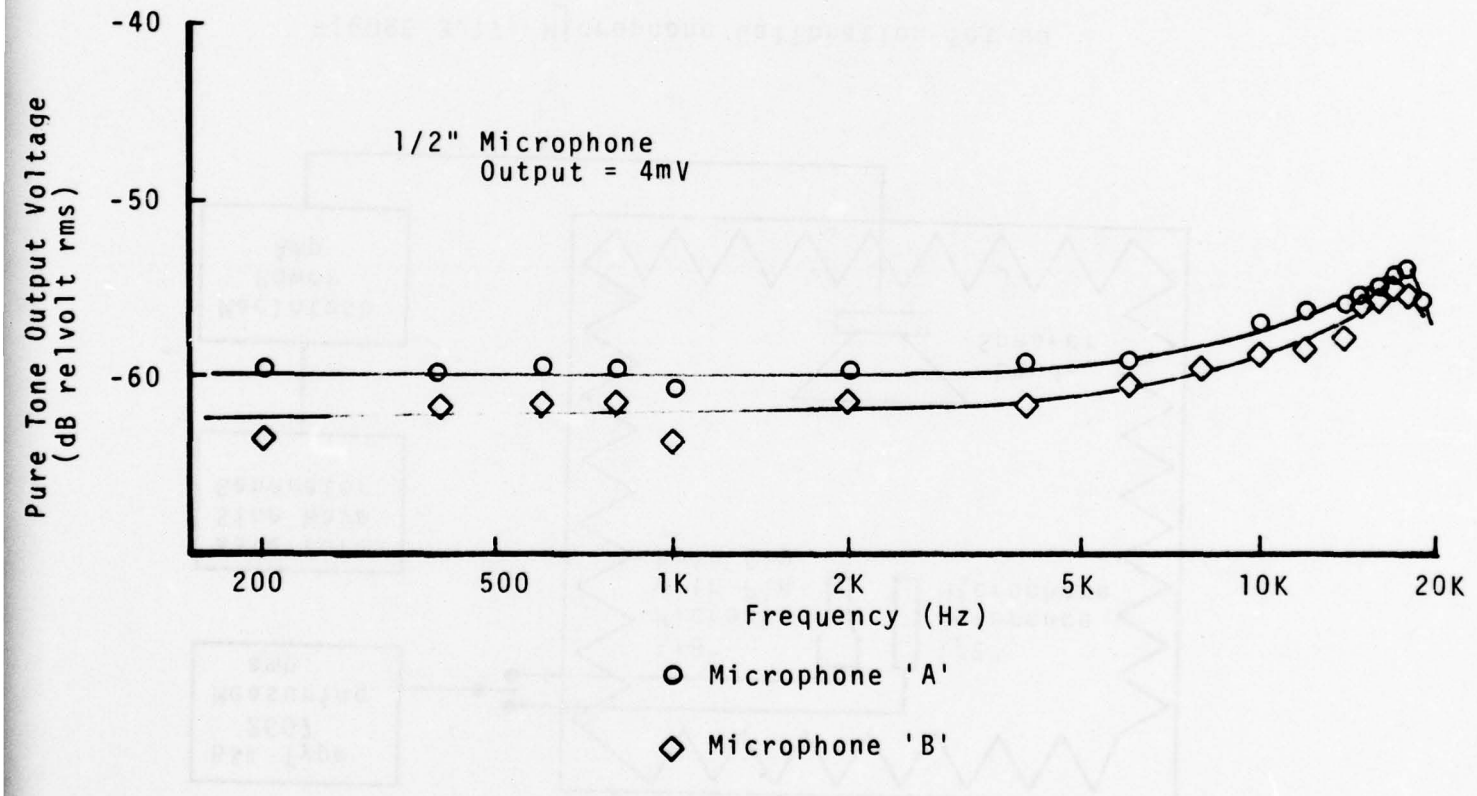

FIGURE 3.18 Frequency Response of Microphones

The first part was a data sampling and an analog to digital conversion. Then a conditioning was done on the data to determine its intermittent characteristics. The method used was similar to that of Hedley and Keffer [21]. Finally, a spectral analysis was done on the conditioned signal.

The conversion was done via two analog to digital (A/D) converters with the subroutine CONVRT (written by G. Holmes, see Appendix A). CONVRT read the A/D converters at a rate equal to twice the maximum frequency of interest to prevent aliasing. This data was stored in a data array for further processing.

A conditioning was then done on the entire data array. The signal was first squared and then differentiated (using a central difference scheme). This magnified the inherent differences between the laminar and turbulent portions of the signal. The signal was then averaged over successive small "smoothing intervals" to smooth out sharp fluctuations. Finally, the conditioned signal was compared to a predetermined "criterion level". The portions of time that the conditioned signal was greater than the criterion level were taken as turbulent spots. Since the characteristics of the turbulent spots were of interest, the laminar

portions of the signal were set equal to zero. This reduced the amount of non-turbulent signal present (i.e. Tollmien-Schlichting waves, noise, etc.). This entire conditioning process is shown schematically in Figure 3.19.

The conditioning process had two variables, smoothing interval and criterion level. These variables were adjusted so that small changes in them would not cause noticeable changes in the resulting conditioned signal. Hedley and Keffer [21] have shown that the burst rate is the statistic most sensitive to changes in the conditioning of the signal. Figures 3.20 and 3.21 show the effect of smoothing interval and criterion level on the burst rate. Figure 3.22 shows a typical raw signal with a "criterion function" superimposed on it. The criterion function was equal to one during turbulent spots and zero during the laminar portions of the signal. This figure provides a good check of the signal conditioning.

The final part of the data acquisition computer program was to perform the statistical calculations. First the intermittency function, burst rate and burst period were calculated for the data array. Then a spectral analysis similar to that of DeJong [22] was performed on the data array.

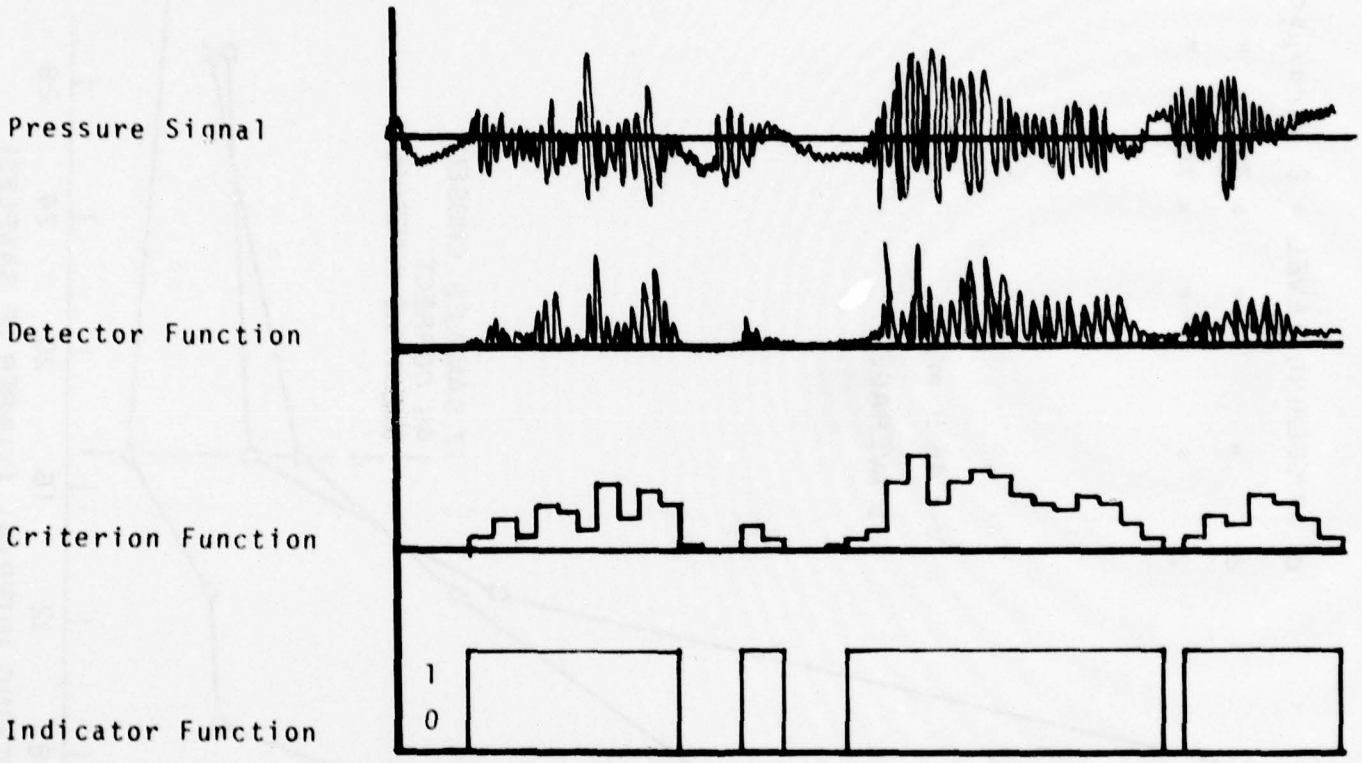

FIGURE 3.19 Signal Conditioning Process. After Hedley and Keffer [21]

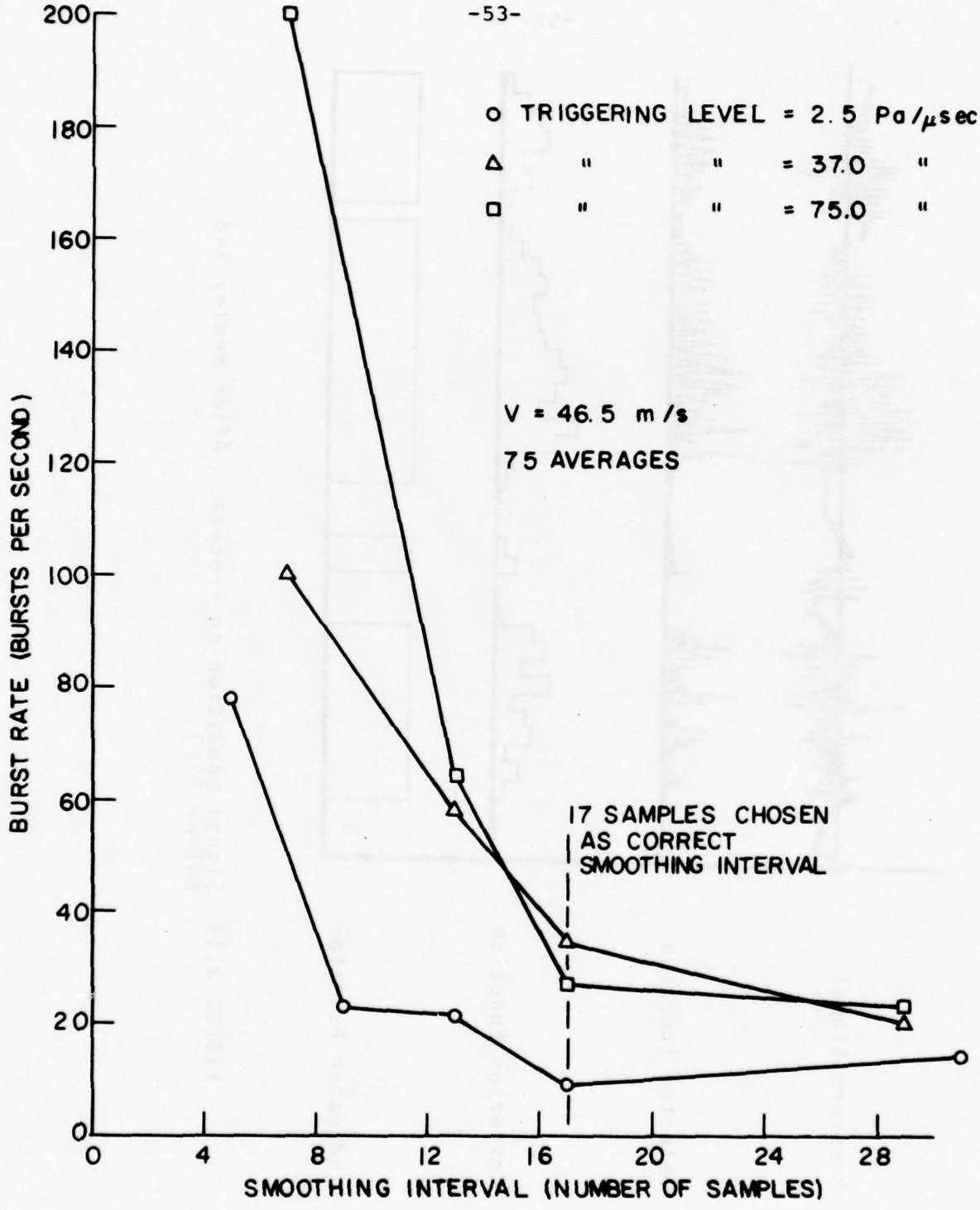

FIGURE 3.20 Burst Rate Versus Smoothing Interval

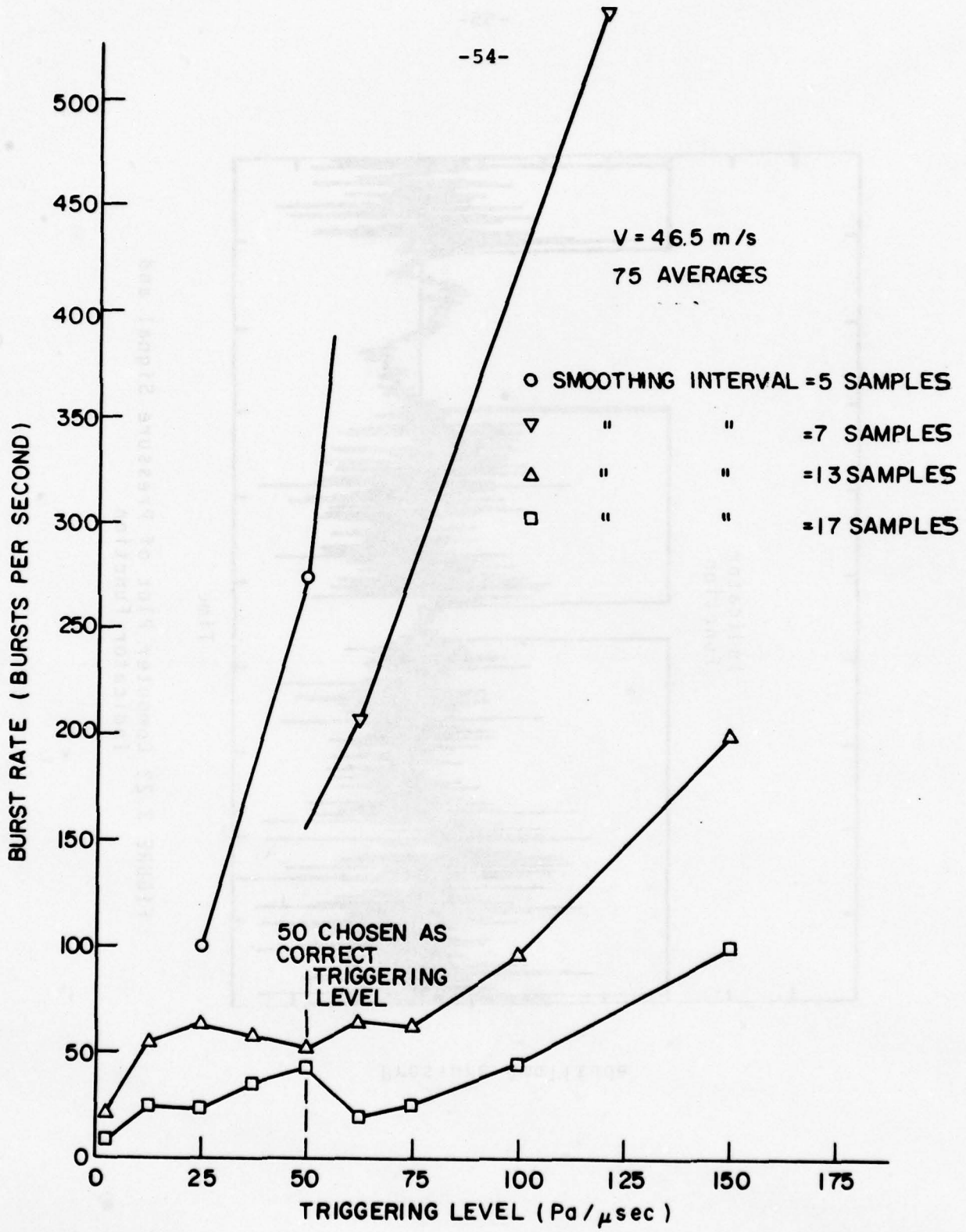

FIGURE 3.21 Burst Rate Versus Triggering Level (Criterion Level)

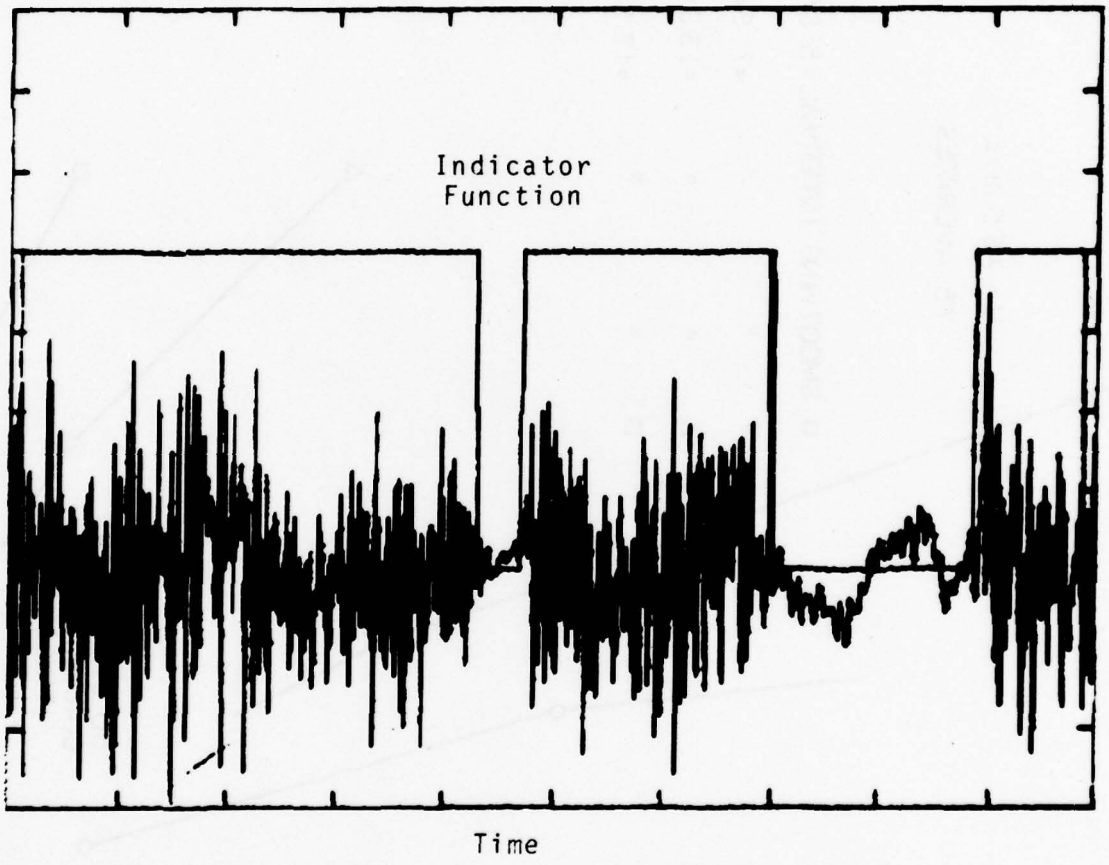

FIGURE 3.22 Computer Plot of Pressure Signal and Indicator Function

The spectral analysis involved calculating spectral estimates from the random pressure signals. The theory of random signal processing is well developed (see Bendat and Piersol [23] or Oppenheim and Schafer [24]). The wall pressure spectral density was defined in Chapter 2 by:

$$\Phi_p(\omega) = \frac{1}{2\pi} \int_{-\infty}^{\infty} R_p(\tau) e^{-i\omega\tau} d\tau, \tag{2.3}$$

where $R_p(\tau)$ was defined as:

$$R_p(\tau) = E[p(t)p(t + \tau)], \tag{2.2}$$

and $p(t)$ must be stationary. If $p(t)$ is also ergodic, (2.2) may be replaced by:

$$R_p(\tau) = \lim_{T\to\infty} \frac{1}{T} \int_{-T/2}^{T/2} p(t)p(t + \tau)dt$$

$$= \langle p(t)p(t + \tau) \rangle \tag{3.2}$$

($\langle\ \rangle$ denotes a temporal average). The assumption of stationarity is good if the statistics of the pressure signals do not change over relatively long periods of time. Although it cannot be rigorously proven, the signals were assumed to be ergodic. This allowed the temporal average to be used, which provided an easier calculation method. The Fourier transform is used extensively in the analysis of random signals. A useful approximation is the finite Fourier transform:

$$P(f,T) = \int_0^T p(t) e^{-i2\pi ft}\, dt. \tag{3.3}$$

P is a function of the integration interval, T and the frequency, f ($f = \omega/2\pi$). p(t) must be stationary. If the assumption of ergodicity is correct, the finite Fourier transform and the temporal average may be used to calculate the spectral density instead of equation (2.4).

$$\Phi_p(f) = \lim_{T\to\infty} \frac{2}{T} \langle |P(f,T)|^2 \rangle \tag{3.4}$$

Notice that since the experimental frequency, f, is being used,

$$\Phi_p(\omega) = \frac{1}{4\pi} \Phi_p(f) \tag{3.5}$$

The finite Fourier transform may be approximated by the sum:

$$\tilde{P}(f,T) = h \sum_{n=o}^{N-1} p(nh) e^{-i2\pi fnh}, \tag{3.6}$$

if the function p(t) is sampled N times with a time interval h. Here T is equal to Nh. An efficient method of computing this sum, is the fast Fourier transform, or FFT, developed by Cooley and Tukey [25]. The FFT requires only $2N \log_2 N$ multiplications, instead of N^2, and provides the value of $\tilde{P}(f,T)$ at frequencies of $f_j = j/T$. The FFT requires N to be an integral power of 2 and the result may be written as:

$$\tilde{P}_j = \frac{1}{h}\tilde{P}(f_j,T),\ j=0,1,\ldots\frac{N}{2}-1. \tag{3.7}$$

An estimate of $\Phi_p(f)$ may now be written as:

$$\tilde{\Phi}_p(f_j) = \frac{2h}{N}|\tilde{P}_j|^2, \quad j = 0,1,\ldots\frac{N}{2}-1. \tag{3.8}$$

Due to the randomness of the function p(t), the standard error of the estimate, $\tilde{\Phi}_p(f_j)$ is 1. If $\tilde{\Phi}_p(f_j)$ is calculated for a large number of data sets, the standard error may be reduced to $\sqrt{1/M}$ (where M is the number of data sets) by taking the average, $\bar{\Phi}_p(f_j)$, of all the $\tilde{\Phi}_p(f_j)$'s. We now have:

$$\bar{\Phi}_p(f_j) = \frac{1}{M}\sum_{k=1}^{M}\tilde{\Phi}_{p,k}(f_j)$$

or

$$\bar{\Phi}_p(f_j) = \frac{1}{M}\sum_{k=1}^{M}\frac{2h}{N}|\tilde{P}_j|^2, \quad j = 0,1,\ldots\frac{N}{2}-1. \tag{3.9}$$

If two random pressure signals, p(t) and q(t), are sampled simultaneously, a joint spectral analysis may be done using the theory of complex numbers. If a complex number is defined as:

$$z(t) = p(t) + i\,q(t), \tag{3.10}$$

Then a complex Fourier transform may be approximated by:

$$\tilde{Z}_j = \sum_{n=o}^{N-1}[p(nh) + i\,q(nh)]e^{i\frac{2\pi jn}{N}},$$

$$j = 0,1,\ldots\frac{N}{2}-1 \tag{3.11}$$

This relation now provides:

$$\tilde{P}_j = \frac{1}{2} (\tilde{Z}_j + \tilde{Z}^*_{N-j})$$

and

$$\tilde{Q}_j = \frac{1}{2i} (\tilde{Z}_j - \tilde{Z}^*_{N-j}) \qquad (3.12)$$

where * denotes complex conjugate. $\tilde{\Phi}_p(f_i)$ and $\tilde{\Phi}_q(f_i)$ may now be obtained from these relations and equation (3.8). The cross-spectral density is defined as:

$$\phi_p(\bar{r},f) = \lim_{T\to\infty} E[P(f,T)Q^*(f,T)]. \qquad (3.13)$$

$\bar{r}$ is the vector between pressures p(t) and q(t).

$\phi_p(\bar{r},f)$ may be approximated by:

$$\tilde{\phi}_p(\bar{r},f_j) = \frac{2}{Nh} \tilde{P}_j \tilde{Q}_j^*. \qquad (3.14)$$

The standard error of $\tilde{\phi}_p(\bar{r},f_j)$ can be reduced by averaging, as with $\tilde{\Phi}_p$.

The data acquisition computer program performed these complex FFT calculations, obtaining the pressure spectral densities and the cross-spectral density. All of the spectra were multiplied by $1/\gamma$ to correct for the intermittency. During the data acquisition M was set at

250 so that the standard error was 6.3%.

Another computer program was used to non-dimensionalize and plot the spectral data and to calculate the convection velocity. Both of these programs may be found in Appendix A.

4. DISCUSSION OF RESULTS

4.1 MEAN VELOCITY MEASUREMENTS

The characteristics of the mean velocity profiles in the intermittent region are listed in Table 4.1 for various flow speeds. In the intermittent region the boundary layer had two distinct behaviors - laminar and turbulent. Dhawan and Narasimha [11] have shown that mean velocity measurements in this region result from time average over a laminar profile and over a turbulent profile. They have also shown that a very good approximation of the flow characteristics are obtained by averaging a Blasius boundary layer with a 1/7 power law turbulent boundary layer. However, a virtual origin at the transition point must be used for the turbulent boundary layer. Figure 4.1 shows a typical mean velocity profile that we measured in the intermittent region. A law of the wall profile and a Blasius profile are also shown for comparison.

The measured displacement thickness, δ_m^*, can be expressed by:

$$\delta_m^* = \gamma \delta_T^* + (1 - \gamma) \delta_L^* \ , \qquad (4.1)$$

where δ_L^* is the displacement thickness of the Blasius boundary layer and δ_T^* is that for the turbulent layer. A similar expression can be written for the coefficient of skin friction, C_{fm}:

$$C_{fm} = \gamma C_{fL} + (1-\gamma) C_{fT} . \qquad (4.2)$$

Since it is the behavior of the flow in the turbulent spots

TABLE 4.1

Velocity (m/s)	$x\|_{\gamma=0.01}$ (m)	$x\|_{\gamma=0.99}$ (m)	$\delta^*_T \times 10^3$ (x=0.91m) Eq. 4.7 (m)	$C_{fT} \times 10^3$ (x=0.91m) Eq. 4.3
		Smooth Condition		
36.0	0.41	1.09	1.22	3.65
37.6	0.36	1.02	1.32	3.56
38.3	0.33	0.94	1.37	3.51
39.0	0.30	0.89	1.43	3.47
39.5	0.28	0.81	1.47	3.44
40.0	0.25	0.76	1.53	3.41
40.5	0.23	0.71	1.56	3.38
44.5	0.20	0.66	1.60	3.30
45.0	0.18	0.63	1.64	3.28
45.5	0.17	0.62	1.65	3.27
		Rough Condition		
22.0	0.64	1.07	0.77	4.49
22.5	0.61	1.02	0.84	4.38
23.0	0.57	0.99	0.94	4.26
24.0	0.39	0.94	1.34	3.90
25.0	0.29	0.79	1.55	3.75
25.5	0.25	0.71	1.63	3.69
26.0	0.23	0.64	1.66	3.66
26.5	0.20	0.53	1.72	3.62
29.0	0.17	0.33	1.76	3.53
29.5	0.15	0.30	1.80	3.51

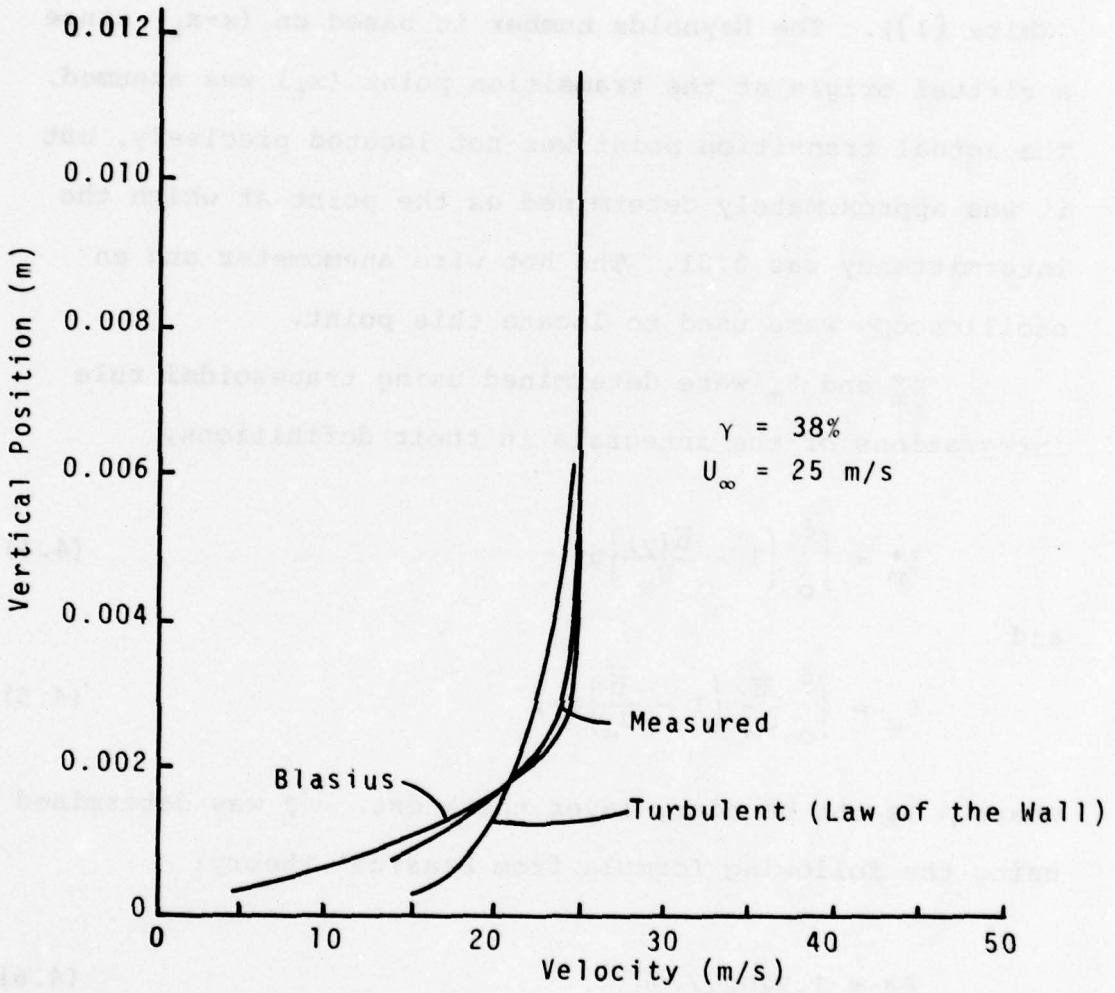

FIGURE 4.1 Velocity Profiles in Intermittent Region

that is of interest, δ_T^* and C_{fT} are the desired parameters. Measurements of skin friction were not made, but C_{fT} was determined from the approximate formula:

$$C_{fT} \cong 0.455/\ell n^2(0.06\ Re(x-x_t)), \tag{4.3}$$

(White [1]). The Reynolds number is based on $(x-x_t)$ since a virtual origin at the transition point (x_t) was assumed. The actual transition point was not located precisely, but it was approximately determined as the point at which the intermittency was 0.01. The hot wire anemometer and an oscilloscope were used to locate this point.

δ_m^* and θ_m were determined using trapezoidal rule integrations of the integrals in their definitions,

$$\delta_m^* = \int_o^\delta \left(1 - \frac{\bar{u}(y)}{U_\infty}\right) dy \tag{4.4}$$

and

$$\theta_m = \int_o^\delta \frac{\bar{u}}{U_\infty}\left(1 - \frac{\bar{u}}{U_\infty}\right) dy, \tag{4.5}$$

where δ is the boundary layer thickness. δ_L^* was determined using the following formula from Blasius' theory:

$$\delta_L^* = 1.7208x/\sqrt{Re_x}\ . \tag{4.6}$$

δ_T^* was then calculated using equation 4.1. For this calculation, γ was measured using the data acquisition computer program with the hot wire probe again placed a distance of about $4\delta_T^*$ above the plate. δ_T^* was also calculated using the approximation:

$$Re_{\delta_T^*} \cong 0.018\ Re_{(x-x_t)}^{6/7}\ , \qquad (4.7)$$

(White [1]). The measured values of δ_T^* are plotted in Figure 4.2 against those calculated from equation 4.7.

4.2 MEAN PRESSURE MEASUREMENTS

Table 4.2 gives a summary of the mean and intermittent characteristics of the wall pressure field. The extent of transition on the test plate is shown in Figure 4.3. The variation of intermittency with Reynolds number (based on x, the distance from the leading edge of the plate) is shown for both the smooth and rough conditions. Recall that in the rough condition, the test plate had a 0.015 inch (0.381 mm) high two dimensional reverse step located 4.25 inches (10.8 cm) behind the leading edge.

In both cases, the variation of intermittency is in the form of a Gaussian integral curve. Similar results have been found experimentally by Schubauer and Klebanoff [4] and DeMetz and Casarella [3] and analytically by Emmons [9]. The effect of the roughness was to reduce the transition Reynolds number from about 2×10^6 to 1.2×10^6.

The non-dimensional burst frequency (f_B^*) is plotted against intermittency in Figures 4.4 and 4.5. Theoretical results and the experimental result of Farabee, et al [10] are also shown. The theoretical results were obtained by

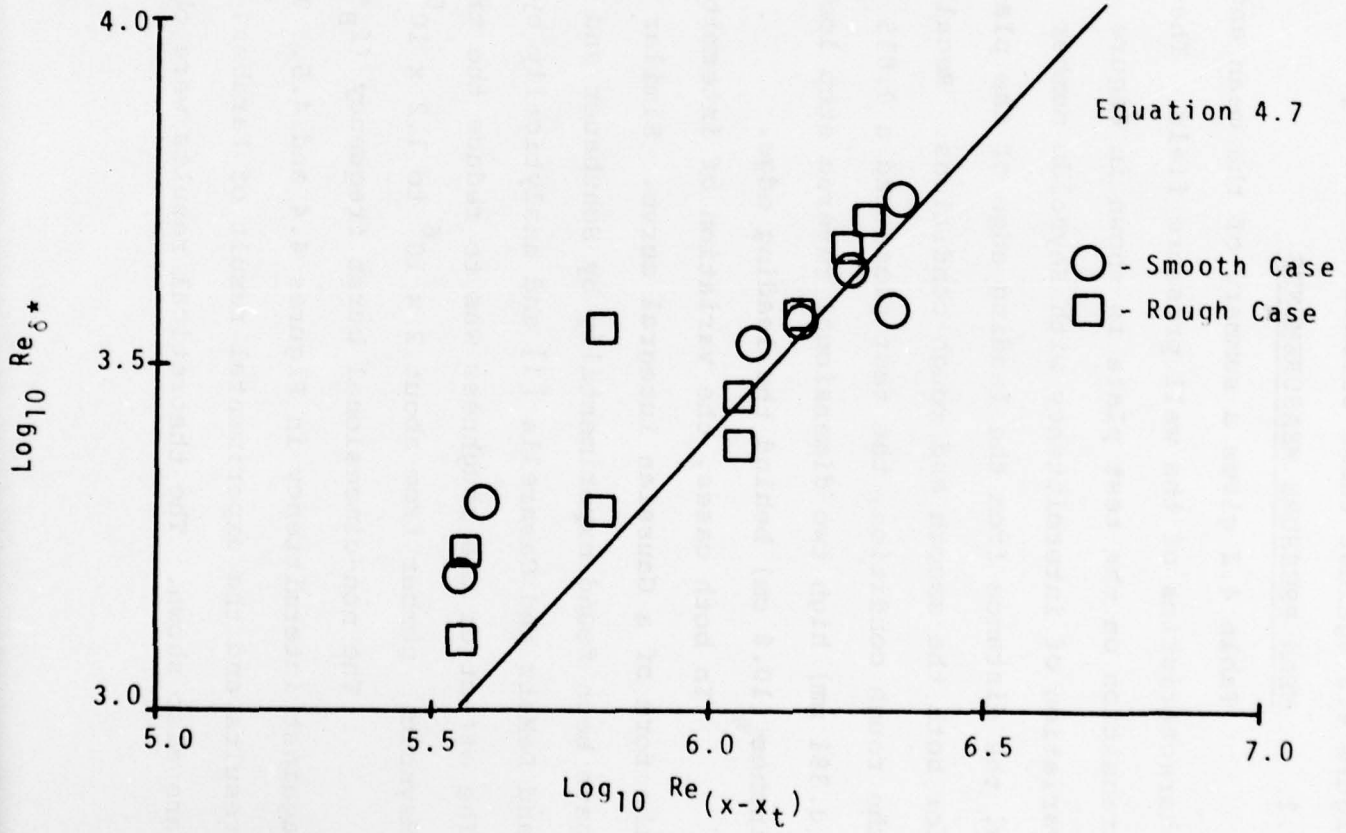

FIGURE 4.2 Boundary Layer Displacement Thickness in Intermittent Region

TABLE 4.2

Run No.	Velocity (m/s)	x (m)	γ	f_B ($\frac{\text{Bursts}}{\text{sec}}$)	τ_B (msec)
			Smooth Condition		
3606	36.0	0.91	0.062	73.2	0.85
3824	38.3	0.91	0.245	60.8	4.03
3825	37.6	0.91	0.254	214.0	1.19
3940	39.0	0.91	0.399	73.7	5.42
3864	38.3	0.91	0.644	69.9	9.22
4069	39.5	0.91	0.688	66.3	10.4
4089	39.5	0.91	0.894	32.2	27.8
4076	40.5	0.91	0.765	64.4	11.9
4499	44.5	0.91	1.000	0.316	3160
4599A	45.0	0.91	0.997	1.50	665
3818	37.6	0.91	0.184	48.7	3.78
3922	39.0	0.90	0.218	52.3	4.16
3840	38.3	0.91	0.397	71.1	5.58
4041	39.5	0.90	0.406	70.8	5.74
3954	39.0	0.91	0.539	77.4	6.96
4046	40.0	0.90	0.464	71.9	6.46
4078	40.0	0.91	0.775	59.2	13.1
4065	40.5	0.90	0.652	76.7	8.50
4599B	45.0	0.91	0.998	1.18	843
4699	45.5	0.90	0.996	2.53	394
			Rough Condition		
2219	22.0	0.91	0.188	43.7	4.31
2322	23.0	0.91	0.219	46.7	4.70
2326	23.0	0.91	0.260	56.0	4.65
2435	24.0	0.91	0.354	70.8	4.94
2440	24.0	0.91	0.401	76.7	5.23
2441	24.5	0.91	0.405	86.1	4.71
2570	25.0	0.91	0.701	81.4	8.62
2670	25.5	0.91	0.698	72.1	9.67
2999A	29.0	0.91	0.996	5.13	197
3099	29.5	0.91	0.993	7.90	126
2225	22.5	0.91	0.247	55.4	4.46
2325	23.0	0.90	0.251	51.5	4.88
2448	24.0	0.91	0.475	80.4	5.91
2639	25.5	0.90	0.389	76.7	5.07
2562	25.0	0.91	0.624	84.9	7.35
2652	26.0	0.90	0.525	82.8	6.34
2685	26.0	0.91	0.847	53.7	15.8
2674	25.5	0.90	0.734	70.9	10.4
2999B	29.0	0.91	0.989	9.24	10.7
2690	26.5	0.90	0.905	38.9	23.3

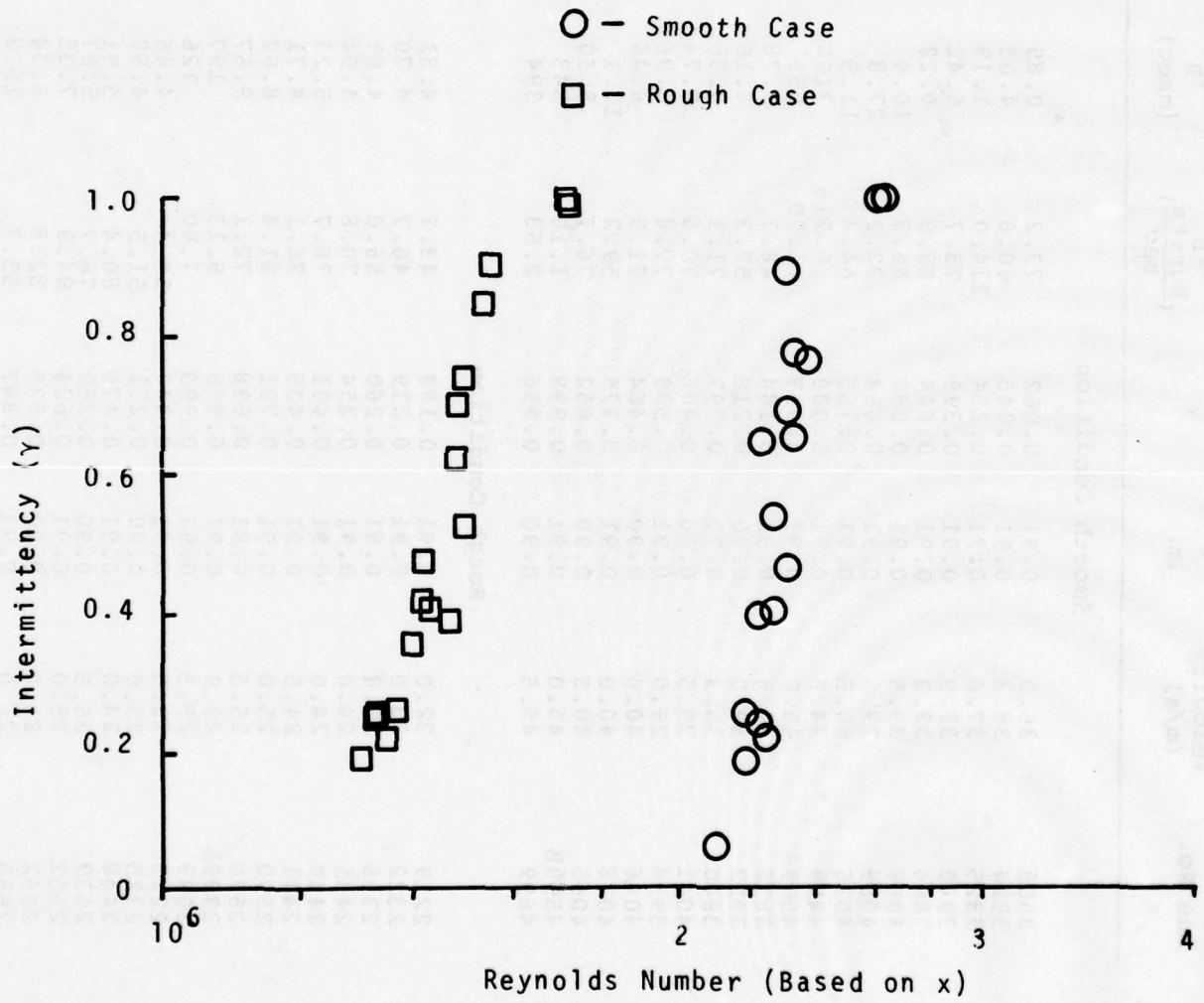

FIGURE 4.3 Extent of Transition Region

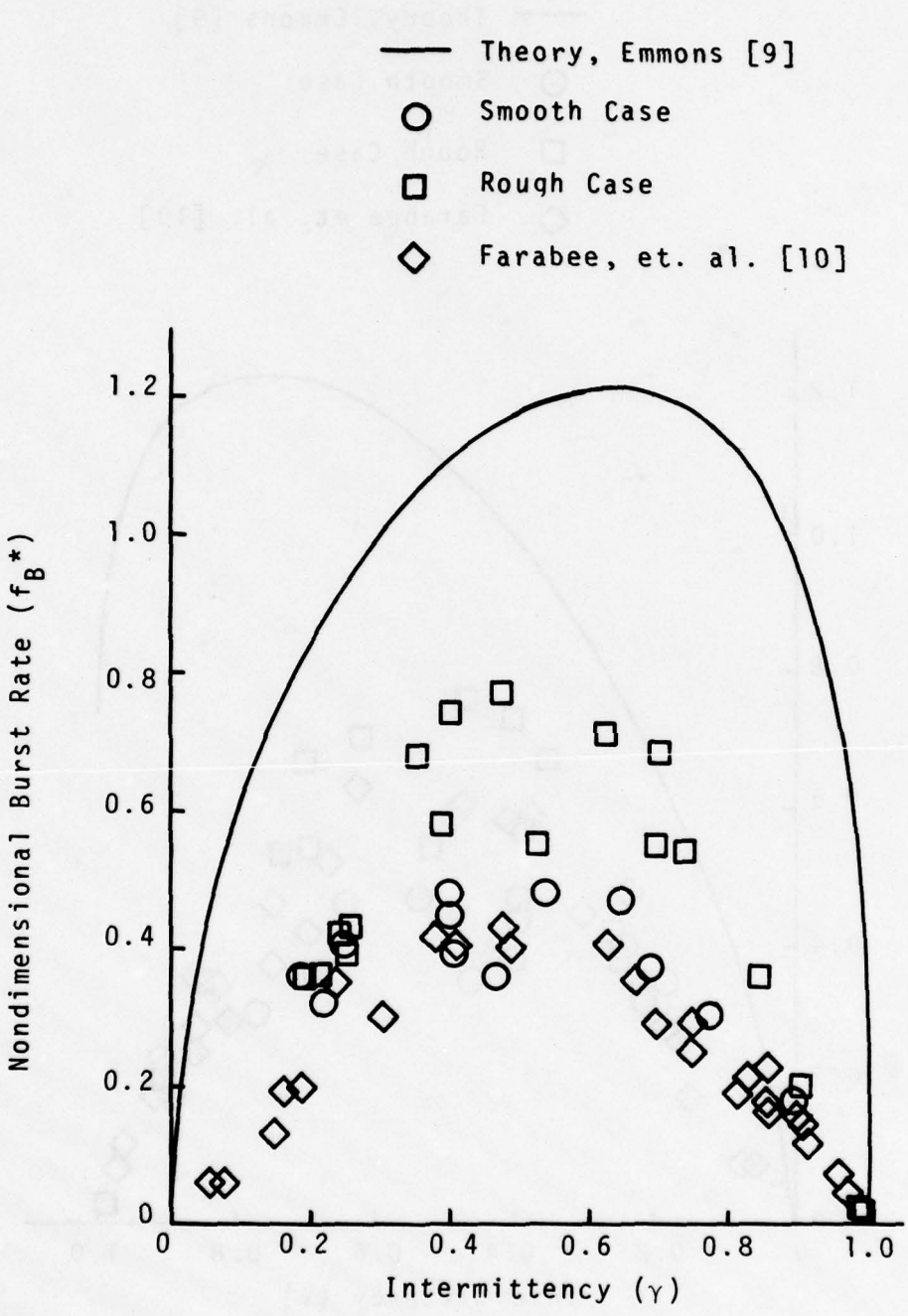

FIGURE 4.4 Normalized Burst Rates (Line Source Density)

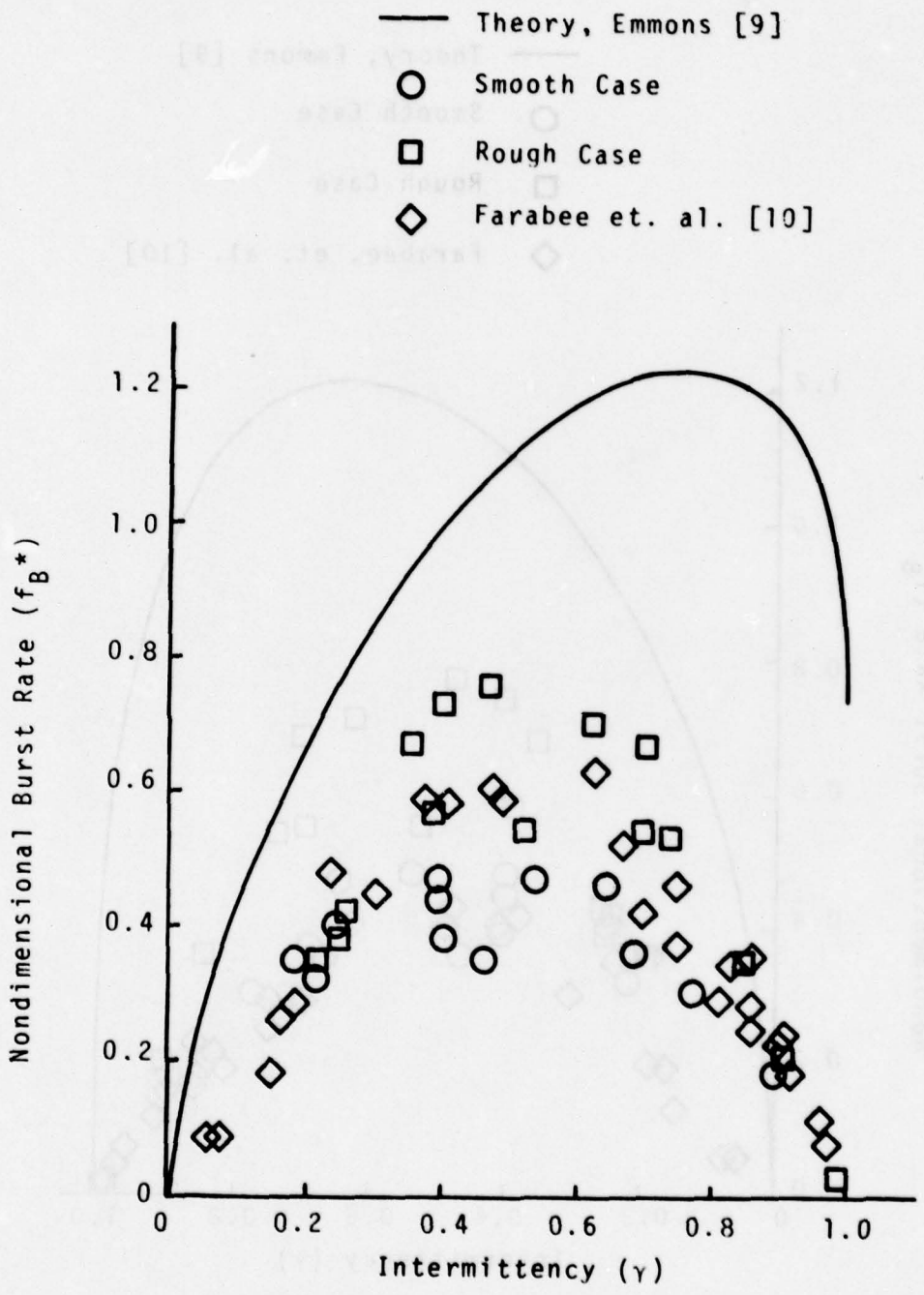

FIGURE 4.5 Normalized Burst Rates (Constant Source Density)

applying Emmons' [9] theory to two different source rate density functions. In Figure 4.4 a line source density function was assumed and a constant source density function was used in Figure 4.5. In the constant case, the source density function was constant downstream of the transition point, but was set to zero upstream. In the line source case Dirac's delta function was used as the source rate function. The delta function was centered on the transition point. The non-dimensionalization was done as in Farabee, et al. For the line source:

$$f_B^* \equiv f_B/n \tan\alpha \sqrt{\frac{U_\infty}{n\sigma^*}} \quad , \tag{4.8}$$

and for the constant source:

$$f_B^* \equiv f_B/g \tan\alpha \left(\frac{U_\infty}{g\sigma^*}\right)^{2/3} \quad , \tag{4.9}$$

where f_B is the burst frequency, n is the line source density and g is the uniform source density. The burst growth angle is α and σ^* is a non-dimensional parameter defined by,

$$\sigma^* \equiv \frac{U_g \, U_\infty}{U_\ell \, U_t} \tan\alpha \; . \tag{4.10}$$

where U_ℓ is the velocity of the leading edge of the burst, U_t is the trailing edge velocity and,

$$U_g = U_\ell - U_t \; . \tag{4.11}$$

The numerical values for U_2, U_t and α were taken from Schubauer and Klebanoff [4] (see Figure 2.1).

If a line source function is used in Emmons' model of the intermittent region, the following relations are obtained,

$$f_B^* = 2\sqrt{(1-\gamma)\,\ell n\left(\frac{1}{1-\gamma}\right)} \tag{4.12}$$

and

$$f_B^* = 0.420\, f_B \frac{\Delta X_T}{U_\infty} \tag{4.13}$$

where

$$\Delta x_T = x|_{\gamma=.99} - x|_{\gamma=.01} \tag{4.14}$$

The use of a constant source function gives the relations:

$$f_B^* = 8.722 \int_0^{\bar{x}} \eta \exp[3.035(\eta^3-\bar{x}^3)]\,d\eta, \tag{4.15}$$

and

$$f_B^* = 0.412\, f_B \frac{\Delta X_T}{U_\infty}. \tag{4.16}$$

where

$$\bar{x} = \frac{x - x_t}{\Delta x_T} \tag{4.17}$$

Equations 4.12, 4.13, 4.15 and 4.16 are obtained in Appendix B. Equations 4.12 and 4.15 were used to obtain the theoretical curves in Figures 4.4 and 4.5. The experimental results were scaled using equations 4.13 and 4.16.

The burst rate measurements of Farabee, et al [10] compare well with the present results for the smooth plate. The rough plate results are higher than the smooth case, but this is most likely due to inaccuracies in the measurement of ΔX_T. The burst rates were measured with the pin-hole microphones and ΔX_T was measured with the hot wire anemometer at a later time. If the source-rate function changed during this time, the measured value of ΔX_T would be in error.

The theoretical curve of Figure 4.4 (line source model) has approximately the same shape as the measured results but its magnitude is too high. Emmons [9] points out that this theory will predict higher burst rates than are measured. When two bursts are separated by a very small laminar region, a transducer may only detect one burst whereas the theory will count two separate burst. (This is due to the smoothing in the data acquisition computer program.) If two or more burstsoverlap, the theory treats them as a single burst and uses the period of the larger burst. However, if the bursts do not completely overlap, the observed period is somewhat longer than this. These effects tend to make the theoretical burst rate higher than the observed rate. A basic assumption in Emmons' theory is that the turbulent spots are completely independent of each other. This assumption is not totally correct but seems to be a good approximation, since strong

burst interaction would change the shape of the curve in Figure 4.4.

The mean square pressure ratio ($\overline{p^2}|_\gamma / \overline{p^2}|_{\gamma=1}$) is plotted against intermittency in Figure 4.6. The mean square pressure ratio is defined as the ratio of the total mean square pressure to the mean square of the turbulent portion only. If the laminar portions of the intermittent signal do not contribute to the mean square pressure then the following relation from Section 2.2 must be true:

$$\overline{p^2}|_{\gamma=1} = \frac{1}{\gamma} \overline{p^2}|_\gamma . \qquad (2.8)$$

The mean square pressure ratio must then be equal to γ. Due to noise and laminar pressure fluctuations (e.g. T-S waves) the mean square pressure ratio was higher than γ when γ was less than about 0.6. The difference increased for smaller γ because of the greater amount of laminar signal.

4.3 STATISTICS OF PRESSURE FLUCTUATIONS

The wall pressure spectral densities for the smooth and rough conditions are shown in Figures 4.7 and 4.8. The spectral density was non dimensionalized by $U_\infty / q^2 \delta^*_T \gamma$, where q is the total head ($1/2\ \rho U_\infty^2$), and the frequency was scaled by δ^*_T / U_∞. Results of Blake [2] and Willmarth and Wooldridge [14] for fully turbulent boundary layers are shown for comparison. The spectral density is shown for

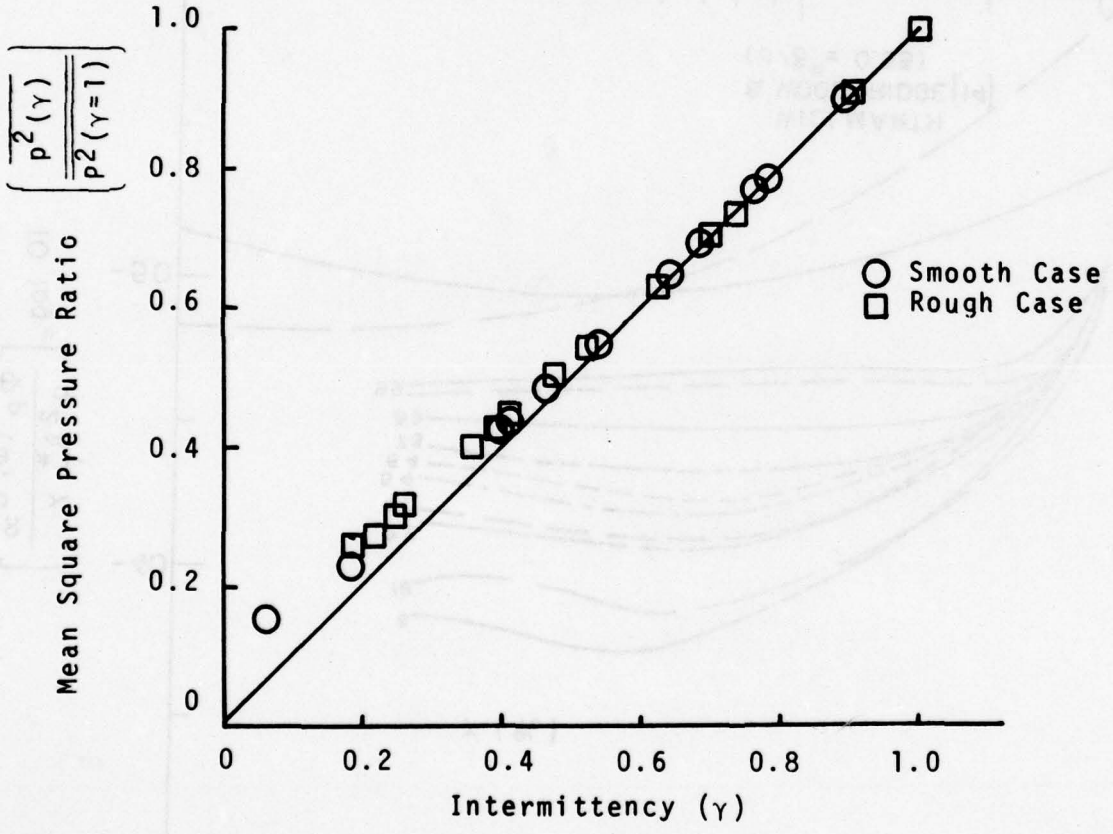

FIGURE 4.6 Mean Square Pressure Ratio

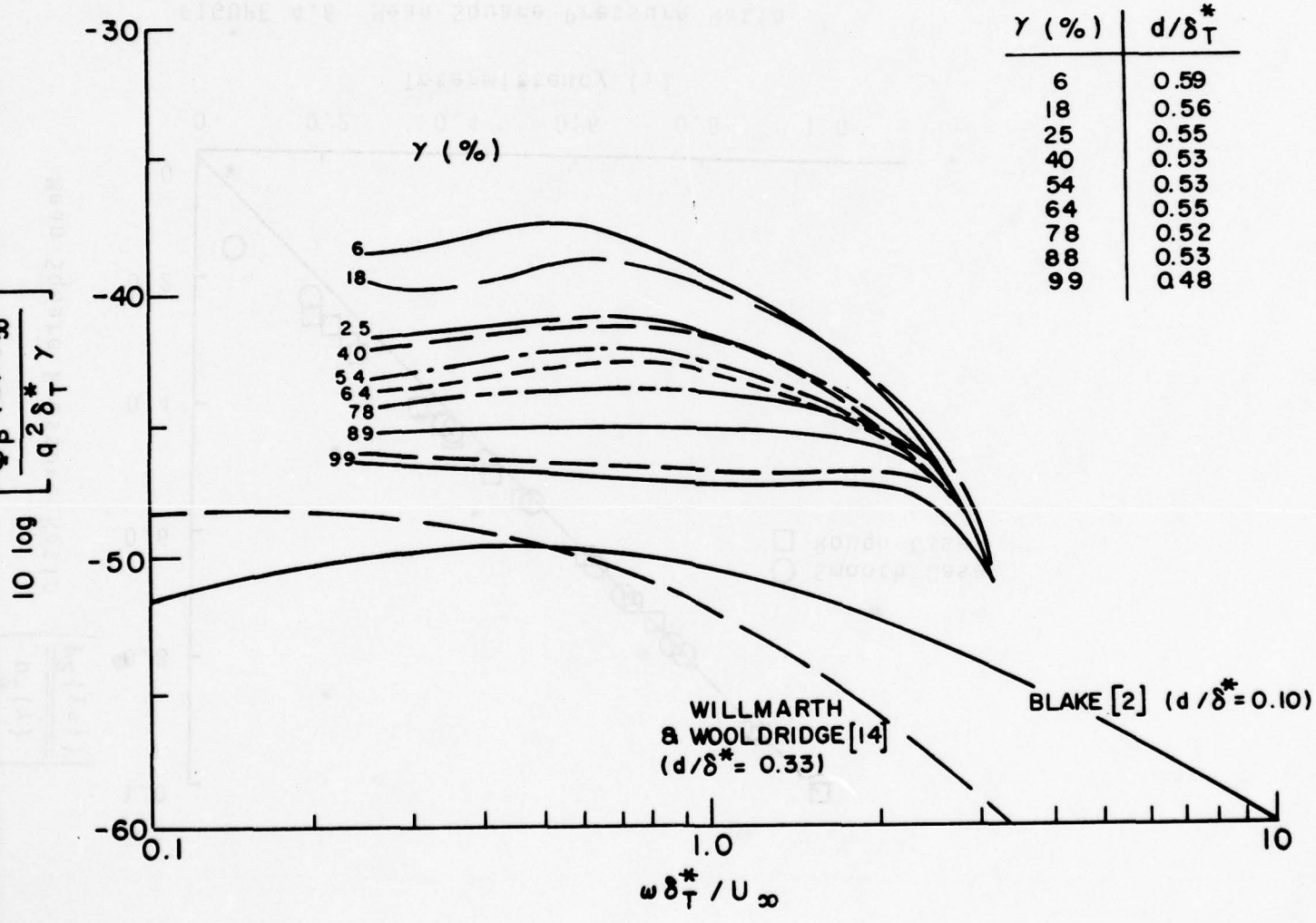

FIGURE 4.7 Wall Pressure Spectral Densities (Smooth Wall). γ is shown in percent.

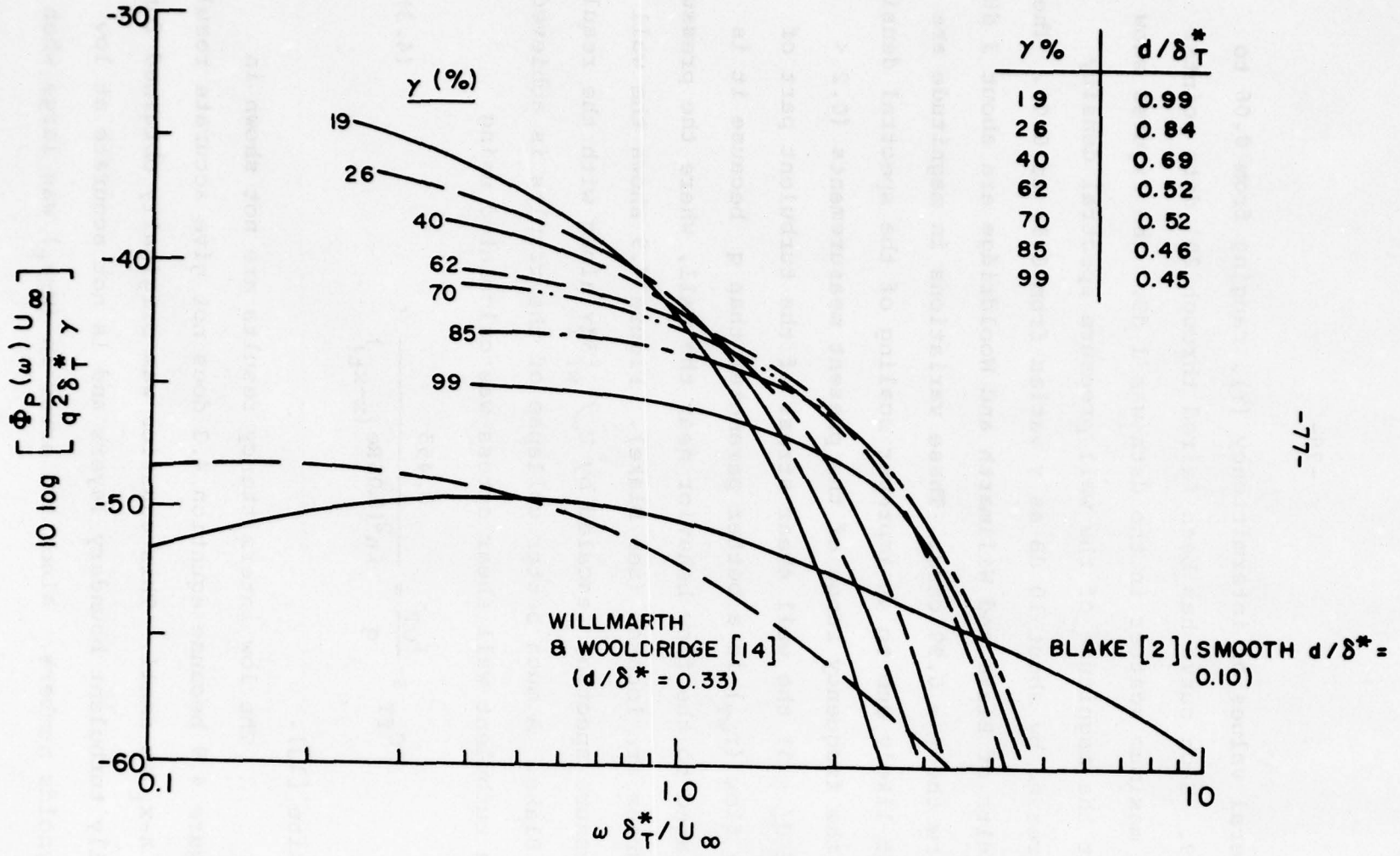

FIGURE 4.8 Wall Pressure Spectral Densities (Rough Wall). γ is shown in percent.

several values of intermittency (γ), ranging from 0.06 to 0.99. Each curve has been faired through 201 data points. The maximum scatter in the data was 1 dB. The figures show that the magnitude of the wall pressure spectral density increased by about 10 dB as γ varied from 0.99 to 0.06. The results of Blake and Willmarth and Wooldridge are about 3 dB below the $\gamma = 0.99$ case. These variations in magnitude are most likely due to an improper scaling of the spectral density. In the frequency range of the present measurements ($0.2 < \omega\delta_T^*/U_\infty < 5$) the wall shear stress of the turbulent part of the flow (τ_{wT}) is a better parameter than q because it is related to the flow behavior near the wall, where the pressure sources are located (see Blake). Figure 4.9 shows the wall pressure spectra, rescaled by $U_\infty/\tau_{wT}^2\delta_T^*\gamma$ along with the results of Blake. A much better collapse of the results is achieved. The turbulent wall shear stress was calculated using

$$C_{fT} \equiv \frac{\tau_{wT}}{q} \cong \frac{0.455}{\ell n^2(0.06 Re_{(x-x_t)})} , \qquad (4.3)$$

(White [1]).

The low intermittency results are not shown in Figure 4.9 because equation 4.3 does not give accurate results if $x-x_t$ is small. This equation was originally obtained for fully turbulent boundary layers and is not accurate at low Reynolds numbers. Also, the error in $(x-x_t)$ was large when

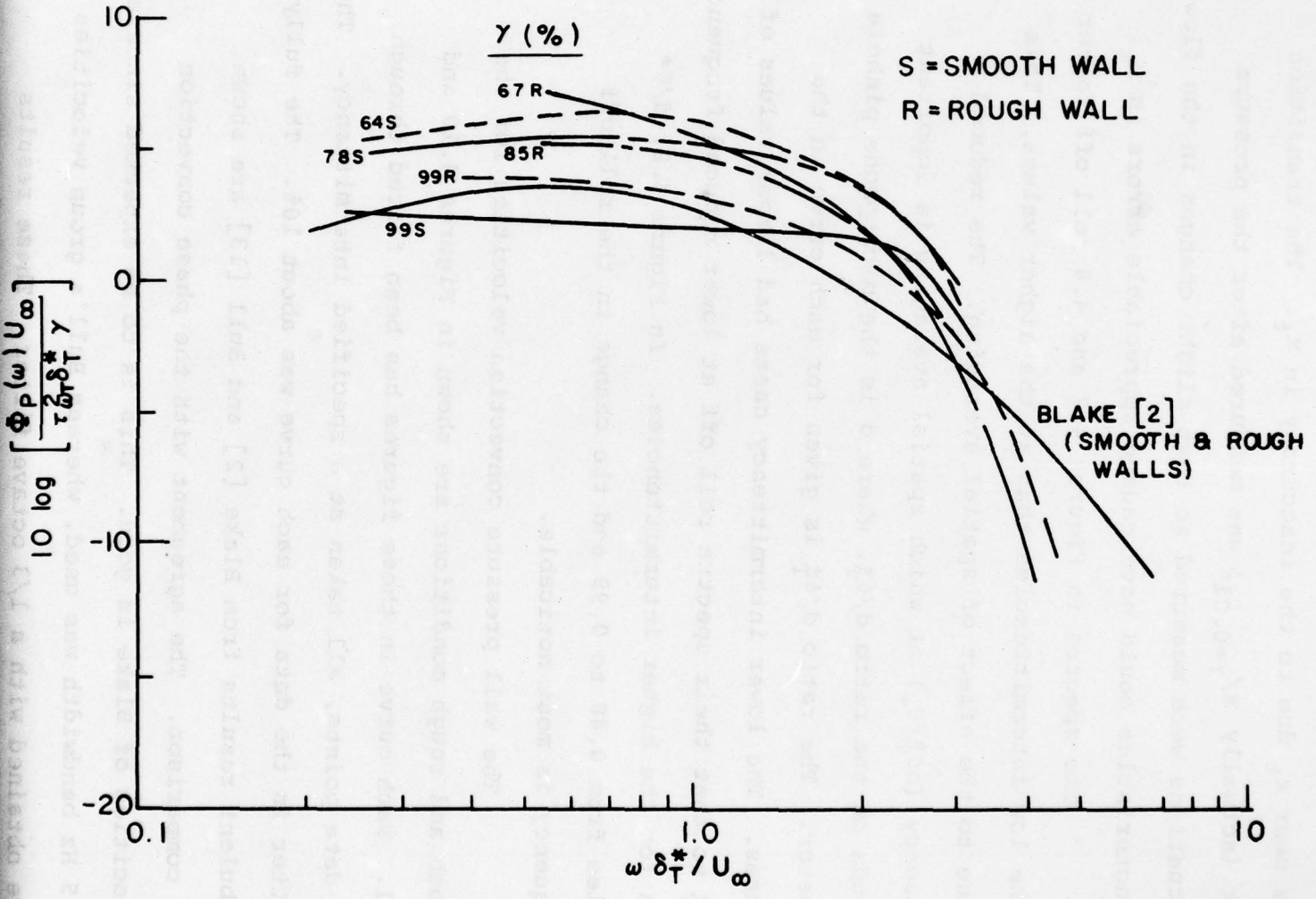

FIGURE 4.9 Wall Pressure Spectral Densities Scaled by the Wall Shear Stress. γ is shown in percent.

x was near x_t due to the inaccuracy in x_t. The transition point (actually $x/_{\gamma=0.01}$) was measured after the pressure fluctuations were measured so that slight changes in the flow characteristics could have caused appreciable errors in x_t.

The spectra in Figures 4.7 and 4.8 roll off faster at the low intermittencies than at the higher values. This is due to the effect of spatial averaging. The reduced frequency ($\omega\delta_T^*/U_\infty$) at which spatial averaging is important depends on the ratio d/δ_T^*, where d is the microphone pinhole diameter. The ratio d/δ_T^* is given for each curve in the figures. The lower intermittency cases had larger values of d/δ_T^* so that their spectra roll off at lower reduced frequencies than for the higher intermittencies. In Figure 4.8, d/δ^* varies from 0.48 to 0.99 and the change in the roll-off frequency is most noticable.

The wall pressure convection velocities for the smooth and rough conditions are shown in Figures 4.10 and 4.11. Each curve in these figures has been faired through 201 data points, all taken at a specified intermittency. The scatter in the data for each curve was about 10%. The fully turbulent results from Blake [2] and Bull [13] are shown for comparison. The agreement with the phase convection velocities of Blake is good. This is to be expected since a 62.5 Hz bandwidth was used, whereas Bull's group velocities were obtained with a 1/3 octave filter. These results

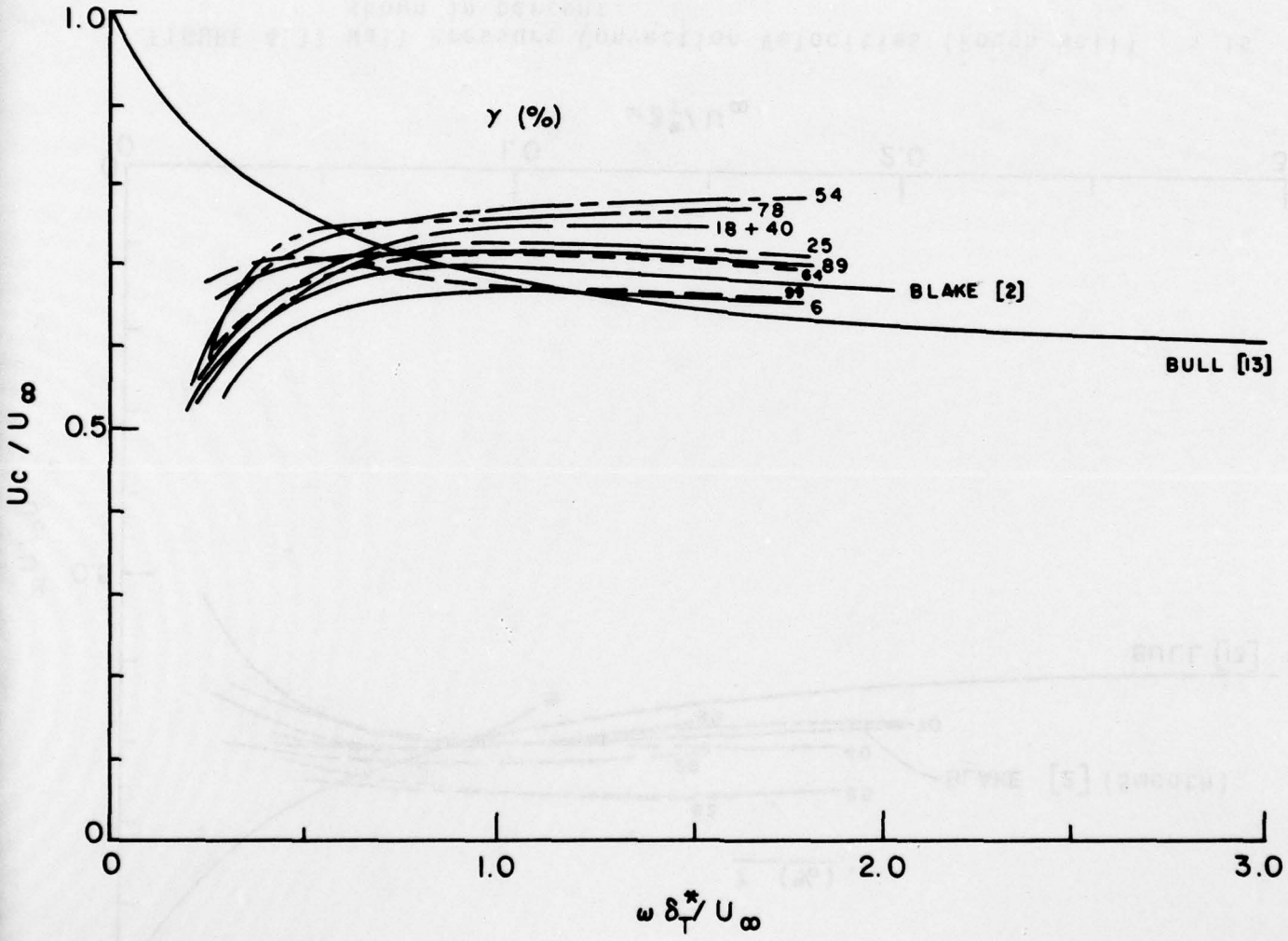

FIGURE 4.10 Wall Pressure Convection Velocities (Smooth Wall). γ is shown in percent.

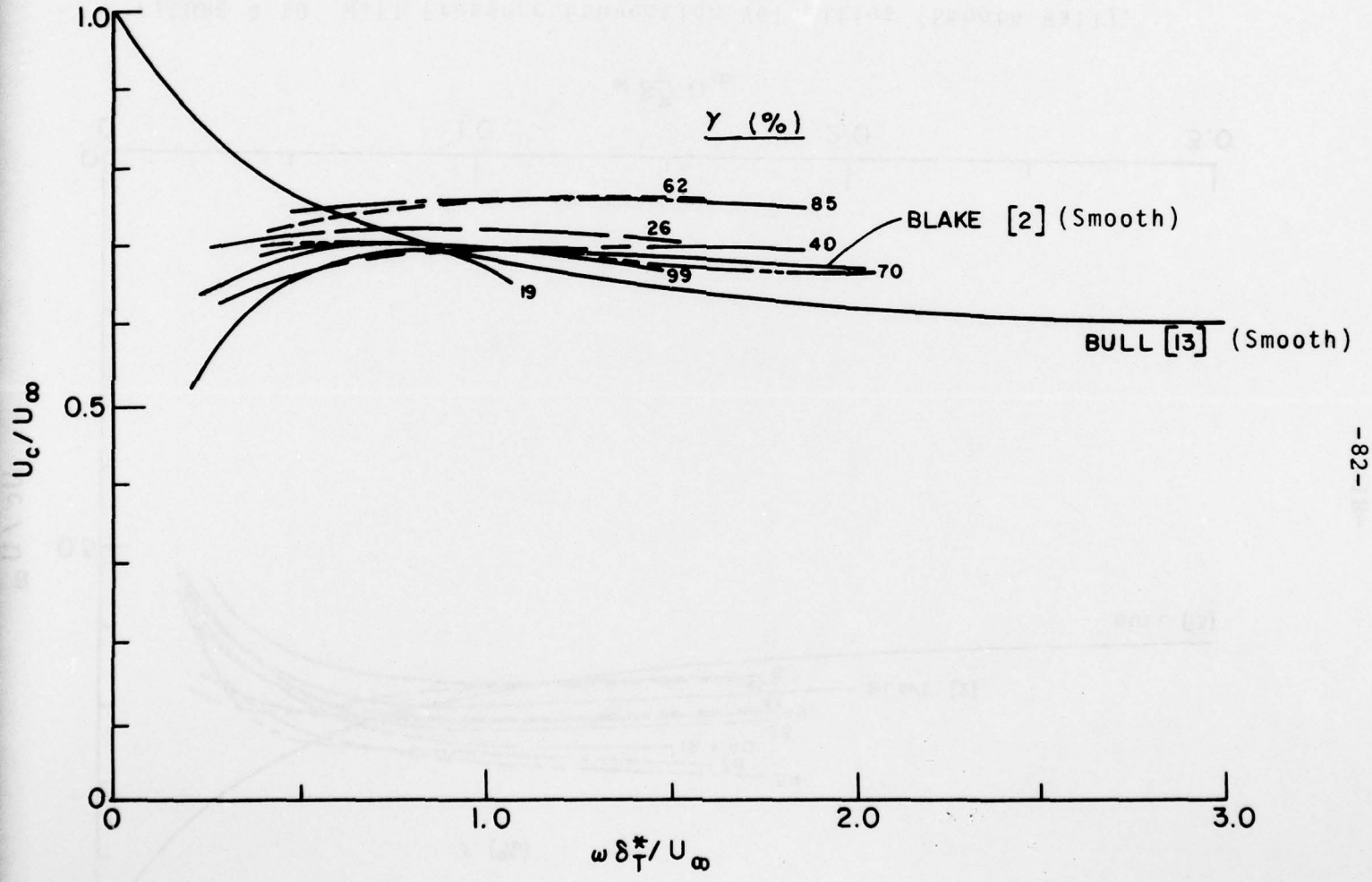

FIGURE 4.11 Wall Pressure Convection Velocities (Rough Wall). γ is shown in percent.

indicate that convection velocity does not depend on intermittency and that the single roughness has no effect. The γ=0.19 curve in Figure 4.11 goes only to $\omega\delta^*/U_\infty$ = 1.0. This is because the magnitude of the wall pressure spectrum dropped abruptly above this frequency and the convection velocity could not be calculated.

Figures 4.12 and 4.13 show the normalized longitudinal cross-spectral density magnitudes of wall pressure for the smooth and rough conditions. Again the curves in these figures have been faired through 201 data points. The scatter in the data was about 10%. The cross-spectral density magnitude was divided by the spectral density and the frequency was non-dimensionalized by r_s/U_c, where r_s is the streamwise microphone separation and U_c is the phase convection velocity. These curves show the coherence in the pressure field versus the microphone separation in wave length units. The results of Blake [2] and Willmarth and Wooldridge [14] are shown for comparison. Our results do not indicate any dependence on intermittency. However, the curves are slightly lower than the results of Blake and Willmarth and Wooldridge. This difference can best be explained by the fact that in the intermittent region, a turbulent spot will not cover both microphones all of the time. Thus, for part of the time one microphone will have a laminar signal while

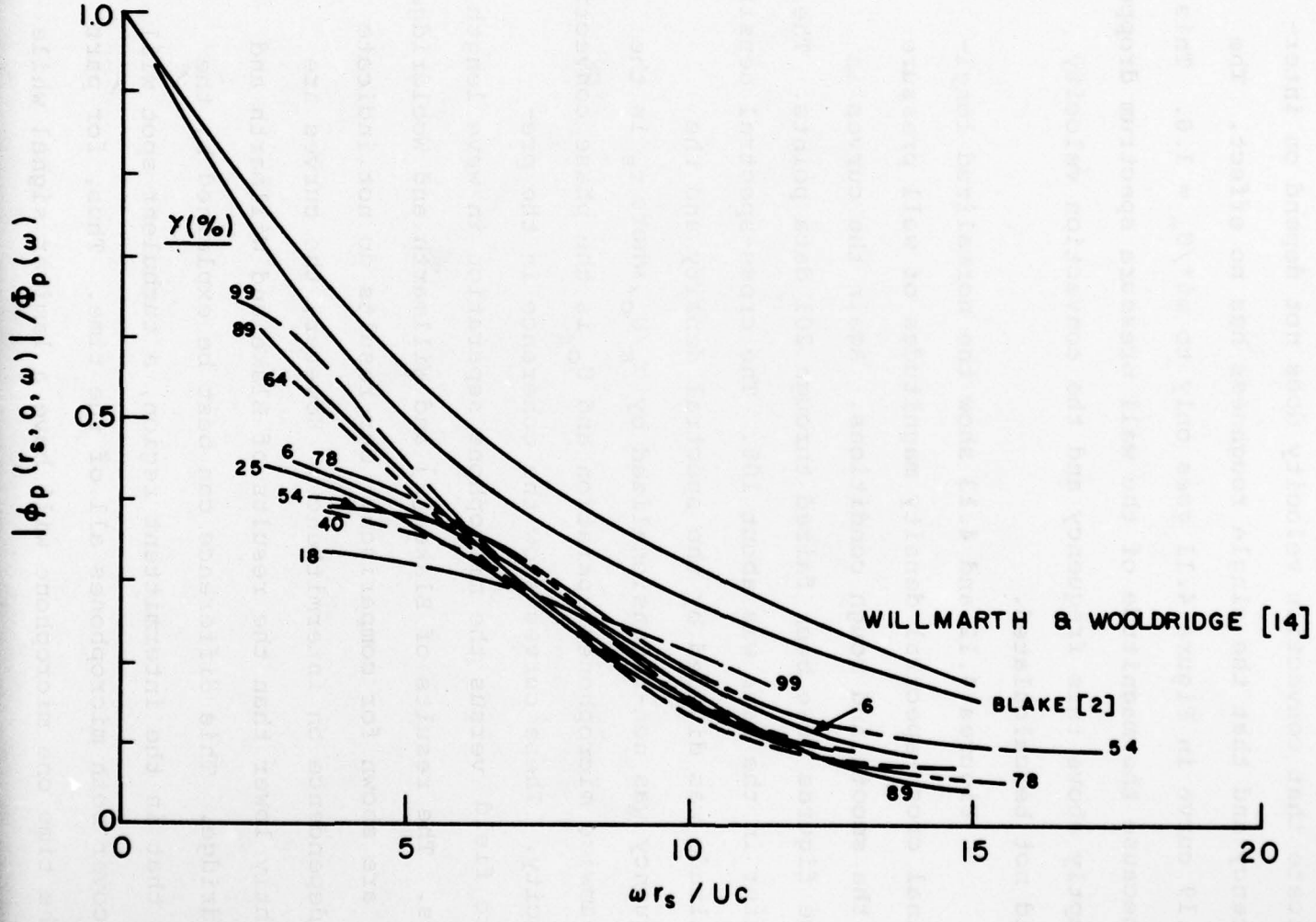

FIGURE 4.12 Normalized Longitudinal Cross-Spectral Densities (Smooth Wall). γ is shown in percent.

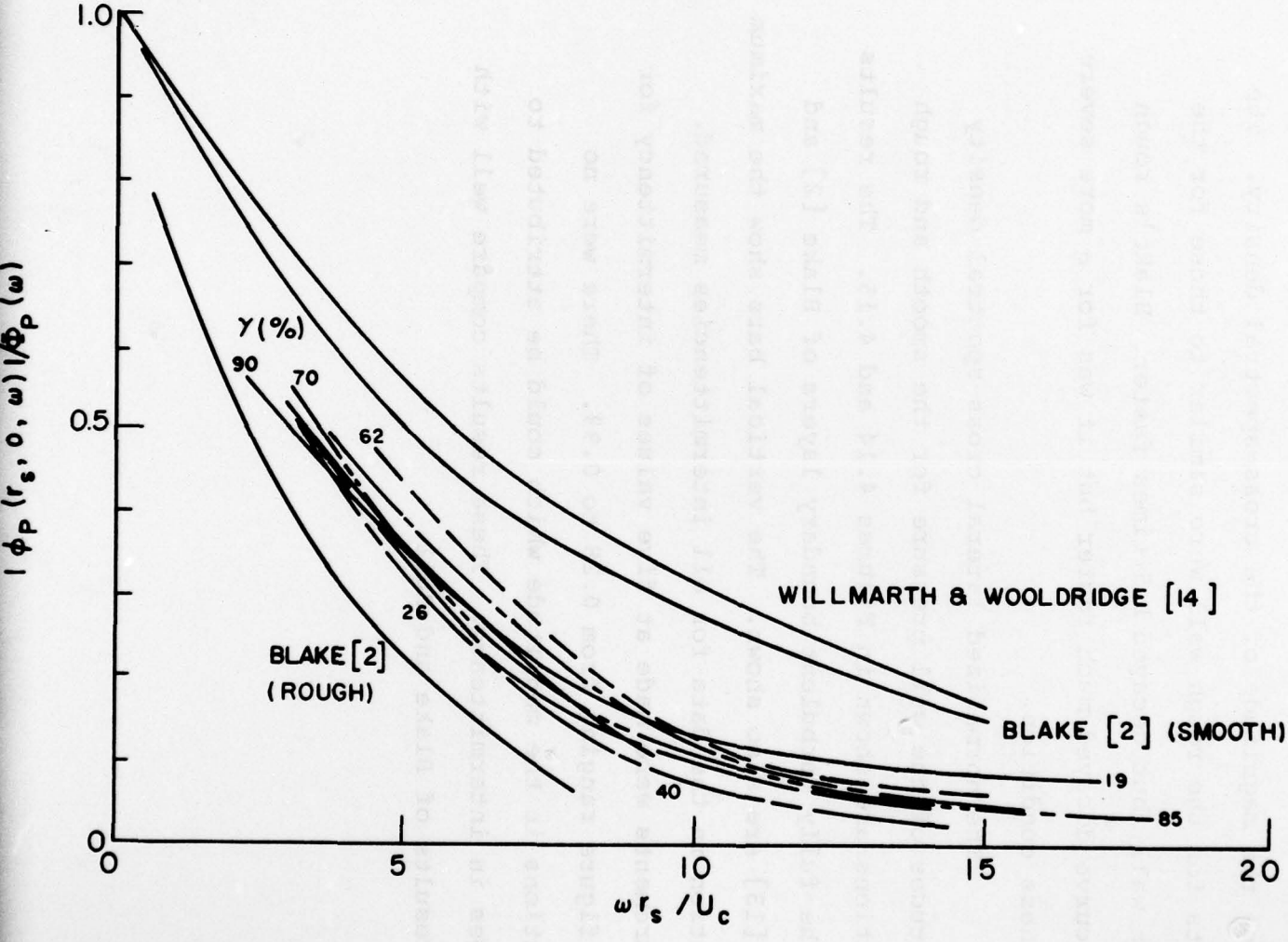

FIGURE 4.13 Normalized Longitudinal Cross-Spectral Densities (Rough Wall). γ is shown in percent.

the other has a turbulent signal (see Figure 2.3). This reduces the magnitude of the cross-spectral density. The results for the rough wall were similar to those for the smooth wall, but decayed 1.5 times faster. Blake's rough wall curve decayed much faster but it was for a more severe roughness condition.

The normalized lateral cross-spectral density magnitudes of the wall pressure for the smooth and rough conditions are shown in Figures 4.14 and 4.15. The results for the fully turbulent boundary layers of Blake [2] and Bull [13] are also shown. The vertical bars show the maximum variation in the data for all intermittencies measured. Measurements were made at five values of intermittency for each figure ranging from 0.28 to 0.99. There were no variations in the magnitude which could be attributed to changes in intermittency. These results compare well with the results of Blake and Bull.

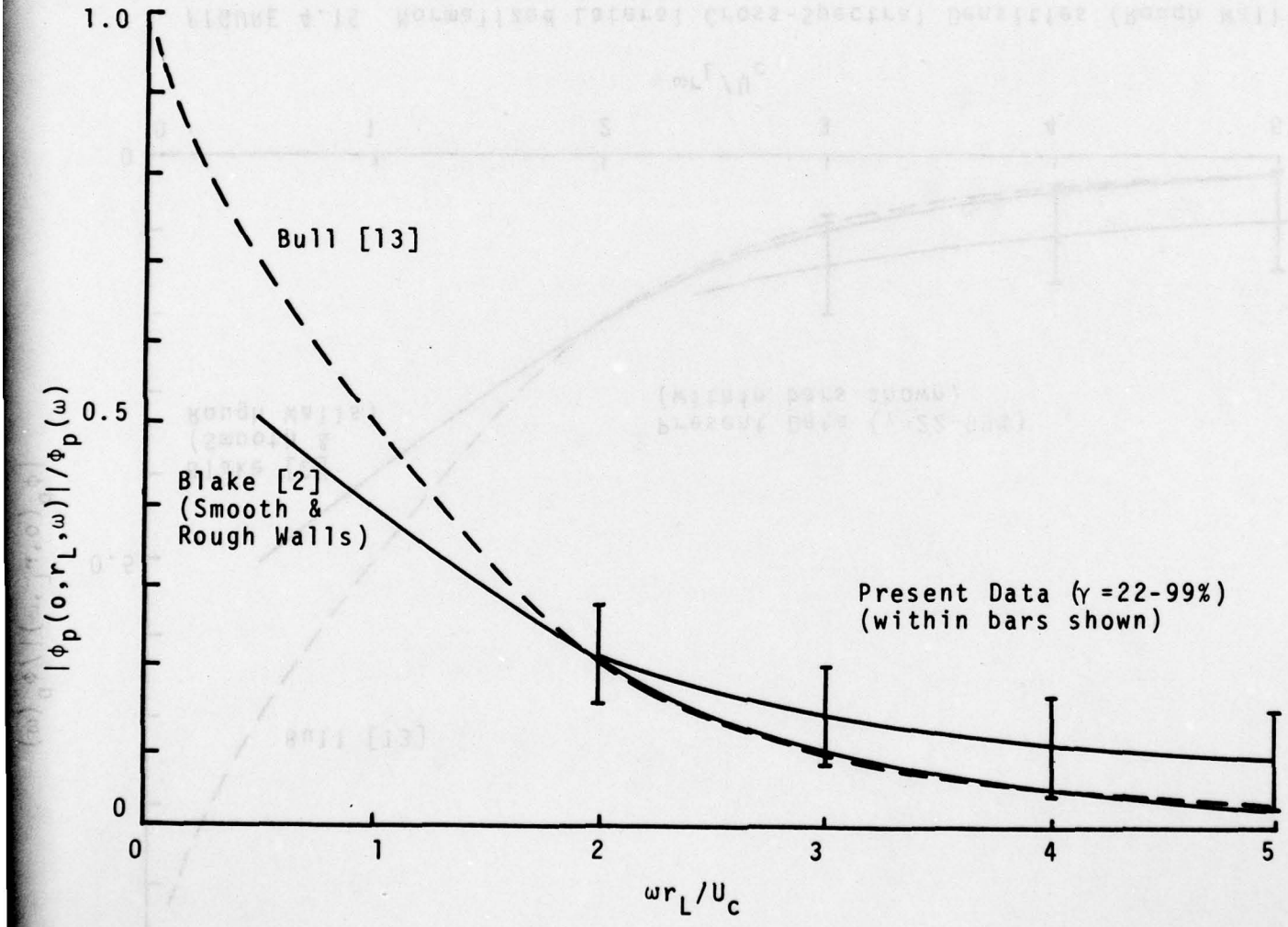

FIGURE 4.14 Normalized Lateral Cross-Spectral Densities (Smooth Wall). γ is shown in percent.

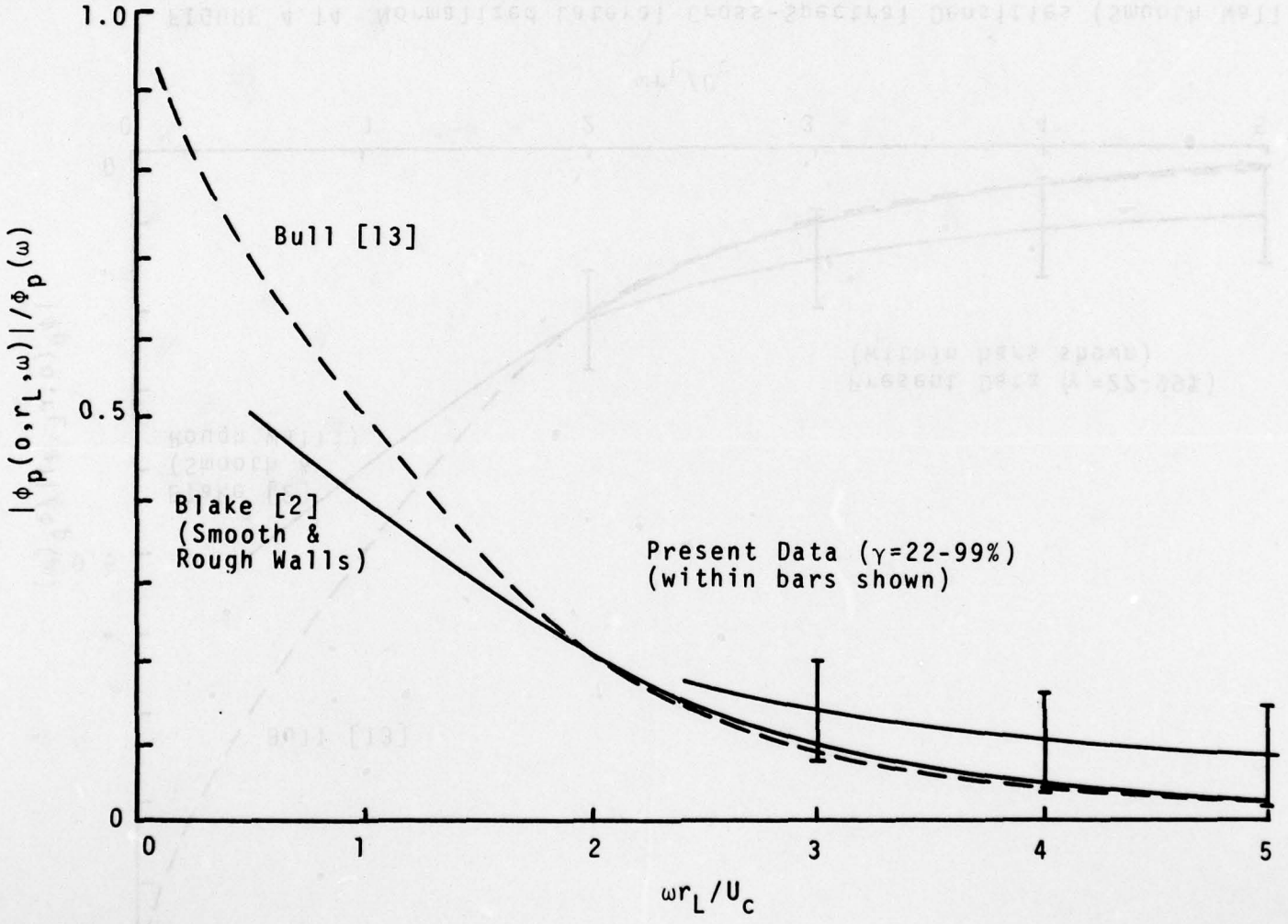

FIGURE 4.15 Normalized Lateral Cross-Spectral Densities (Rough Wall). γ is shown in percent.

5. CONCLUSIONS

Measurements of the statistics of the wall pressure fluctuations in the intermittent region of a viscous boundary layer on a flat plate have been presented. They were found to be similar to the results obtained in the fully turbulent region by Blake [2], Bull [13], Willmarth and Wooldridge [14] and others. When properly scaled, the statistics agreed with the results cited in previous reports for the fully turbulent region (to experimental accuracy). The wall pressure spectral densities did not all collapse to the same curve, but this was due to the inaccurate determination of the wall shear stress and the effect of spatial averaging over the microphone pinhole. The wall shear stress is essential to the correct scaling of the spectral density. The reduced frequency $(\omega\delta_T^*/U_\infty)$ at which spatial averaging becomes important depends on the ratio of the microphone pinhole diameter to the turbulent boundary layer displacement thickness. The similarities in the properties of turbulent spots and turbulent boundary layers seem to indicate that the underlying physical phenomenon is the same in each case.

The structural excitation due to the intermittent region of a boundary layer may therefore be determined by using results for fully turbulent layers if the effect of the intermittency is accounted for. The location of the

transition point and the variation of intermittency must be estimated first. These calculations should include the influence of surface roughness, free stream turbulence and other external effects. The variations in intermittency measured here were found to be similar to previous analytical and experimental results (Emmons [9], DeMetz and Casarella [3] and Schubauer and Klebanoff [4]).

The burst frequency was also measured and the results agreed well with the previous measurements of Farabee et. al. [10]. However, the burst rate computed with an Emmons type spot growth model was shown to be inaccurate.

When a small, two dimensional, downstream facing step was put in the plate near the leading edge, most of the statistics of the pressure field did not change. The only exception was the longitudinal cross-spectral density magnitude. With the step in place this function showed about a 1.5 times faster decay. The step also decreased the transition Reynolds number from about 2×10^6 to 1.2×10^6 (based on x).

Further studies of the intermittent region of the boundary layer are warranted. The study of surface roughness effects should be extended to include several types of two and three dimensional roughnesses commonly found in marine and aircraft structures (i.e. seams and rivets).

An improvement of Emmons' [9]theory to account fully for overlapping bursts in the computation of the burst rate and burst period would be valuable. Precise measurements of the turbulent wall shear stress in the intermittent region would also be useful. This would aid in the prediction of the wall shear stress for low Reynolds numbers.

REFERENCES

1. White, F. M., Viscous Fluid Flow, McGraw-Hill, New York, 1974.

2. Blake, W. K., "Turbulent Boundary-Layer Wall-Pressure Fluctuations on Smooth and Rough Walls", MIT Acoustics and Vibration Lab., Report No. 70208-1, January 1969, also J. Fluid Mech., Vol. 44, Part 4, pp. 637-660, December 1970.

3. DeMetz, F. C. and Casarella, M. J., "An Experimental Study of the Intermittent Properties of the Boundary Layer Pressure Field During Transition on a Flat Plate", NSRDC, Report No. 4140, November 1973.

4. Schubauer, G. B. and Kelbanoff, P. S., "Contributions on the Mechanics of Boundary Layer Transition", National Advisory Committee for Aeronautics, Report No. 1928, 1956.

5. Schubauer, G. B. and Skramstad, H. K., "Laminar Boundary Oscillations and Transition on a Flat Plate", National Advisory Committee for Aeronautics, Report No. 909, April 1943.

6. Klebanoff, P. S., Tidstrom, K. D. and Sargent, L. M., "The Three-Dimensional Nature of Boundary Layer Instability", J. Fluid Mech., Vol. 12, pp. 1-34, 1962.

7. Cantwell, B., Coles, D. and Dimotakis, P., "Structure and Entrainment in the Plane of Symmetry of a Turbulent Spot", J. Fluid Mech., Vol. 87, Part 4, pp. 641-672, 1978.

8. Schlichting, H., Boundary Layer Theory, Pergamon Press, London, 1955.

9. Emmons, H. W., "The Laminar-Turbulent Transition in a Boundary Layer - Part 1", J. Aero. Sciences, Vol. 18, p. 490, 1951.

10. Farabee, T. M., Casarella, M. J. and DeMetz, F. C., "Source Distribution of Turbulent Bursts During Natural Transition", NSRDC, Report No. SAD-89E-1942, August 1974.

11. Dhawan, S. and Narasimha, R., "Some Properties of Boundary Layer Flow During the Transition from Laminar to Turbulent Motion", J. Fluid Mech., Vol. 3, pp. 418-436, 1958.

12. Crandall, S. H. and Mark, W. D., Random Vibration in Mechanical Systems, Academic Press, New York, 1963.

13. Bull, M. K., "Wall-Pressure Fluctuations Associated with Subsonic Turbulent Boundary Layer Flow", J. Fluid Mech., Vol. 28, Part 4, pp. 719-754, 1967.

14. Willmarth, W. W. and Wooldridge, C. E., "Measurements of the Fluctuating Pressure at the Wall Beneath a Thick Turbulent Boundary Layer", J. Fluid Mech., Vol. 14, p. 187, 1962.

15. Hanson, C. E., "The Design and Constructing of a Low-Noise, Low-Turbulence Wind Tunnel", MIT Acoustics and Vibration Lab., Report No. 79611-1, 1969.

16. Tani, I., "Boundary-Layer Transition", Annual Review of Fluid Mech., Vol. 1, pp. 169-196, 1969.

17. Spangler, J. G. and Wells, C. S. Jr., "Effects of Free Stream Disturbances on Boundary-Layer Transition", AIAA Journal, Vol. 6, Part 3, pp. 543-545, March 1968.

18. Martin, N. C., "Wavenumber Filtering by Mechanical Structures", Ph.D. Thesis, Massachusetts Institute of Technology, January 1976.

19. Shapiro, P. J., "The Influence of Sound Upon Boundary Layer Instabilities", MIT Acoustics and Vibration Lab., Report No. 83458-83560-1, September 1977.

20. Moeller, M. J., "Low Wavenumber Levels of a Turbulent Boundary Layer in Zero and Adverse Gradients", MIT S.M. Thesis, 1977.

21. Hedley, T. E. and Keffer, J. F., "Some Turbulent/Non-Turbulent Properties of the Outer Intermittent Region of a Boundary Layer", J. Fluid Mech., Vol. 64, Part 4, pp. 645-678, 1974.

AD-A075 379 MASSACHUSETTS INST OF TECH CAMBRIDGE ACOUSTICS AND V--ETC F/G 20/4
WALL PRESSURE FLUCTUATIONS DURING TRANSITION ON A FLAT PLATE.(U)
APR 79 C J GEDNEY N00014-77-C-0084
UNCLASSIFIED A/V-84618-1 NL

2 OF 2
AD A075379

END
DATE FILMED
11-79
DDC

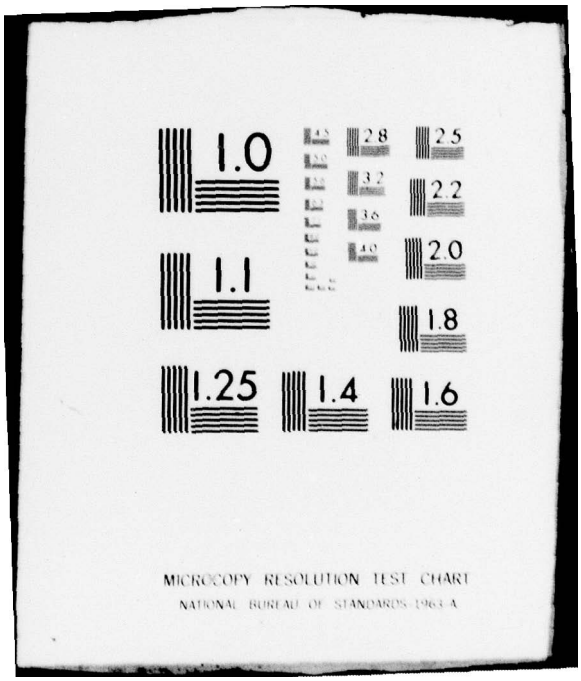
1.0
1.1
1.25
1.4
1.6
2.8
3.2
3.6
4.0
2.5
2.2
2.0
1.8
MICROCOPY RESOLUTION TEST CHART
NATIONAL BUREAU OF STANDARDS 1963-A

22. DeJong, R., "Vibrational Energy Transfer in a Diesel Engine", MIT Ph.D. Thesis, 1976.

23. Bendat, J. S. and Piersol, A. G., Random Data Analysis and Measurement Procedures, Wiley-Interscience, New York, 1971.

24. Oppenheim, A. V. and Schafer, R. W., Digital Signal Processing, Prentice Hall, New Jersey, 1975.

25. Cooley, J. W. and Tukey, J. W., "An Algorithm for the Machine Calculation of Complex Fourier Series", Math. Comp., Vol. 19, April 1965.

APPENDIX A

COMPUTER PROGRAM LISTINGS

A.1 DATA AQUISITION PROGRAM (FORTRAN CODE)

```
C
C     CONDITIONALLY AVERAGED CROSS-SPECTRAL DENSITY PROGRAM
C
C     THIS PROGRAM IS DESIGNED TO SAMPLE DATA AND THEN
C     CONDITIONALLY REJECT OR KEEP THE DATA DEPENDING ON A
C     PRESET TRIGGERING LEVEL.
C     CHANNEL Y IS THE TRIGGER IN TWO CHANNEL MODE, AND
C     CHANNELS X AND Y ARE THEN INPUT INTO THE CROSS-SPECTRAL
C     ANALYSIS PROGRAM OF RICK DEJONG.
C     OUTPUT INCLUDES THE RMS BEFORE AND AFTER CONDITIONING,
C     AND THE CROSS-SPECTRAL OUTPUT FOR CPLOT.
C
C     THIS IS VERSION E     NOV '77   CHARLES SEDNEY
C
C
      IMPLICIT INTEGER*2 (I-N)
      DIMENSION PSX(256),PSY(256),CO(256),QUAD(255),TAB(256)
      DIMENSION SENS(2),GAIN(2),SCALEX(2),NDATA(2,512)
      DIMENSION RMS(2),CRMS(2),RMSRAT(2),DRMS(2),BAND(2)
      DIMENSION SQRN(2),SQRN(2),DUMMY(4),IDATA(2,2048)
      DATA SENS,GAIN,BAND/0.0,0.0,0.0,0.0,0.0,15000./
      DATA ISAMP,NSAMP,MSAMP/2048,512,514/
      DATA NDEV,NBITS,NOUT/6,8,255/
      DATA FREQ,SMO,AVE/15000.,21.0,250./
C
C     INITIALIZE
C
      CALL PRIV
      CALL SINTAB(TAB,NBITS)
   11 WRITE(NDEV,12)
   12 FORMAT(' CERTAIN VARIABLES ARE PRESET',/,' TO ACCEPT, HIT RETURN',
     1       /,' TO MODIFY, TYPE NEW VALUES',/)
C
      SENS(1)=0.0
  100 CONTINUE
      WRITE(NDEV,101)SENS,GAIN
  101 FORMAT('   SENSITIVITY(X,Y)  AND  GAIN(X,Y)  (DB) (SENS-RE 1V/REF)
     1',/1X,4F10.5)
      READ(NDEV,102)(DUMMY(I),I=1,4)
  102 FORMAT(4F10.2)
      IF(DUMMY(1).EQ.0.0)GO TO 110
      DO 103 I=1,2
      J=I+2
      SENS(I)=DUMMY(I)
  103 GAIN(I)=DUMMY(J)
      GO TO 100
C
  110 WRITE(NDEV,111)FREQ,BAND
  111 FORMAT('  MAX FREQ  LO-OUTPUT BANDS-HI  (HZ)',/,1X,3F10.1)
```

```
      READ(NDEV,112)(DUMMY(I),I=1,3)
  112 FORMAT(3F10.2)
      IF(DUMMY(1).EQ.0.0) GO TO 113
      FREQ=DUMMY(1)
      BAND(1)=DUMMY(2)
      BAND(2)=DUMMY(3)
      GO TO 110
  113 INTVL=IFIX(0.2E07/FREQ+0.5)
      FREQ=0.2E07/FLOAT(INTVL)
C
      TRIG=0.0
  120 WRITE(NDEV,121)TRIG
  121 FORMAT('  TRIGGERING LEVEL (VREF/MICROSEC)'/1X,F10.5)
      READ(NDEV,122)DUMMY(1)
  122 FORMAT(F10.5)
      IF(DUMMY(1).EQ.0.0) GO TO 123
      TRIG=DUMMY(1)
      GO TO 120
  123 CONTINUE
      JSAMP=ISAMP
  140 WRITE(NDEV,141)SMO
  141 FORMAT('     SMOOTHING INTERVAL',/,1X,F8.0,'  SAMPLES')
      READ(NDEV,142) DUMMY(1)
  142 FORMAT(F10.5)
      IF(DUMMY(1).EQ.0.0) GO TO 143
      SMO=DUMMY(1)
      ISMO=(IFIX(SMO)/2)*2+1
      SMO=FLOAT(ISMO)
      GO TO 140
  143 ISMO=IFIX(SMO)
      TRIG=TRIG*TRIG*SMO*10.**(GAIN(2)/10.)*10.**(SENS(2)/10.)/FREQ/
     1FREQ*2.58419E12
      KSMO=(ISMO+1)/2
      JSMO=JSAMP-KSMO-1
      LSAMP=JSMO-KSMO+1
      KSAMP=JSAMP-1
C
  150 WRITE(NDEV,151) AVE
  151 FORMAT(1X,F10.2,' AVERAGES')
      READ(NDEV,152)DUMMY(1)
  152 FORMAT(F10.5)
      IF(DUMMY(1).EQ.0.0) GO TO 153
      AVE=DUMMY(1)
      GO TO 150
  153 LIMIT=IFIX(AVE)
C
      WRITE(NDEV,160)
  160 FORMAT(' FOR INTERMITTANCY ONLY, TYPE 0',/,
     1       ' FOR SPECTRAL ANALYSIS, TYPE 1')
      READ(NDEV,161)IFFT
  161 FORMAT(I1)
C
      WRITE(NDEV,170)
  170 FORMAT(' TYPE 1 TO MODIFY VARIABLES',/,
     1       ' TYPE 0 TO START SAMPLING')
      READ(NDEV,171) ID
  171 FORMAT(I1)
```

```
      IF(ID.NE.0) GO TO 100
C
C
C     CLEAR OUTPUT ARRAYS
 1000 DO 1001 I=1,NOUT
      PSX(I)=1.E-30
      PSY(I)=1.E-30
      CO(I) =1.E-30
 1001 QUAD(I)=1.E-30
      GAMTOT=0.0
      DO 1002 I=1,2
      RMS(I)=0.0
      DRMS(I)=0.0
 1002 CRMS(I)=0.0
      ICOUNT=0
      BURST=0.0
C
C     MAIN AVERAGING LOOP
C
      AKK=0.0
 1003 ICOUNT=ICOUNT+1
      IF(ICOUNT.GT.LIMIT)GO TO 1200
      DO 1004 I=1,2
      SQRN(I)=0.0
 1004 SQRM(I)=0.0
C
C     AVERAGING LOOP FOR DATA COLLECTION
C
 1100 IGAM=0
      ITER=0
      LERR=0
C
C     READ DATA
C
 1101 CALL CONVRT  (IDATA,0,ISAMP,INTVL,LERR)
      IF(LERR)91,1103,91
   91 CONTINUE
      WRITE(NDEV,1102)LERR
 1102 FORMAT(' A/D FAILED',I2))
      GO TO 1500
 1103 CALL UNPACK(IDATA,ISAMP)
      DO 210 I=1,2
      NSUM=0.0
      DO 200 J=1,ISAMP
  200 NSUM=NSUM+IDATA(I,J)/ISAMP
      DO 210 J=1,ISAMP
  210 IDATA(I,J)=IDATA(I,J)-NSUM
      IFLG=1
C
C     DEFINE INTERMITTANCY FUNCTION
C
      DO 1112 J=KSMO,JSMO
      DETEK=0.0
      DO 1109 I=1,ISMO
      M=J-KSMO+I+1
      IDIF=IDATA(2,M+1)/4-IDATA(2,M-1)/4
      DIFFY=FLOAT(IDIF)
```

```
      DIFFY=DIFFY*DIFFY
      DETEK=DETEK+DIFFY
 1109 CONTINUE
      IF(DETEK.LT.TRIG)GO TO 1111
      IF(IFLG.LT.1)BURST=BURST+1.0
      IFLG=1
      IGAM=IGAM+1
      DO 1110 I=1,2
      ADAT=FLOAT(IDATA(I,J))
      SQRM(I)=SQRM(I)+ADAT*ADAT
 1110 CONTINUE
      GO TO 1112
 1111 IFLG=0
      DO 1105 I=1,2
      ADAT=FLOAT(IDATA(I,J))
      SQRM(I)=SQRM(I)+ADAT*ADAT
      IDATA(I,J)=0.0
 1105 CONTINUE
 1112 CONTINUE
C
C     IS DATA ARRAY FILLED ?
C
      KEND=KSMO+NSAMP-1
      DO 1115 I=1,2
      DO 1115 J=KSMO,KEND
      JJ=J-KSMO+1
 1115 NDATA(I,JJ)=IDATA(I,J)
      AKK=AKK+1.0
      ITER=ITER+1
      IF(IGAM.GE.NSAMP)GO TO 1123
      IF(ITER.GT.100)GO TO 1121
      GO TO 1101
 1121 WRITE(NDEV,1122)
 1122 FORMAT(' GAMMA TOO LOW')
      GO TO 1500
C
C     FIND CONTIONAL RMS RATIOS
C
 1123 GAM=FLOAT(IGAM)
      GAMTOT=GAM+GAMTOT
      SAMP=LSAMP*ITER
      DO 1124 I=1,2
      RMS(I)=(SQRM(I)+SQRM(I))/SAMP+RMS(I)
      CRMS(I)=SQRM(I)/GAM+CRMS(I)
      DRMS(I)=SQRM(I)/(SAMP-GAM+1.E-30)+DRMS(I)
      IF((SAMP-GAM).LE.0.0)DRMS(I)=0.0
 1124 CONTINUE
C
      IF(IFFT.NE.0)GO TO 1125
      GO TO 1003
C     CALCULATE FOURIER TRANSFORM AND ADD TO RESULTS
C
 1125 WEIGHT=(SAMP/(GAM+1.E-30))**.25
      CALL FFTC(NDATA,TAB,NBITS,1)
      CALL CPS (NDATA(1,1),X1)
      CALL CPS(NDATA(2,1),Y1)
      PSX(1)=PSX(1)+4.*X1*X1*WEIGHT*WEIGHT
```

```
      PSY(1)=PSY(1)+4.*Y1*Y1*WEIGHT*WEIGHT
      CO(1)=CO(1)+4.*Y1*X1*WEIGHT*WEIGHT
      DO 1126 J=2,NOUT
      CALL CFS(NDATA(1,J),X1)
      CALL CFS(NDATA(2,J),Y1)
      JJ=NSAMP-J
      CALL CFS(NDATA(1,JJ),X2)
      CALL CFS(NDATA(2,JJ),Y2)
      XR=(X1+X2)*WEIGHT
      XI=(Y1-Y2)*WEIGHT
      YR=(Y1+Y2)*WEIGHT
      YI=(X2-X1)*WEIGHT
      PSX(J)=PSX(J)+XR*XR+XI*XI
      PSY(J)=PSY(J)+YR*YR+YI*YI
      CO(J)=CO(J)+YR*XR+YI*XI
 1126 QUAD(J)=QUAD(J)-YR*XI+YI*XR
      GO TO 1003
C
C
C     INTERMITTANCY OUTPUT
C
 1200 WRITE(NDEV,1201)
 1201 FORMAT('     RMS (LAM,TURB,TOTAL)')
      FACTR=.0001526/SQRT(AVE)
      DO 1202 I=1,2
      RMS(I)=SQRT(RMS(I))*FACTR
      CRMS(I)=SQRT(CRMS(I))*FACTR
      DRMS(I)=SQRT(DRMS(I))*FACTR
      RMSRAT(I)=CRMS(I)/DRMS(I)
 1202 WRITE(NDEV,1203)DRMS(I),CRMS(I),RMS(I)
 1203 FORMAT(1X,3F10.5)
      SAMTOT=FLOAT(LSAMP)*AKK
      GAM=GAMTOT/SAMTOT
      WRITE(NDEV,1204)
 1204 FORMAT('    RMS RATIO(X,Y)      GAMMA')
      WRITE(NDEV,1203)RMSRAT(1),RMSRAT(2),GAM
      BURATE=BURST*FREQ*2./SAMTOT
      BURPER=GAM/(BURATE+1.E-30)
      IF(BURATE.EQ.0.0)BURPER=0.0
      WRITE(NDEV,1205)
 1205 FORMAT('     AVE BURST RATE, PERIOD')
      WRITE(NDEV,1206)BURATE,BURPER
 1206 FORMAT(1X,2E10.3,' (SEC)')
C
C     RETURN TO BEGINNING TO RESET VARIABLES
C
      IF(IFFT.EQ.0) GO TO 100
C
C     OUTPUT FOR SPECTRAL ANALYSIS SECTION
C
C     CALCULATE SCALING FACTORS
C
      FAK=5.*5.*256.
      SCALE=4.34294*ALOG(FAK/(FREQ*AVE))
      SCALEX(1)=SCALE-SENS(1)-GAIN(1)
      SCALEX(2)=SCALE-SENS(2)-GAIN(2)
      SCALE=0.5*(SCALEX(1)+SCALEX(2))
```

```
C
C     PRINTED OUTPUT OR PUNCHED TAPE ?
C
 1300 WRITE(NDEV,1301)
 1301 FORMAT(' CHOOSE PRINT(05),PUNCH(01),RESTART(00),STOP(-1)')
      READ(NDEV,1302) ICH
 1302 FORMAT(I2)
      IF(ICH.EQ.0) GO TO 100
      IF(ICH.LT.0) GO TO 1500
      WRITE(NDEV,1303)
 1303 FORMAT('  FREQ   PSD-X   PSD-Y CPSD-XY PHASE   COHER',/)
      DF=FREQ/256.
      NL=IFIX(BAND(1)/DF+1.5)
      NU=IFIX(BAND(2)/DF+1.5)
      IF(NU.GT.NOUT)NU=NOUT
      DO 1304 I=NL,NU
      FR=DF*FLOAT(I-1)
      PSXOUT=4.34294*ALOG(PSX(I))+SCALEX(1)
      PSYOUT=4.34294*ALOG(PSY(I))+SCALEX(2)
      XMAG=CO(I)*CO(I)+QUAD(I)*QUAD(I)
      COHER=XMAG/(PSX(I)*PSY(I))
      XMAG=2.17147*ALOG(XMAG+1.E-30)+SCALE
      PH=ATAN2(QUAD(I),CO(I))*57.29578
 1304 WRITE(ICH,1305)FR,PSXOUT,PSYOUT,XMAG,PH,COHER
 1305 FORMAT(1X,F6.0,4F7.1,F5.2)
      GO TO 1300
C
C     QUIT PROGRAM
C
 1500 CONTINUE
      STOP
      END
```

A.2 DATA ACQUISITION SUBPROGRAMS (INTERDATA ASSEMBLY CODE)

```
*SUBROUTINE UNPACK
*ARGUMENTS    NDATA   DATA ARRAY
*             NSAMP   NO. SAMPLES
*UNPACK CONVERTS STORAGE OF NDATA FROM BYTE TO HALFWORD FORM
 ENTRY UNPACK
UNPACK STM RX,SAVE SAVE REGISTERS
 LH  NDATA,2(15) FETCH ADDRESSES
 LH  NSAMP,4(15)
 LH  NSAMP,0(NSAMP) LOAD CONSTANT
*SET POINTERS
 AHR NSAMP,NSAMP NSAMP=NSAMP*2
 SIS NSAMP,1
 LHR RID,NDATA
 AHR RID,NSAMP
 AHR NSAMP,NSAMP
```

```
 LHR TOP,NDATA
 AHR TOP,NSAMP
*UNPACK DATA
LOOP LB TEMP,0(MID)
 EXBR TEMP,TEMP
 STH TEMP,0(TOP)
 SIS TOP,2 BLIP POINTERS
 SIS MID,1
 CLHR TOP,NDATA
 BNL LOOP
 LM R6,SAVE RESTORE REGISTERS
 B 6(15) RETURN
SAVE DS 10
R6 EQU 11
NDATA EQU 11
NSAMP EQU 12
MID EQU 13
TOP EQU 14
TEMP EQU 15
 END
 ENTRY PRIV
*    CALL PRIV TO ALLOW I/O INSTRUCTIONS   PRIV NEEDS TO BE CALLED ONLY
*     ONCE PER PROGRAM(MAINLINE) EXECUTION, BUT ADDITIONAL CALLS DON'T HURT
*
*     ASSUMES FORTRAN CALL   SO  R11 + 14 CAN BE BASHED
*
PRIV LH 14,X'9C' GET OLD SVC 0 PARMS
 LHI 11,PRG SET POINTER TO PRG
 STH 11,X'9C'
 SVC 0,0 SWAP PSW'S
PRG STH 14,X'9C' RESTORE OLD
 B 2(15) RETURN
 END
 TITLE UNPACK DATA FROM ADC
 ENTRY UPSAMP
* UPSAMP(IA,NSAMP)
* IA IS INTEGER*2 ARRAY FROM CNVRT
* NSAMP IS NUMBER OF DATA SAMPLES TAKEN
* DATA IS UNPACKED TO ARRAY FORMAT (2,NSAMP
UPSAMP STM 8,RSAVE
 LH N,4(15)
 LH N,0(N)
 LH AADR,2(15)
 AHR N,N
  AHR AADR,N
 LHR BADR,AADR
 AHR BADR,N
 LIS TWO,2
 SHR BADR,TWO
 SHR AADR,TWO
 LHI L1,LD1
 LIS FOUR,4
LD1 LB D1,0(AADR)
 LB D2,1(AADR)
 EXBR D1,D1
 EXBR D2,D2
 STH D1,-2(BADR)
```

```
 STH D2,0(BADR)
 SHR AADR,TWO
 SHR BADR,FOUR
 SHR N,TWO
 BPR L1
 LM 0,RSAVE
 AH 15,0(15)
 BR 15
RSAVE DS 16
N EQU 9
AADR EQU 9
BADR EQU 10
TWO EQU 11
FOUR EQU 12
D1 EQU 13
D2 EQU 14
L1 EQU 15
 END
```

A.3 SUBPROGRAM 'CONVRT' (INTERDATA ASSEMBLY CODE)

```
 TITLE ************   SAMPLE A/D CONVERTER ************
 ENTRY CONVRT (A,NCHAN,NSAMP,PERIOD,LERR)
* FORTRAN CALLABLE SUBROUTINE
* A IS INTEGER*2 A(2,NSAMP/2) ARRA OF DATA (NCHAN=0)
*        INTGER*2 A(NSAMP/2) IF NCHAN NOT ZERO
* PERIOD IS INTEGER GIVING NUMBER OF MICROSECONDS BETWEEN CONVERSIONS
* NSAMP IS NUMBER OF CONVERSIONS TO BE MADE
* LERR IS LOGICAL VARIABLE
*        RETURNED TRUE IF EROR OCCURS, ELSE .FALSE.
* NCHAN IS CHANNEL TO SAMPLE
*        0  BOTH CHANNELS. FIRST DATA WILL BE CHANNEL A
*        1 CHANNEL A ONLY
*        2 CAHNNEL B ONLY
* EVERY CONVERSION TAKES UP ONE BYTE OF SPACE
* OUTPUT DATA IS BIPOAR, (8 BIT SIGNED SCALED FRACTION)
CONVRT STH 0,RSAVE
 LHI 11,X'20' SET UP COMMAND
 LIS 10,1 TWO BYTES PER SAMPLE
 LH 12,2(15) GET ADDRESS OF ARGS
 LHR 3,12 SET BEGINNING OD DATA AREA
 LH 13,0(13) GET NCHAN
  BZS BOTH DOING BOTH CHANNELS
 OHR 11,13 OR IN CHANNEL NUMBER
 OHI 11,2 TURN ON ONE CHANNEL MODE
 LIS 10,0 ONE BYTE PER SAMPLE
BOTH EQU *
 LH 14,0(14) GET NSAMP
 SLHL 14,0(10) MULTIPLY BY LENGTH OF ITEM
 AHR 12,14
```

THIS PAGE IS BEST QUALITY PRACTICABLE
FROM COPY FURNISHED TO DDC

```
 AIS 12,1 GET END OF BUFFER
 LHR 4,12 SET END OF DATA AREA
 LHI 1,X'56'
 DC  1,STOP STOP IF FIRST
 LH  12,0(15)
 SIS 12,1
 WHR 1,12
 LIS 12,0
 SPSR 0,12 FORCE 0 STATUS, SAVE OLD STATUS
 OCR 1,11 OUTPUT START COMMAND
 RBR 1,3 READ THE DATA
 SPSR 12,0 RESTORE OLD STATUS, SAVE ERROR FLAG
 DC  11,STOP STOP IF AGAIN
 LHR 12,12 TEST ERROR
 BZS OK
 LCS 12,1 -1 = FORTRAN .TRUE., 0=.FALSE.
OK LH 15,RSAVE+30
 LH  15,10(15)
 STH  12,0(15) STORE ERROR PARAMTER
 LM  0,RSAVE RETURN TO FORTRAN PROGRAM
 AH  15,0(15)
 BR  15
STOP DB X'10'
 DB  *
RSAVE DS 32
 END
```

A.4 PRESSURE STATISTICS PLOTTING PROGRAM (FORTRAN CODE)

```
C
C PROGRAM TO PLOT THE WALL PRESSURE STATISTICS MEASURED IN A BOUNDARY LAYER
C
C THIS PROGRAM INPUTS POWER AND CROSS SPECTRAL DENSITIES FROM
C THE DATA AQUISITION PROGRAM, NON-DIMENSIONALIZES THEM AND
C PLOTS THEM.
C
      INTEGER*2 XL,ID
      DIMENSION ARRAY(2,6,201),XS(4),XL(40),ID(8),A(11,201),RET(2)
     1,ROUGH(2),NVAR(11)
      LOGICAL NVAR
      DATA ROUGH /3HSMO,3HROU/
      DEFINE FILE 10(20,1250,U,NRP)
      DO 5 I=1,11
    5 NVAR(I)=.FALSE.
C INPUT DATA
C       GENERAL
      READ(8,10)NRUNS
   10 FORMAT(I3)
      DO 190 IT=1,NRUNS
C       TAPE DATA
```

THIS PAGE IS BEST QUALITY PRACTICABLE
FROM COPY FURNISHED TO DDC

```
      READ(8,20)(ID(L),L=1,8),NRP,LOC,NPLOT,NPB,NMAX,LR
   20 FORMAT(8A2/6I7)
C       TEST CONDITIONS
      READ(8,30)US,UL,RS,RL,DS,DPH,TS,GAMS
   30 FORMAT(8F10.3)
C FIND DATA
      GO TO (40,100),LOC
C DATA ON FILE (ASCII)
   40 DO 60 K=1,2
C     READ(12,50)((ARRAY(K,I,J),I=1,6),J=1,NMAX)
      READ(8,55)((ARRAY(K,I,J),I=1,6),J=1,NMAX)
C  50 FORMAT(1X,F7.0,4F7.1,F6.2)
   55 FORMAT(1X,F7.0,4F7.1,F6.2)
   60 CONTINUE
C CALCULATE DENSITY
      RO=-0.0023*TS+1.352
C STATISTICAL CALULATIONS
C   INITIALIZE
      MPH=113
      BRCH=0.0
      LFLAG=0
      QS=RO*US*US*0.5
      RSOU=RS/US
      RLOU=RL/UL
      RSOUP=RSOU*57.29578
      DSOU=DS/US
      PSDIM=0.0795798/DSOU/QS/QS/SQRT(GAMS)
C    SPECTRAL CALCULATIONS
      IF(ARRAY(1,5,1).LE.0.0)BRCH=BRCH+360.0
      IF(ARRAY(1,5,1)-ARRAY(1,5,2).GE.DPH)LFLAG=1
      DO 90 J=1,NMAX
      J1=J+1
      J2=J+2
      W=ARRAY(1,1,J)*5.28319
C ADD 2 PI TO PHASE FOR EACH BRANCH OF ARCTAN CROSSED
      ARRAY(1,5,J)=ARRAY(1,5,J)+BRCH
C  ADD ANOTHER 2 PI IF CROSSING A BRANCH
      BRCH=BRCH+360.0*FLOAT(LFLAG)
      LFLAG=0
      IF(J.GE.NMAX-2)GO TO 70
C TEST FOR BRANCH
      IF(ARRAY(1,5,J1)-ARRAY(1,5,J2).GE.DPH  )LFLAG=1
      IF(ARRAY(1,5,J2)-ARRAY(1,5,J1).GE.DPH  )LFLAG=-1
C CALCULATE NON-DIMENSIONAL STATISTICS AND ERRORS
   70 A(1,J)=W*RSOUP/ARRAY(1,5,J)
      A(2,J)=W*DSOU
      A(3,J)=W*RSOU/A(1,J)
      A(4,J)=W*RLOU/A(1,J)
      DO 80 K=1,2
      N1=K+4
      N2=K+6
      ARRAY(K,2,J)=0.5*(ARRAY(K,2,J)+ARRAY(K,3,J))
      A(N1,J)=2.0*(ARRAY(K,3,J)-ARRAY(K,2,J))
      A(N2,J)=10.**((ARRAY(K,4,J)-ARRAY(K,2,J)    )/10.0)
   80 CONTINUE
      A(9,J)=10.0*ALOG10(10.**(ARRAY(1,2,J)/10.0)*PSDIM)
      A(10,J)=ARRAY(1,1,J)
```

```
      A(11,J)=ARRAY(1,5,J)
   90 CONTINUE
C WRITE NON-DIMENSIONAL SPECTRA ON FLOPPY DISK (BIN)
      WRITE(10'NRP)((A(I,J),I=1,11),J=1,NMAX)
      GO TO 110
C READ NONDIMENSIONAL SPECTRA FROM FLOPPY DISK (BIN)
  100 READ(10'NRP)((A(I,J),I=1,11),J=1,NMAX)
C PRINT NUMBERS ON LP ?
  110 GO TO (120,150),NPR
  120 WRITE(5,130)(ID(L),L=1,8),US,RS,TS,RO,DS,UL,RL,ROUGH(LP)
  130 FORMAT(1H1,8A2/12X,'UINF       SEP.',T33,'TEMP       DENS       DELST
     1'/' (STR)',4X,5E10.3/' (LAT)',4X,2E10.3/10X,A3)
      WRITE(5,140)((A(I,J),I=1,11),J=1,NMAX)
  140 FORMAT('0   UC/J    W.DS/U',T28,'W.R/UC',T43,'ERROR       PHI(R)/PH
     1I(W)      PHI(W)    FREQ    PHASE'/'     (STR)     (STR)      (STR)
     2(LAT)  (STR)  (LAT)   (STR)    (LAT) (NON-DIM)  (HZ)   (DEG)'/
     3(F9.4,3F9.3,F6.1,F7.1,2F9.4,F8.1,2F10.1))
C MAKE PLOTS
  150 IF(NPLOT.EQ.0)GO TO 190
      DO 155 J=MPH,NMAX
      A(1,J)=0.
      A(3,J)=0.
      A(4,J)=0.
  155 CONTINUE
      DO 180 IP=1,NPLOT
      READ(8,160)NV,IS,NX,XS,XL
  160 FORMAT(3I7,4F7.0/40A2)
      DO 170 L=1,8
      XL(L)=ID(L)
  170 CONTINUE
      NVAR(NV)=.TRUE.
      CALL PICTR(A,11,XL,XS,NVAR,NMAX,NX,-1,1004,IS,FT,1)
      NVAR(NV)=.FALSE.
      PAUSE
  180 CONTINUE
  190 CONTINUE
      CALL EXIT
      END
```

APPENDIX B

CALCULATION OF THE THEORETICAL INTERMITTENCY AND BURST RATE FUNCTIONS

Emmons [9] derived the following relations for the intermittency and burst rate at point P(x,y) on a flat plate.

$$\gamma(P) = 1-\exp\left[-\int_R g(P_o)\,dV_o\right] \tag{B.1}$$

$$f_B(P) = \int_R \frac{g(P_o)}{\Delta t} \exp\left[-\int_{R'} g(P'_o)\; dV'_o\right] dV_o \tag{B.2}$$

where the point P_o is in the "retrograde cone" R and the point P'_o is in the "truncated cone" R' in the (x,y,t) coordinate system (see Figure B.1). $g(P_o)$ is the source rate probability density function and Δt is the duration of the burst at point P.

The integrals in equation B.1 and B.2 can be solved if the volume element dV_o is written (assuming a triangular burst shape),

$$dV_o = \frac{\sigma^*}{U_\infty} (x-x_o)^2 dx_o, \tag{B.3}$$

where, $$\sigma^* = \frac{U_g U_\infty}{U_\ell \eta_t} \tan\alpha \ , \tag{B.4}$$

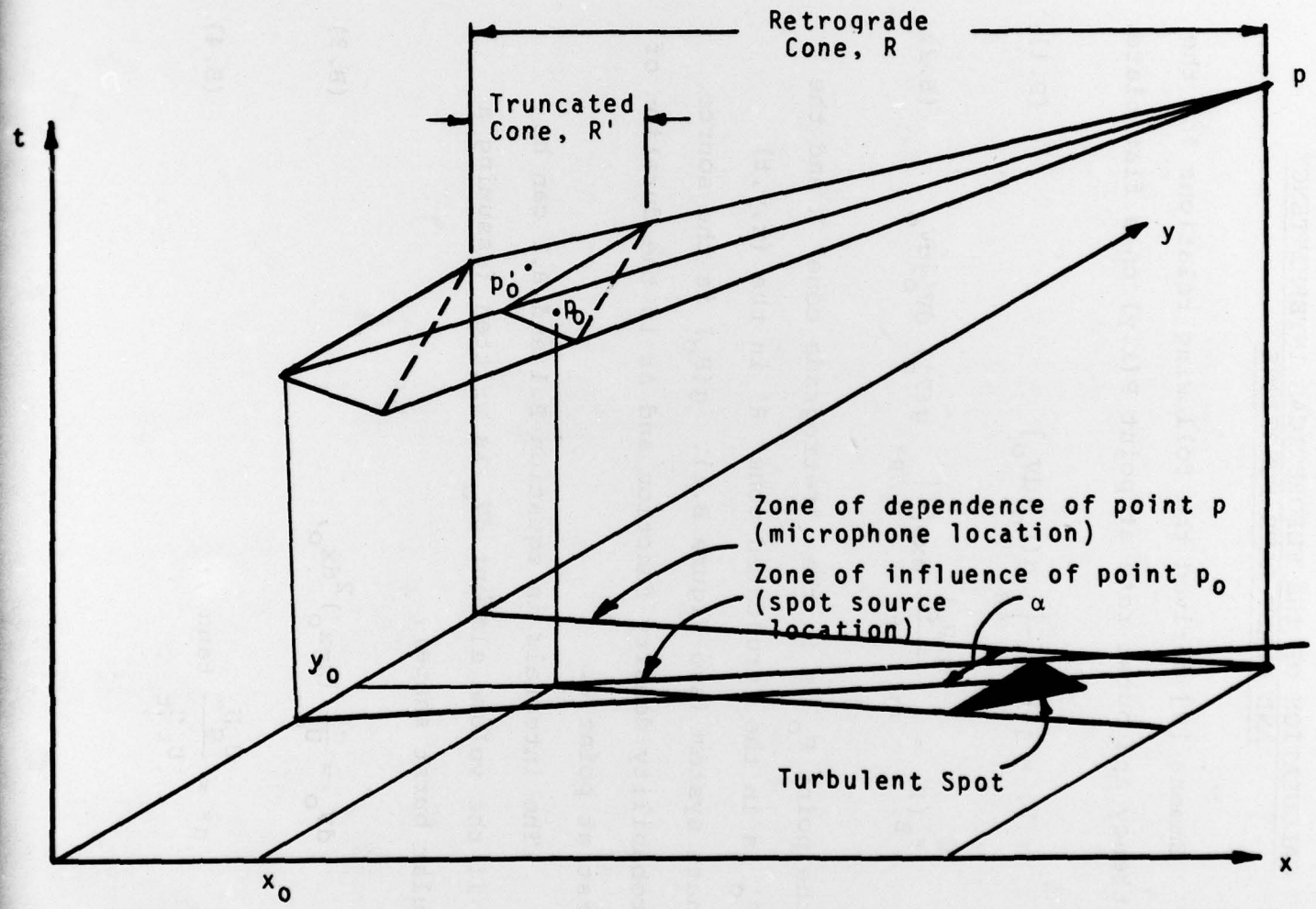

FIGURE B.1 Rectrograde and Truncated Cones Shown in the x,y,t, Coordinate System After Emmons [9]. (A Triangular Turbulent Spot Shape is Assumed).

U_∞ = freestream velocity,

U_ℓ = leading edge velocity of bursts,

U_t = trailing edge velocity of bursts,

α = half angle of spread of bursts,

and $U_g = U_\ell - U_t$.

dV_o can also be written in terms of Δt ,

$$dV_o = \Delta t dx_o dy_o \ . \tag{B.5}$$

Case 1: Line Source

The first assumed form of $g(P_o)$ is Dirac's Delta function,

$$g(P_o) = n\delta(x_o - x_t) \tag{B.6}$$

where n is the number of sources per unit length per unit time along the line $x = x_t$. Substitution into equation B.1 yields,

$$\gamma(P) = 1 - \exp\left[-\frac{n\sigma^*}{U_\infty}(x - x_t)^2\right] \ . \tag{B.7}$$

The inner integral in equation B.2 becomes,

$$\int_o^{x_o} n\delta(x'_o - x_t)\frac{\sigma^*}{U_\infty}(x - x'_o)^2 \, dx_o =$$

$$n\frac{\sigma^*}{U_\infty}(x - x_t)^2 H(x_o - x_t) \ . \tag{B.8}$$

Where the Heaviside function, H(x) is used since the value of this integral strongly depends on the relative locations of x_o and x_t. Equation B.2 becomes

$$f_B = \int_o^x \int_{y-d}^{y+d} n\delta(x_o - x_t)\exp[-\frac{n\sigma^*}{U_\infty}(x - x_t)^2 H(x_o - x_t)]dy_o dx_o \tag{B.9}$$

where $$d = (x - x_o)\tan\alpha \tag{B.10}$$

Solving the integrals in equation B.9 gives

$$f_B = 2n\tan\alpha(x - x_t)\exp[-\frac{n\sigma^*}{2U_\infty}(x - x_t)^2] \ . \tag{B.11}$$

The nondimensionalization of f_B is done as in Farabee et. al [10]:

$$f_B^* = f_B/n\ \tan\alpha\sqrt{\frac{U_\infty}{n\sigma^*}} \ . \tag{B.12}$$

Combining equations B.7, B.11 and B.12 yields,

$$f_B^* = 2\sqrt{(1-\gamma)\ln(\frac{1}{1-\gamma})} \tag{4.12}$$

and

$$f_B^* = 0.420\ f_B\ \Delta X_T/U_\infty \ . \tag{4.13}$$

Case 2: Constant Source

The second form of $g(P_o)$ is a constant for $x_o \geq x_t$,

$$g(P_o) = \begin{cases} 0 & (x_o < x_t) \\ g & (x_o \geq x_t) \end{cases} \tag{B.13}$$

Equation B.1 now becomes,

$$\gamma(P) = 1 - \exp[-\frac{g\sigma^*}{3U_\infty}(x - x_t)^3] \tag{B.14}$$

and B.2 becomes

$$f_B = 2\tan\alpha\ g\ \Delta X_T^2 \int_o^{\bar{x}} \eta \exp[\frac{\sigma^* g}{3U_\infty}\Delta X_T^3(\eta^3 - \bar{x}^3)]d\eta \tag{B.15}$$

where $$\bar{x} = \frac{x - x_t}{\Delta X_T} \tag{B.16}$$

and $$\Delta X_T = X|_{\gamma=0.99} - X|_{\gamma=0.01} \tag{B.17}$$

Combining B.14 and B.17 yields,

$$\Delta X_T = 1.45 \sqrt[3]{\frac{3U_\infty}{g\sigma^*}}\ . \tag{B.18}$$

Rewriting equation B.15,

$$f_B = 8.72\ g\tan\alpha\,(\frac{U_\infty}{g\sigma^*})^{2/3} \int_o^{\bar{x}} \eta \exp[3.04(\eta^3 - \bar{x}^3)]d\eta. \tag{B.19}$$

Nondimensionalizing f_B again as in Farabee et. al. [10],

$$f_B^* \equiv f_B/g\tan\alpha\ (\frac{U_\infty}{g\sigma^*})^{2/3}\ . \tag{B.20}$$

Combining equations B.18, B.19 and B.20 gives the desired relations,

$$f_B^* = 8.72 \int_o^{\bar{x}} \eta \exp[3.04(\eta^3 - \bar{x}^3)]d\eta \tag{4.15}$$

and

$$f_B^* = 0.412\ f_B\ \Delta X_T/U_\infty\ . \qquad (4.16)$$